AD-A091 064 FOREIGN TECHNOLOGY DIV WRIGHT-PATTERSON AFB OH F/G 20/4
AERODYNAMICS OF HIGH VELOCITIES (COLLECTION OF ARTICLES).(U)
SEP 80

UNCLASSIFIED FTD-ID(RS)T-0590-80 NL

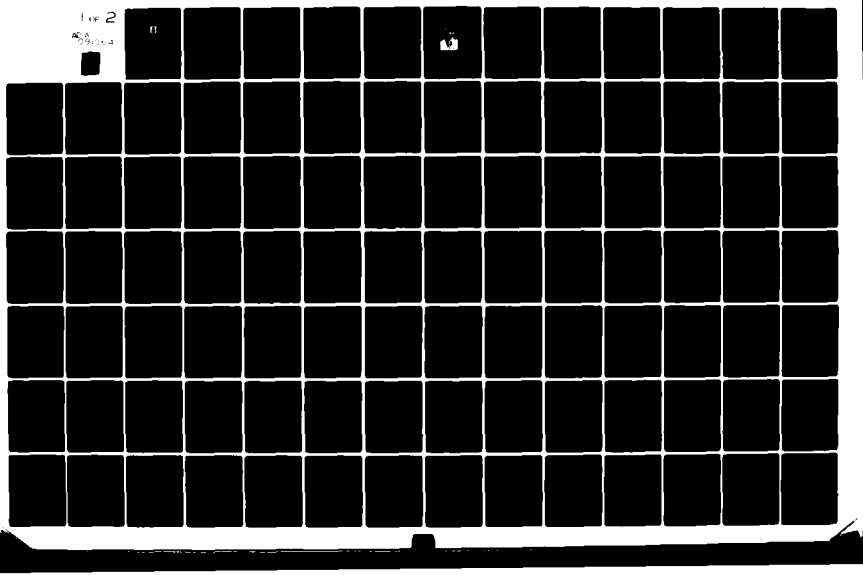

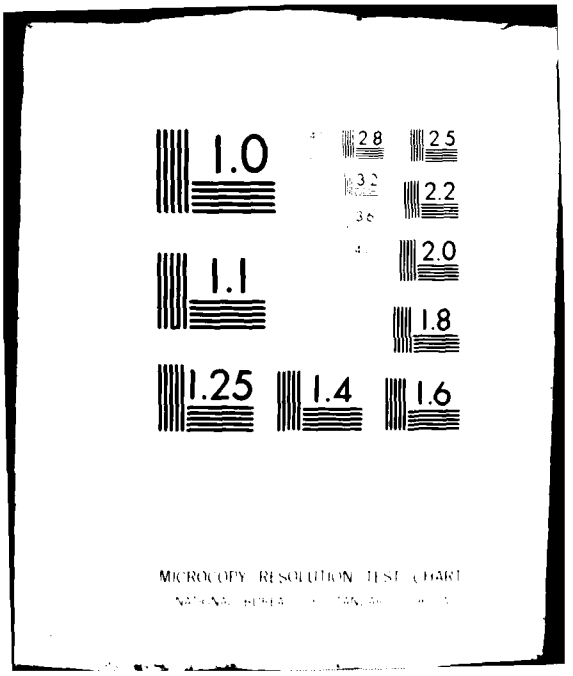
1.0
2.8
2.5
3.2
2.2
3.6
2.0
1.1
1.8
1.25
1.4
1.6
MICROCOPY RESOLUTION TEST CHART

FTD-ID(RS)T-0590-80

(2)

FOREIGN TECHNOLOGY DIVISION

AERODYNAMICS OF HIGH VELOCITIES
(Collection of Articles)

Nr. 19, 1972

Approved for public release;
distribution unlimited.

(11) 24 Sep 80

EDITED TRANSLATION

(14) FTD-ID(RS)T-0590-80 (12) 174

24 September 1980

(6) MICROFICHE NR: FTD-80-C-001033

AERODYNAMICS OF HIGH VELOCITIES (Collection of Articles). ~~No. 19, 1972~~

English pages: 168

(21) Edited trans. of Source: Institut Mekhaniki MGU, Nauchnyye Trudy, ~~Nr. 19, Moscow, 1972, pp. 1-93, 96-99, 102-151. Pages 94-95, 100-101 missing in original document~~

Country of origin: (USSR) n 19 p1-13, 16-18, 101-151 1972.
Translated by: SCITRAN
F33-657-78-D-0619
Requester: FTD/TQTA
Approved for public release; distribution unlimited.

THIS TRANSLATION IS A RENDITION OF THE ORIGINAL FOREIGN TEXT WITHOUT ANY ANALYTICAL OR EDITORIAL COMMENT. STATEMENTS OR THEORIES ADVOCATED OR IMPLIED ARE THOSE OF THE SOURCE AND DO NOT NECESSARILY REFLECT THE POSITION OR OPINION OF THE FOREIGN TECHNOLOGY DIVISION.	PREPARED BY: TRANSLATION DIVISION FOREIGN TECHNOLOGY DIVISION WP-AFB, OHIO.

142600

Graphics and Other Merged Materials have been Reproduced from the Best Materials Available.

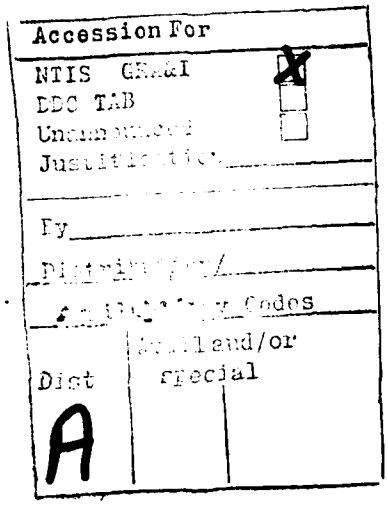

TABLE OF CONTENTS

FOREWORD 3

I. Flows of an Ideal Gas 5

1. About the establishment method 5

2. Flow past a sphere and cylinder with a flat leading part 16

3. Flow around blunt bodies 20

4. Flow around convexo-concave bodies 23

5. Nonequilibrium gas flows around surfaces 30

6. Solving the direct problem for a Laval nozzle 38

A Difference Scheme of the Third Order of Accuracy for Calculating Two-dimensional Flows with Contact Separation 44

Investigation of Supersonic Flow Around a Sphere by a Flow of Air with a High Static Temperature 54

Boundaries of Applicability of the Law of Binary Similarity During the Flow of a Dissociating Gas Around Bodies 65

Conditions on the Incident and Reflected Shock Waves in an Equilibrium Gas 71

Investigation of a Spatial, Supersonic Flow Around the Leading Part of Blunt Bodies by the Establishment Method 80

Calculating Viscous Flow Around a Sphere by a Hypersonic Flow of a Gas Mixture Containing Carbon Dioxide Gas 112

Stability of an Axisymmetrical Compressed, Non-viscous Wake 157

U. S. BOARD ON GEOGRAPHIC NAMES TRANSLITERATION SYSTEM

Block	Italic	Transliteration	Block	Italic	Transliteration
А а	*А а*	A, a	Р р	*Р р*	R, r
Б б	*Б б*	B, b	С с	*С с*	S, s
В в	*В в*	V, v	Т т	*Т т*	T, t
Г г	*Г г*	G, g	У у	*У у*	U, u
Д д	*Д д*	D, d	Ф ф	*Ф ф*	F, f
Е е	*Е е*	Ye, ye; E, e*	Х х	*Х х*	Kh, kh
Ж ж	*Ж ж*	Zh, zh	Ц ц	*Ц ц*	Ts, ts
З з	*З з*	Z, z	Ч ч	*Ч ч*	Ch, ch
И и	*И и*	I, i	Ш ш	*Ш ш*	Sh, sh
Й й	*Й й*	Y, y	Щ щ	*Щ щ*	Shch, shch
К к	*К к*	K, k	Ъ ъ	*Ъ ъ*	"
Л л	*Л л*	L, l	Ы ы	*Ы ы*	Y, y
М м	*М м*	M, m	Ь ь	*Ь ь*	'
Н н	*Н н*	N, n	Э э	*Э э*	E, e
О о	*О о*	O, o	Ю ю	*Ю ю*	Yu, yu
П п	*П п*	P, p	Я я	*Я я*	Ya, ya

*ye initially, after vowels, and after ъ, ь; e elsewhere.
When written as ë in Russian, transliterate as yë or ë.

RUSSIAN AND ENGLISH TRIGONOMETRIC FUNCTIONS

Russian	English	Russian	English	Russian	English
sin	sin	sh	sinh	arc sh	$\sinh^{-1}$
cos	cos	ch	cosh	arc ch	$\cosh^{-1}$
tg	tan	th	tanh	arc th	$\tanh^{-1}$
ctg	cot	cth	coth	arc cth	$\coth^{-1}$
sec	sec	sch	sech	arc sch	sech^{-1}
cosec	csc	csch	csch	arc csch	csch^{-1}

Russian	English
rot	curl
lg	log

GEORGIY IVANOVICH PETROV

(for his 60th birthday)

On May 31, 1972, the eminent Soviet Mechanical Scientist Georgiy Ivanovich Petrov celebrated his 60th birthday and 37 years of scientific, educational and social activity.

In the years of his youth, Georgiy Ivanovich intimately entwined his scientific interests with the work of the Progressive Soviet School of Aerodynamics, which was headed at that time by academician Sergey Alekseyevich Chaplygin. In 1934, a year before graduating from the Mechanical-Mathematical Department of Moscow State University, Georgiy Ivanovich began to work at TsAGI. His basic works of this period were devoted to questions of the propagation of vibrations in a viscous fluid and the theory of hydrodynamic stability.

During the years of World War II, Georgiy Ivanovich participated in work, vitally important for our country, in perfecting aerodynamics and combat characteristics of aircraft.

In 1955, already being a well-known scientist, G. I. Petrov was chosen head of the Department of Aeromechanics and Gasdynamics of the Mechanical-Mathematical faculty of Moscow State University. Since that time, a significant part of Georgiy Ivanovich's scientific and educational activity has taken place within the walls of his alma mater. In addition to work in the department, G. I. Petrov is the scientific supervisor of the Department of Aeromechanics of the Institute of Mechanics of Moscow State University, formed in 1960, and of a number of subunits of the computer center of Moscow State University.

Georgiy Ivanovich was among the first scientists who collectively and worthily evaluated the role of computer technology in

the development of science, and specifically, in theoretical and applied mechanics. Already many years ago, a seminar led by him was at work at the computer center at Moscow State University. The trends associated with the use of numerical methods in different branches of mechanics are being successfully developed in the works of his students, who are chiefly graduates of the Department of Aeromechanics and Gasdynamics of Moscow State University.

Many young, or already not so young, students of Georgiy Ivanovich consider the scientific research seminar which functions within the Institute of Mechanics to be a brilliant school of development. The variety of themes of reports given at the seminar reflects the breadth of scientific interests of Georgiy Ivanovich - from the flight mechanics of insects and aerodynamically low velocities to the hydrodynamics of processes that occur on the sun and the machanics of formation of lunar craters. Unchanging goodwill, a burning interest in anything new, no matter how small a result with respect to the seminar leader, serves as good payment for the risk for each young person who sets out on the thorny path of scientific investigations.

The collective of the Institute of Mechanics of Moscow State University congratulates Georgiy Ivanovich from the heart and wishes him strong health and new, great creative successes in his scientific, educational, and social activity for the good of our great motherland.

FOREWORD

This publication of scientific transactions is the second edition of a collection of articles on the aerodynamics of high velocities. In this edition, the results of investigations of a number of two-dimensional and three-dimensional problems of exterior aerodynamics are presented, as are the results of certain problems associated with the stability and the excitation of self-excited vibrations in gas flows.

The first four articles examine axisymmetrical, supersonic streamlining of bodies by a nonviscous, perfect, and real gas. The article by M. G. Lebedev, L. V. Pchelkina and K. G. Savinov presents the results of extensive calculations made by the method of establishing supersonic streamlining of bodies of different shape. The next article presents a differential system of a high order of accuracy developed by V. V. Yeremin and Yu. M. Lipnitskiy. This system makes it possible to use the establishment method to calculate complex two-dimensional flows without the explicit separation not only of shock waves, but also tangential discontinuities, and examples of such calculations are given for the first time. The work of Ye. G. Shapiro is devoted to the systematic investigation of supersonic streamlining of a body by a gas with a high static temperature; the basic flow characteristics are presented in the form of universal relationships with certain parameters; the possibility of describing an equilibrium gas flow in the examined case with the aid of the effective adiabatic exponent is shown. V. P. Stulov's article evaluates the applicability of the law of binary similitude during streamlining of bodies and obtains a boundary equation of the region of change in parameters p_∞ , R_0, where this law is valid.

V. N. Mirskiy's work describes the algorithm of calculating conditions on the incident and reflected shock waves in an equilibrium gas of random composition. The work gives an example of

calculation for a mixture of H_2O + Ar.

The next two articles are devoted to investigating supersonic, three-dimensional streamlining of blunt bodies. The article by Yu. M. Lipnitskiy, Yu. A. Mikhaylov and K. G. Savinov describes the differential system of calculating spatial, supersonic streamlining of blunt bodies with the presence of angles of attack and sideslip; the results of investigating streamlining of triaxial ellipsoids are given. The work of A. K. Burdel'nyy, V. B. Minostsev and V. P. Shkadova examines nonequilibrium, supersonic, spatial streamlining of segmentally conical bodies.

The articles by G. N. Andreyev and V. G. Gromov are devoted to supersonic streamlining of bodies by a viscous gas. The first of these gives a detailed investigation of a three-dimensional boundary layer on the flow line of segmentally conical bodies and spherically blunted cones. Finally, attention is given to studying the effect of the character of pressure distribution on the appearance of separation. In the second article, a solution to the Navier-Stokes equations in the vicinity of the critical line is given for a case of supersonic streamlining of a sphere by carbon dioxide gas. The results of calculations for a broad range of Reynolds numbers are given.

The article by M. G. Lebedev and G. F. Telenin is devoted to an investigation, suggested by the authors in the first collection, of the mechanism of excitation of self-excited vibrations of supersonic streams. The problem is solved in the complete statement for plane and axisymmetrical streams. A comparison is made with experimental data. The article by S. Ya. Gertsenshteyn and A. V. Kashko cites an investigation of the stability of an axisymmetrical wake in a supersonic flow. The problem is solved within the framework of an ideal fluid.

I. FLOWS OF AN IDEAL GAS

SOLVING PROBLEMS OF GASDYNAMICS BY THE ESTABLISHMENT METHOD

M. G. Lebedev, L. V. Pchelkina, K. G. Savinov

Beginning in 1966, M. G. Lebedev and K. G. Savinov, at the Institute of Mechanics of Moscow State University, and Yu. N. D'yakonov (deceased), and L. V. Pchelkina, at the Computer Center of Moscow State University, conducted numerical investigations of various gas flows by the establishment method [3]. The obtained results have been partly reflected in the works of authors [5-12]. In this article, a survey of the basic obtained results of both gasdynamic and methodological characters is given. In this case, a great deal of attention is given to earlier unpublished results.

1. About the establishment method

In 1961, K. I. Babenko and G. P. Voskresenskiy suggested a finite-difference method of calculating supersonic, spatial, steady state gas flows [1]. A monograph [2] contains a detailed presentation and the foundation of the method. The method has been extensively used for calculating the supersonic, spatial streamlining of sharp and blunt cones and bodies of certain other shapes. The results of the conducted investigations are in works [1-4].

One should take note of the important role which the works of Yu. N. D'yakonov [5,6] played in the development of this method. The methodological investigations carried out by Yu. N. D'yakonov made it possible to make a number of important improvements in the method [1] and to apply it to solving a number of gasdynamic problems for which this method was unsuited in its initial form

[5-7, 13-15].*

The experience of making calculations by the finite-difference method [1] makes it possible to obtain numerical solutions with high accuracy to various complex problems of gasdynamics, without at the same time making extreme demands on the speed and memory of the computer used for making the calculations.

In 1964, V. V. Rusanov [3, 21] suggested a modification of a method [1] applicable to solving two-dimensional, unsteady equations of gasdynamics. Inasmuch as particular attention attaches to steady state solutions which can be obtained from unsteady equations when $t \to \infty$ and from boundary conditions of the problem which do not change in time, the method [3], like other methods of the solution to unsteady problems, is frequently called the establishment method.

The establishment method examined by the authors was presented in detail in [3,4,6]; but inasmuch as we intend to dwell on certain results of a methodological character in this article, it seems useful to briefly describe the course of solving the gasdynamic equations by this method. We shall do this based on the example of a problem of flow arund a blunt body.

Let (Fig. 1) a blunt rotational body be flowed past by a supersonic gas flow running along the body axis of symmetry. Let the equation of contour of the body in the polar coordinate system in the meridional plane be $r = G(\theta, t)$ (we assume that the body contour can change in time according to a certain assigned law), and let $r = f(\theta, t)$ be the equa-

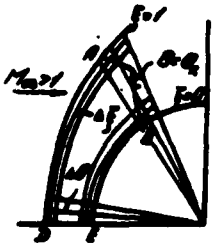

Fig. 1

*We note that there are also other modifications of the examined method today (for example, see the article by Yu. M. Lipnitskiy, Yu. Ya. Mikhaylov and K. G. Savinov, in this collection).

tion of the regressed shock wave. We shall insert the coordinate ξ with the relationship:

$$\xi = \frac{r - G(\theta,t)}{F(\theta,t) - G(\theta,t)} \tag{1.1}$$

such that $\xi = 0$ on the body surface, and $\xi = 1$ on the shock wave. The gasdynamic equations for a perfect gas and the variables t, ξ, θ can be written in the form:

$$\frac{\partial X}{\partial t} + A\frac{\partial X}{\partial \xi} + B\frac{\partial X}{\partial \theta} + \Gamma = 0 \tag{1.2}$$

where

$$X = \begin{vmatrix} u \\ v \\ \rho \\ p \end{vmatrix}, \quad A = \begin{vmatrix} a & 0 & \xi_r \rho^{-1} & 0 \\ 0 & a & r^{-1}\xi_\theta \rho^{-1} & 0 \\ \xi_r \gamma p & r^{-1}\xi_\theta \gamma p & a & 0 \\ \xi_r \rho & \xi_\theta \rho & 0 & a \end{vmatrix}$$

$$B = \frac{1}{r}\begin{vmatrix} v & 0 & 0 & 0 \\ 0 & v & \rho^{-1} & 0 \\ 0 & \gamma p & v & 0 \\ 0 & \rho & 0 & v \end{vmatrix}, \quad \Gamma = \frac{1}{r}\begin{vmatrix} -v^2 \\ uv \\ \gamma p(2u + v\,ctg\,\theta) \\ \rho(2u + v\,ctg\,\theta) \end{vmatrix}$$

u, v -- velocity components in the direction r, θ, ρ -- pressure, ρ -- density, γ -- adiabatic exponent

$$a = \xi_t + \xi_r u + r^{-1}\xi_\theta v, \quad \xi_r = (F - G)^{-1},$$

$$\xi_t = -\frac{\partial\theta/\partial t + \xi(\partial F/\partial t - \partial G/\partial t)}{F - G}, \quad \xi_\theta = -\frac{\partial G/\partial\theta + \xi(\partial F/\partial\theta - \partial G/\partial\theta)}{F - G}$$

The precise solution to problems of the mathematical statement of the problem of steady state flow past a blunt body with a regressed shock wave, i.e., questions of the existence, singularity and continuous relationship with the boundary conditions, poses great difficulties because of the nonlinearity of the gasdynamic equations. Model problems which conserve the basic aspects of the studied problem are usually used for the qualitative examination

of questions of uniqueness and the continuous relationship with the boundary conditions. One can use plane, potential transonic currents, described in the plane of a hodograph by an equation of the Tricomi type (Chaplygin equation), as well as certain linear equations in the vertical plane of such models [18,4].

Let characteristics of the second and first families, which intersect at a point c (Fig. 1), correspondingly be drawn from points A of a shock wave and B of the contour of a body in which a flow is supersonic. Then the relationships in the region of the shock wave AD, the boundary condition on the part of the contour BE, and the conditions of symmetry on the part of the axis DE will uniquely determine the steady state solution to the system of gas-dynamic equations in the region of the shock layer DACBE and ensure a continuous relationship with the boundary conditions. For the existence of solutions with limited derivatives of the gas-dynamic parameters, it is sufficient that the body contour not have breaks in the subsonic flow region, and that the distribution of parameters of the advancing flow and the body contour in the supersonic flow region ensure the absence of boundary lines. It should be noted that the appearance of singularities with infinite derivatives in the isolated points on the sonic line does not disrupt the uniqueness of the problem (for example, when the sonic line leaves the point of inflection on the surface of the body or when the body is streamlined by a stream of sufficiently small cross section).

We finally note that positions closest to the axis of all the possible positions of points A and B (Fig. 1) are determined from the condition such that the characteristics AC and BC which originate from these points limit the minimum region of effect of the supersonic region of effect on the subsonic region.

We shall now assume that the vector x and the position F of the shock wave has been totally assigned at a moment of time t = 0

in a region of the shock layer $0 \le \xi \le 1, 0 \le \theta \le \theta_*$. Then, in order to determine the gas parameters in this region when t > 0, it is necessary to solve a mixed Cauchy problem for system (2) with initial data when t = 0 and boundary conditions on the contour of the body, the shock wave, and the axis of symmetry. In order that the unsteady problem be correctly stated, it is necessary to draw a boundary ray $\theta = \theta_k$ such that the velocity component v normal to the ray exceeds the local velocity of sound c everywhere on it.*

We insert a grid with nodes

$$t > 0, 0 \le \xi \le 1, \quad 0 \le \theta \le \theta_*$$

in the investigated region (t^n, ξ_m, θ_l). We designate (Fig. 2)

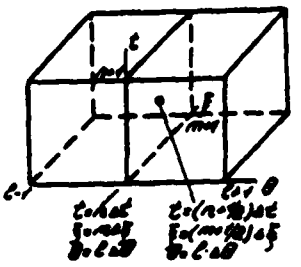

Fig. 2

$$t^n = t^{n-1} + \Delta t, \quad \xi_m = \xi_{m-1} + \Delta\xi,$$

$$\theta_l = \theta_{l-1} + \Delta\theta, \quad \xi_0 = \theta_0 = t_0 = 0,$$

$$\xi_M = 1, \quad \theta_L = \theta_*,$$

$$f(t^n, \xi_m, \theta_l) = f^n_{m,l},$$

$$n = 0, 1, 2, \ldots; \quad m = 0, 1, \ldots, M;$$

$$l = 0, 1, \ldots, L.$$

We replace derivatives in the points $(n+1/2, m+1/2, l)$ with the difference relationships according to the following formulas:

$$\left(\frac{\partial x}{\partial t}\right)^{n+\frac{1}{2}}_{m+\frac{1}{2},l} = \frac{1}{2\Delta t}\left(x^{n+1}_{m+1,l} - x^{n}_{m+1,l} + x^{n+1}_{m,l} - x^{n}_{m,l}\right) - \frac{\sigma}{4\Delta\theta}\left(x^{n}_{m+1/2,l+1} - 2x^{n}_{m+1/2,l} + x^{n}_{m+1/2,l-1}\right), \tag{1.3a}$$

$$\left(\frac{\partial x}{\partial \xi}\right)^{n+\frac{1}{2}}_{m+\frac{1}{2},l} = \frac{1}{2\Delta\xi}\left[\alpha\left(x^{n+1}_{m+1,l} - x^{n+1}_{m,l}\right) + \beta\left(x^{n}_{m+1,l} - x^{n}_{m,l}\right)\right], \tag{1.3b}$$

---

*Here, too, we note that, as the experience of calculations shows, in certain cases one can obtain a numerical solution to the problem without significant errors, and without satisfying the conditions v > c, when $\theta = \theta_k$, and even without drawing the boundary ray into the region of supersonic velocities. It is usually sufficient for this purpose that velocity on the boundary ray be a magnitude of precisely the same order as the speed of sound. Certainly, the question of the permissibility of drawing the boundary ray in the subsonic region requires an examination in each specific case. One of such cases is presented in Sec. 5.

$$\left(\frac{\partial X}{\partial \theta}\right)^{n+1/2}_{m+1/2,\ell} = \frac{1}{2\Delta\theta}\left[\alpha\left(X^{n+1}_{m+1/2,\ell+1} - X^{n+1}_{m+1/2,\ell-1}\right) + \beta\left(X^{n}_{m+1/2,\ell+1} - X^{n}_{m+1/2,\ell-1}\right)\right] . \qquad (1.3c)$$

The value of X in the point $(n+1/2,\ m+1/2,\ \ell)$ is defined as the mean arithmetical value of X in the four nearby nodes

$$(X)^{n+1/2}_{m+1/2,\ell} = \frac{1}{2}\left[X^{n+1}_{m+1/2,\ell} + X^{n}_{m+1/2,\ell}\right] . \qquad (1.3d)$$

In formulas (1.3)

$$x_{m+1/2,\ell} = \frac{1}{2}\left(x_{m+1,\ell} + x_{m,\ell}\right) .$$

The parameters of the difference system α, β satisfy condition $\alpha > 0,\ \beta > 0,\ \alpha + \beta = 1$; in most of the calculations that were made, it was assumed that $\alpha = 0.52,\ \beta = 0.48$.

The second term in (1.3a) is artificial viscosity of the difference system; the coefficient of artificial viscosity is $\sigma > 0$. In certain cases, it proves that one cannot obtain a numerical solution to the problem (see Sec. 4) without inserting artificial viscosity.

By substituting (1.3) and (1.2) for the point $(x^{n+1/2},\ \xi_{m+1/2},\ \theta_\ell)$ we proceed to the system of difference equations:

$$a^{n+1/2}_{m+1/2,\ell} X^{n+1}_{m+1,\ell} + b^{n+1/2}_{m+1/2,\ell} X^{n+1}_{m,\ell} = C^{n+1/2}_{m+1/2,\ell} , \qquad (1.4)$$

where

$$a = E + 2\alpha\tau_1 A , \quad b = E - 2\alpha\tau_1 A ,$$

$$c = -2\Delta t\Gamma + (E - 2\beta\tau_1 A)X^{n}_{m+1} + (E + 2\beta\tau_1 A)X^{n}_{m} - \qquad (1.5)$$

$$- \tau_1 B\left[\alpha\left(X^{n+1}_{\ell+1} - X^{n+1}_{\ell-1}\right) + \beta\left(X^{n}_{\ell+1} - X^{n}_{\ell-1}\right)\right] +$$

$$+ \sigma\tau_1\left(X^{n}_{\ell+1} - 2X^{n}_{\ell} + X^{n}_{\ell-1}\right) ,$$

$\tau_1 = \frac{\Delta t}{\Delta \xi}$, $\tau_2 = \frac{\Delta t}{\Delta \theta}$, E -- unit matrix.

During the subsequent presentation, as in (1.5), the obvious indices shall be omitted.

Thus, the boundary value problem for the system (1.2) pertains to a boundary value problem for the system of difference equations (1.4) with initial data when t = 0 and boundary conditions on the surface of the body and the shock wave.

It is evident from the structure of the system (1.3) that it is situated on (L + 1) independent subsystems. In this connection, it is sufficient to examine the solution to difference equations on the ray θ = const. Inasmuch as the coefficients of the equation depend upon values of the functions for "n" and "n+1" layers, in the process of solution one uses a method of iteration according to the following scheme: At the first iteration, during the determination of matrix elements a, b and column c, the values of all parameters are assumed to equal their values at the previous step. The obtained vector X^{n+1} is used for the subsequent iteration, etc.

The trial and error method is employed for solving the system of difference equations of each ray. In addition to (1.4), we shall examine the system

$$a \bar{X}_{m+1}^{n+1} + b \bar{X}_m^{n+1} = \bar{c} \quad , \tag{1.6}$$

which is obtained from (1.2) by means of discarding the last equation, and $x = [u, v, p]'$ (the stroke signifies transposition). The boundary condition on the body surface is presented in the form

$$\mu_0^{n+1} \bar{X}_0^{n+1} = g_0^{n+1} \quad , \tag{1.7}$$

where

$$\mu_0^{n+1} = [G^2 + (\partial G/\partial \theta)^2]^{-1/2} [G, -\partial G/\partial \theta, 0] \quad ,$$

$$g_0^{n+1} = [G^2 + (\partial G/\partial \theta)^2]^{-1/2} G \cdot (\partial G/\partial \xi) \quad .$$

One can obtain the recurrent formulas for calculating μ_m and $g_m\ (m=1,2,\ldots,M)$ in the following relationship, with the aid of (1.6) and (1.7):

$$\mu_m \tilde{x}_m = g_m \tag{1.7a}$$

These formulas have the form

$$\mu_{m+1} = \frac{\mu_m(\tilde{\delta}^{-1}\tilde{a})_{m+1/2}}{|\mu_m(\tilde{\delta}^{-1}\tilde{a})_{m+1/2}|}, \quad g_{m+1} = \frac{\mu_m(\tilde{\delta}^{-1}\tilde{c})_{m+1/2} - g_m}{|\mu_m(\tilde{\delta}^{-1}\tilde{a})_{m+1/2}|}. \tag{1.7b}$$

The conditions of conservation on the shock wave (for $t = t^{m+1}$, $\theta = \theta_\ell$) can be written in the form:

$$\begin{aligned}
&V_\tau - V_{\tau\infty} \\
&\rho(V_n - N) - \rho_\infty(V_{n\infty} - N) \\
&p - \rho(V_n - N)V_n = p_\infty + \rho_\infty(V_{n\infty} - N)V_{n\infty} \\
&\rho(V_n - N)\frac{V_n^2}{2} + \frac{\gamma}{\gamma-1}pV_n - \frac{1}{\gamma-1}pN = \\
&= \rho_\infty(V_{n\infty} - N)\frac{V_{n\infty}^2}{2} + \frac{\gamma}{\gamma-1}p_\infty V_{n\infty} - \frac{1}{\gamma-1}p_\infty N .
\end{aligned} \tag{1.8}$$

Here the indices $m+1$; ℓ are omitted everywhere; values with the index "∞" are determined by conditions in the free-stream flow and are considered known. N, V_n, V_τ -- respectively, velocity of the shock wave and the components of gas velocity that are normal and tangential to the shock wave; they are determined through the position of the shock wave and the velocity components u, v according to the formulas:

$$\begin{aligned}
N &= (F^2 + F_\theta^2)^{-1/2} F F_t , \\
V_n &= (F^2 + F_\theta^2)^{-1/2}(uF - vF_\theta) , \\
V_\tau &= (F^2 + F_\theta^2)^{-1/2}(uF_\theta + vF) .
\end{aligned} \tag{1.9}$$

If the values F, F_θ are considered to be known according to the previous iteration in equations (1.8), then (1.8) is a system of four equations relative to five unknowns u, v, ρ, p, F_ξ. The trial and error relationship

$$\mu_m \tilde{x}_m + g_m \tag{1.10}$$

when m = M closes the system of equations on the shock wave.

One can solve the system (1.8), (1.10), for example, by the Newton method. Having thereby determined the vector X_m^{n+1}, one can successively find X_m^{n+1} for m = M - 1, M - 2,.... 0, i.e., carry out an inverse trial and error run. For this purpose, one should use the system consisting of four equations obtained by means of a linear combination (1.4), (1.7 a). As a rule, a system consisting of the first, second and fourth equations of (1.4) and the trial and error relationship (1.7 a) was used.

Finally, the new position of the shock wave can be calculated according to the formula:

$$F^{n+1} = F^n + \frac{\Delta t}{2}(F_t^n + F_t^{n+1}) \quad . \tag{1.11}$$

Moving from layer to layer and determining the gas parameters for $t = 0, 1, \ldots, L$ for each of them, we find the vector X in the entire region of interest to us $t > 0,\ 0 < \xi < 1,\ 0 < \theta < \theta_*$.

The conditions of stability of the trial and error method impose limitations on the use of the method in the described form. One can derive the conditions of stability of the trial and error method and the establishment method similar to the way this was done in [2]. They have the form:

$$\xi_t + \xi_x u + \varepsilon^{-1}\xi_\theta v < 0 \tag{1.12}$$

$$\frac{\xi_t + \xi_x u + \varepsilon^{-1}\xi_\theta v}{\sqrt{\xi_x^2 + (\varepsilon^{-1}\xi_\theta)^2}} + c > 0 \quad . \tag{1.13}$$

Conditions (1.12) and (1.13) can be rewritten in a form which makes the kinematic meaning explicit. If $V_{\nu\xi}$ is the gas velocity component normal to the line ξ = const (equation 1.1)), and N_ξ is the rate of displacement of this line, then we have the following from (1.12) and (1.13):

$$V_{\nu\xi} < N_\xi \qquad (1.12a)$$

$$V_{\nu\xi} > N_\xi - c \qquad (1.13a)$$

In the case of a steady state flow $N_\xi = 0$; then it follows from (1.12a) that angle ω between the flow line and the line ξ = const should be positive, as in Fig. 3a; it follows from (1.13a) that the normal velocity $V_{\nu\xi}$ in this case should be less than the speed of sound with respect to its absolute value.

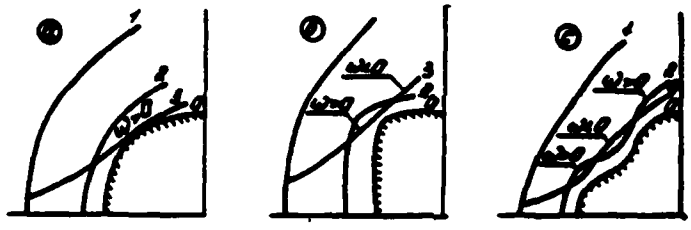

Fig. 3

0 - line $\xi = 0$, 1 - line $\xi = 1$, 2 - intermediate line ξ = const, 3 - flow line

The condition of stability (1.13 a) was always satisfied for all of the flows we calculated. With respect to condition (1.12a), in a number of cases it was violated. For example, in the case of flow past blunt bodies, it follows from (1.1) that the line ξ = const, drawn near the contour of the streamlined body, will trace the form of the latter; this cannot be stated about the flow line drawn near the contour, if the shape of the contour is insufficiently smooth. In these cases, condition (1.12a) will be violated; in the steady state flow in this case, there will be $\omega < 0$ at certain points, as in Fig. 3b,c.

The situation depicted in Fig. 3b existed when making the calculations described in Secs. 2 and 4. However, it proved that if condition (1.12a) is violated in a small number of grid nodes, then this does not have an effect on the convergence of the process of establishment and the accuracy of numerical solutions. However, in those cases when nonsatisfaction of condition (1.13) leads to the impossibility of obtaining a solution, one can use the system with recalculation developed in [5] or the system of two directions, which ensure stability of the inverse trial and error method.

The described algorithm of the numerical solution to gasdynamic equations was programmed on the computer. The program, devised at the Institute of Mechanics (subsequently, the IM program) was written for a differential grid with 11 x 21 points (11 in the ξ direction, 21 in the θ direction); the program written at the Computer Center (subsequently, the VTs program) was written for a grid with 9 x 17 points. The algorithms realized by the IM and VTs programs differ from each other in certain details as well as from that described above. For example, the VTs program selected values [illegible] and [illegible] as dependent variables in the gasdynamic equations, while the IM program directly used p and ρ. The singularity of the equations of gasdynamics on the axis of symmetry was revealed differently; derivatives according to θ on the boundary ray $\theta = \theta_k$, etc., were approximated according to different nonsymmetrical schemes.

We note that the VTs program made it possible to calculate the gas flow with the presence of equilibrium physico-chemical transformations, while the IM program was only developed for calculating flows of a perfect gas.

A check of the satisfaction of certain finite relationships which identically follow from the system of gasdynamic equations was provided for controlling accuracy of the obtained numerical solutions in the written programs. But these finite relationships

do not follow from the approximating system of difference equations, namely the Bernoulli equation, conditions of constancy of the entropy function [illegible] along the streamline (specifically, along the streamlined surface), as well as conditions of flow conservation in the investigated region of the shock layer. The accuracy of the numerical solution to the specific problems we have examined will be stated in the appropriate sections.

Section 2. Flow past a sphere and cylinder with a flat leading part

The calculations of flow past a sphere were made with M_∞ numbers of the free-stream flow [illegible]. The numerical solutions for the sphere are distinguished by high accuracy. For example, when $M_\infty = 4$ in a point of the outer ray lying on the surface of the body [illegible], the Bernoulli equation is satisfied with an accuracy of [illegible], and the condition of entropy constancy is satisfied with an accuracy of [illegible] (with calculations made according to the IM program). One notes good correspondence of the obtained results with the data of other numerical methods, specifically, G. F. Telenin [18].

One should, however, make one remark on the subject of comparing the numerical solutions obtained by the two methods with small M_∞. The results of calculations of flow past a sphere when $M_\infty < 2$ made by the G. F. Telenin method were presented in [16]. It was concluded on the basis of analyzing the numerical data when $M_\infty = 1.2$ in [16] that the angle δ between the shock wave and the sonic line is approximately 90°, and that, consequently, when $M_\infty \leqslant 1.2$ the characteristic bounding the minimum region of effect in the shock layer proceeds from the sonic point on the shock wave. The positions of the sonic points in the vicinity of the shock wave when $M_\infty = 1.2$, calculated by the establishment method, coincide with the corresponding positions in the calculation made according to the G. F. Telenin method with an accuracy of several percentages.

However, differences in the size of the angle δ proved to be greater, inasmuch as the latter is obtained during numerical differentiation of equations of the sonic line and the shock wave. One obtains $\delta < 90^\circ$ in the calculation made by the establishment method. We note that V. V. Rusanov recently demonstrated analytically that during the axisymmetrical flow past bodies when $M_\infty > 1$, angle δ is always less than 90° (with certain entirely natural assumptions made about the shape of the regressed shock wave).

It should be noted that differences in the results of calculating flow past a sphere when $M_\infty = 1.2$ by the two methods exist only in a small region of the shock layer near the shock wave and at a great distance from the axis. Outside this region, when $M_\infty = 1.2$, as well as throughout the entire shock layer when $M_\infty > 1.2$, the numerical solutions obtained by the establishment and G. F. Telenin methods coincide with good accuracy.

Detailed information is given in [6] about the results of calculations of flow past a sphere by equilibrium air when $2 \leq M_\infty \leq \infty$, made by the establishment method. We note here that the equilibrium physico-chemical transformations have a weak effect on the distribution of pressure in the shock layer, in comparison with the case of the perfect gas. A different picture is observed with respect to the other gasdynamic values, primarily density. With hypersonic velocities in the free-stream flow, the magnitude of density in the shock layer can be more than two times greater than the corresponding density value during flow by a perfect gas. The equilibrium dissociation and ionization have an effect as well on the qualitative picture of density distribution in the shock layer. Thus, when a perfect gas with $M_\infty = \infty$ flows past bodies, density ρ_w directly behind the shock wave is constant and is $(\gamma+1)/(\gamma-1)\rho_\infty$. The distributions of density through the shock wave during the flow of equilibrium air around a sphere depending on the angle θ with hypersonic M_∞ are plotted in Fig. 4. The characteristic points of these curves (the extremum, the inflection) correspond to the cessation or initiation of any particular equilibrium processes with the

change in temperature and pressure behind the shock wave (both of these values diminish monotonically with the increase in angle θ). Thus, the inflection points on curves for $M_\infty = 20$ and 25 correspond to conditions under which atmospheric oxygen is practically totally dissociated, and the dissociation of nitrogen has still not started. The maximum point on the curve for $M_\infty = 60$ when $\theta \sim 90^\circ$ corresponds to conditions under which both oxygen and nitrogen are totally dissociated, but the ionization of the atoms has still not begun; the other extremums on this curve are due to the occurrence of ionization of nitrogen and oxygen atoms.

We note that the calculations of flow past a sphere, whose results are given in Fig. 4, were made by the establishment method according to the VTs program up to $\theta = 66^\circ$, while the purely supersonic flow when $\theta > 66^\circ$ was calculated by the method of grids [1].

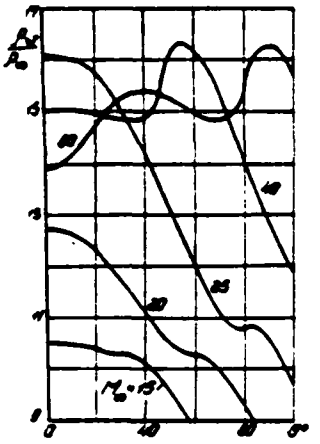

Fig. 4

Calculations of flow around cylinders with a flat leading part and circular edges were made according to the IM program (11 x 21 points) with ratios R/d = 0.4, 0.3, 0.2 and 0.1 (R - rounding radius, d - one-half the middle diameter). The geometrical picture of their flow when $M_\infty = 3$ is shown in Fig. 5. The pole of the polar coordinate system (r, θ) was located a distance d from the critical point. When R/d = 0.2 and the position of the outer ray $\theta_k = 0.835$ at a point on the surface of the body $\xi = 0$, $\theta = \theta_k$, the accuracy of satisfying the Bernoulli integral is $\Delta\delta = 1\%$ and the conditions of entropy constancy $\Delta J = 2\%$. In this case, the normal velocity component v to the ray is greater than the local speed of sound c throughout the entire shock layer on the ray $\theta = \theta_k$. Calculation was also made with the outer ray passing through a point c of conjugation of rounding with the cylinder ($\theta_k = 0.8955$). In this calculation, when $\Delta\delta = 14\%$ However, in this case, pressure on the body surface is calculated sufficiently accurately, while the high magnitude of errors $\Delta J = 20\%$

and Δ_3 is chiefly due to inaccuracy in determining density and velocity. This is confirmed by comparison with the calculation of supersonic flow on the curve made by the method [1], which was made by V. I. Uskov from our initial data when $\theta = 0.835$.

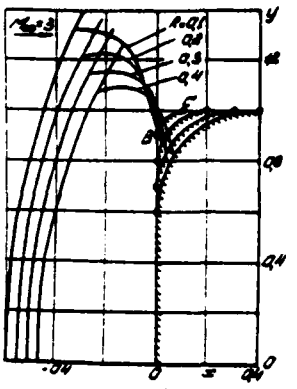

Fig. 5

When $R/d = 0.1$, the accuracy of solution in a point $\xi = 0$, $\theta = \theta_k$ is not high: when $\theta_k = 0.8125$ $\Delta_6 \sim 2\%$, $\Delta_3 \sim 7\%$, when $\theta_k = 0.8313$ (the outer ray passes through c), $\Delta_6 \sim 10\%$, $\Delta_3 \sim 33\%$. We note that even when $\theta_k = 0.8313$ in certain points on the ray $\theta = \theta_k$ comprising velocities $v < c$. One can obviously obtain a solution with $v > c$ when $\theta = \theta_k$ with significantly higher accuracy by shifting the poles of the coordinate system closer to the critical point and by drawing the outer ray through the point on the body where velocity slightly exceeds sonic velocity (we note that with small R/d, the sonic point on the body is very close to point B of conjugation of the flat leading part with the rounding).

We also note that the accuracy of the numerical solution in the point $\xi = 0$, $\theta = \theta_k$ is the worst; outside its small vicinity (a radius on the order of 2-3 steps of the differential grid), error Δ_6 was no more than 1% in all calculated variations.

The distributions of pressure p related to pressure in the critical point p_0, along the surface of the examined bodies, are plotted in Fig. 6 depending on the ordinate y. The distribution p/p_0 along the surface of the cylinder with a flat leading part and a point of inflection (R/d = 0) calculated by the G. F. Telenin method with the identification of a singularity in the point of inflection with the aid of the asymptotic solution [22] is also given here. The points in Fig. 6 plot Yu. Ya. Karpeyskiy's experimental data, which

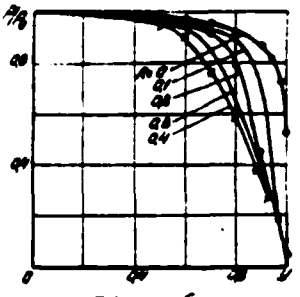

Fig. 6

coincide well with the calculation results.

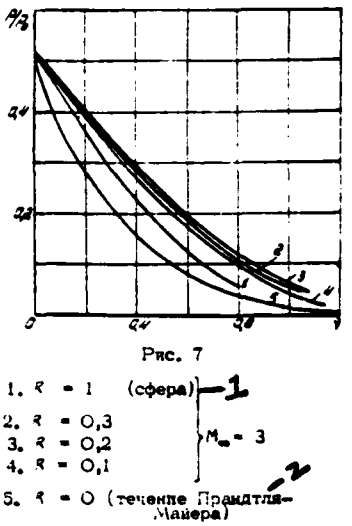

Рис. 7

Fig. 7

1 - sphere; 2 - Prandtl-Meyer flow

We note that such values that characterize the flow as a whole as the regression of the shock wave on the axis of symmetry, the velocity gradient in the critical point, and certain others change with the change in the rounding radius from R/d = 1 (sphere) to R/d = 0 (disc) approximately linearly. At precisely the same time, the local flow properties on the rounded edge can change extremely sharply, particularly with small R/d. Figure 7 plots the p/p_0 distributions along the rounded surface of various radii depending on the angle of turn ν of the flow on the rounded edge ($\nu = 0$ in the sonic point). When R/d = 0 in the inflection point (more accurately, in its infinitely small vicinity), a Prandtl-Mayer flow takes place which begins with M = 1 [22]. As is evident from the data of Fig. 7, the supersonic flow on the surface of a sphere (R/d = 1) is similar to a Prandtl-Meyer flow. However, with a decrease in the size of rounding, the difference between flow on the rounded edge and Prandtl-Mayer flow increases, and only with R/d ≈ 0.2 does flow on the rounded edge begin to tend toward the limiting case.

In conclusion, we shall illustrate the effect of the M_∞ number on flow around a cylinder with a flat leading part when R/d = 0.2 (Fig. 8).

Section 3. Flow around blunt bodies

Most of the data available in the literature on flow around blunt bodies relates to geometrical shapes in which curvature

of the surface is either constant (a sphere) or increases with distance from the critical point (for example, ellipsoids with a ratio of the vertical axis to the horizontal axis of $\delta > 1$, cylinders with a flat nose part, segmental bodies, etc.). This is because it is precisely such shapes which are favorable from the viewpoint of reducing aerodynamic heating of bodies streamlined by a supersonic gas flow. Together with this, the flow around bodies with reducing (beginning from the critical point) surface curvature can also be of known gasdynamic interest.

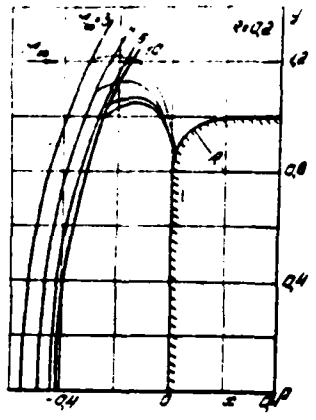

Fig. 8

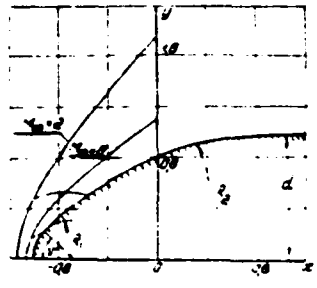

Fig. 9

Figure 9 gives the geometrical pictures of flow past a rotational body when $M_\infty = 2$ and 6. The contour of the rotational body consists of two conjugated arcs of circles. The radius R_1 of the circles which intersects the axis of symmetry ("of bluntness") is less than the radius of the second circles ("lateral surface"); the ratio $R_2:R_1 = 8.5$. The angle φ, comprised by the axis of symmetry and the line which connects the conjugation point with the center of bluntness is greater than the angle θ_* of the sonic point on the surface of a sphere streamlined by a flow with $M_\infty = 6$. Therefore, when $M_\infty = 6$, the lateral surface has no effect on flow around the blunt part; the region of the shock wave ahead of the blunt point, the sonic line in the shock layer coincide with the corresponding lines during flow around a sphere. The pressure distributions on the surface of a sphere with a radius R_1 (dash line) and the examined body are plotted in Fig. 10. It is evident from this graph how acceleration of the gas flow decreases on the surface of a complex body behind the point of conjugation.

When $M_\infty = 2$, the angle $\varphi < \theta_*$; in this case, flow around a blunt body is affected by the shape of the lateral surface. As

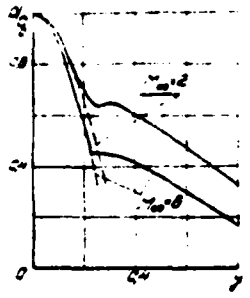

Fig. 10

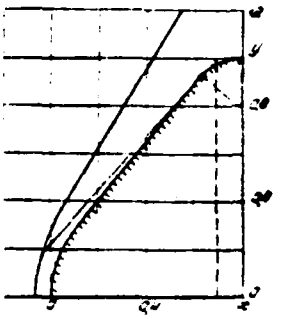

Fig. 11

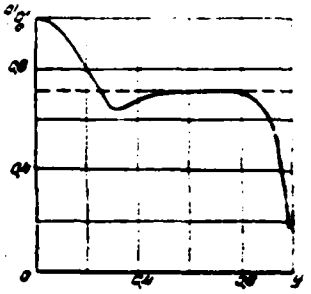

Fig. 12

is evident from Fig. 10, pressure differences on the sphere and on blunting of a complex body only become noticeable in the vicinity of the conjugate point. The gas slows in this region of the body; at a certain distance from the conjugate point, the acceleration of the gas again begins, but occurs significantly more slowly than against the blunt part of the body. In accordance with this, the sonic line is displaced significantly higher during flow around a complex body than in the case of the sphere.

Flow around a blunt cone of finite length with a large expansion angle when $M_\infty = 6$ was also calculated by the establishment method according to the VTs program. The radius of spherical blunting was taken to be $R/d = 0.45$, while the angle of inclination of the conical surface to the axis of symmetry was $\theta_c = 51^\circ$. The examined body had a slight rounding in the region of the middle in the form of a circumferential arc with a radius $r/d = 0.2$, conjugated with a conical surface. We note that the angle $\theta_c = 51^\circ$ is less than the maximum angle for flow around a sharp cone by a flow with $M_\infty = 6$, although it was similar to it. We note further that the angular coordinate of the sonic point on a sphere streamlined by a flow with $M_\infty = 6$, $\theta_c > 30^\circ - \theta_c = 39^\circ$; thus, the lateral surface affects flow around a blunt body.

Figures 11 and 12 show the geometrical picture of flow around a cone and the distribution of pressure on the surface. We note the presence of a point of inflection on the shock wave and the fact that the sonic line, running practically from the conjugate

point of the conical surface with rounding nearly "spreads out" along the body over its entire course. The distribution of pressure in the vicinity of conjugation of the cone with the spherical blunting is "spoon shaped"; similar behavior of pressure in this region is also characteristic for the flow around cones with small expansion angles, when flow in this region is supersonic [6]. Pressure on the surface of a cone with $0.55 \leq y \leq 0.75$ is nearly constant and is similar to pressure on the surface of a sharp cone with precisely the same angle θ_c. However, other gasdynamic parameters significantly differ from the corresponding values on the surface of the sharp cone. Thus, when a sharp cone is streamlined, the local Mach number in the examined case is $M = 1.25$; in the case of a blunt cone, a subsonic value with $M = 0.7$ corresponds to precisely the same surface pressure value.

The examples examined above show that the presence of regions where a flow of gas with negative acceleration occurs is possible on the surface of bodies whose curvature increases, beginning with the critical point. This effect appears significantly more sharply when there is flow around bodies whose curvature changes sign; this question is examined in the next section.

Section 4. Flow around convexo-concave bodies

We shall examine a family of bodies with the equation of the contour generatrix (in the polar system of coordinates in the meridional plane)

$$G(\theta) = 1 - m\sin^2 2\theta \quad . \tag{4.1}$$

When $m = 0$, a body with a contour (4.1) is a sphere with a unit radius; when $m > 0$, the examined body has a depression whose maximum depth is achieved when $\theta = 45^\circ$ and is determined by the parameter m. Parameter K characterizes curvature of the depression.

The establishment method was used to make calculations of flow around bodies (4.1) by a perfect gas ($\gamma = 1.4$) and equilibrium

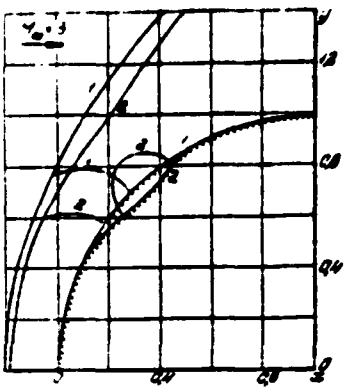

Fig. 13

1. Sphere $\begin{matrix} m=0 \\ k=8 \end{matrix}$; 2. $m = 0.08$.

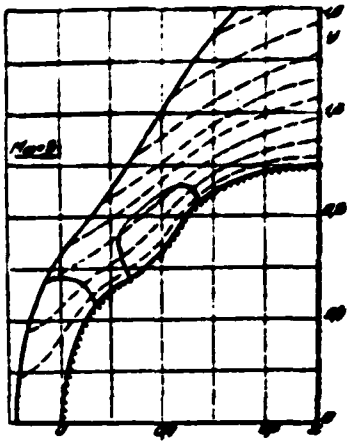

Fig. 14

$m = 0.1$, $k = 8$

air in the range of change of parameters which determine the body shape: $0 \leq m \leq 0.2$, $2 \leq k \leq 8$. Calculations were made according to the IM program for $3 \leq M_\infty \leq 6$ with position of the outer ray $\theta_k = 90^\circ$, and according to the VTs program for $6 \leq M_\infty \leq 20$ when $\theta_k = 90^\circ$ and 70°. When $M_\infty = 6$, a comparison of results obtained according to the two different programs was made; these results coincided.

Figure 13 compares the geometrical pictures of flow past a sphere and a body with a slight depression ($m = 0.05$) when $M_\infty = 3$. As is evident, even a slight change in the shape of the body causes a noticeable change in the picture of flow in the shock layer. Gas accelerates more rapidly on the lower part of a body with a depression, where the inclination of the contour to the axis decreases more rapidly than in a sphere and the gas accelerates more rapidly than on a sphere. This is due to lowering of the sonic line in the shock layer ahead of the body with a depression, in comparison with the sonic line position in the sphere. The change in the sign of surface curvature on the body depression (4.1) leads to gas deceleration in this region and to the appearance of a local zone of subsonic flow which "lies" in the depression. With a repeated change in the sign of curvature of the surface, the velocity of the gas again reaches supersonic values and subsequent gas expansion occurs approximately as on a sphere. The described flow characteristics due to the double change in the sign of surface curvature, extend through the

shock layer and lead to the appearance of two inflection points on the regressed shock wave, which are distinguishable in Fig. 13. We also note that the thickness of the shock layer during the transition from the sphere to the body with the depression decreases.

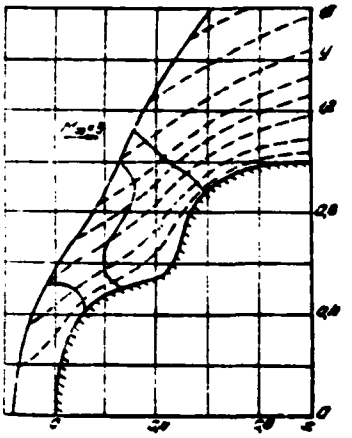

Fig. 15

Figures 14 and 15 show more detailed pictures of flow in bodies with depression m = 0.1 and m = 0.2 (when M_∞ = 3). Shock waves, sonic lines and (dash line) streamlines are plotted here. The deepening of the depression leads (Figs. 13-15) to a certain decrease in the thickness of the shock layer in the region of subsonic and transonic flow and to a sharper curvature of the shock wave (the inflection points on the shock wave are the more clearly pronounced, the deeper the depression), and to an increase in the dimensions of the local zone of subsonic flow in the depression both in absolute units, and relative to the thickness of the shock layer. When m = 0.2, the inflection of the shock wave is so strong that a local subsonic zone forms on the wave which connects with the region of subsonic flow lying in the depression (Fig. 15).

Deceleration of the gas to subsonic velocities during flow around the depression can lead to the appearance of suspended shock waves in the shock layer and the triple points on the shock wave. The programs that were written do not provide for the explicit identification of characteristics of this type, and therefore the suspended shock waves which arose will be "blurred" by the difference scheme.

Figure 16 compares the geometrical pictures of flow around a body with a depression k = 8, m = 0.1 when M_∞ = 3, 4, 6 and 20. We note that the position of the shock wave changes strongly with the change in M_∞ from 3 to 6, and slightly with the change in M_∞ from 6 to 20. When M_∞ increases, the sonic line is displaced to the axis of symmetry -- slightly on the surface of the body, and

quite strongly on the shock waves. The dimensions of the local zone of subsonic flow in the depression decrease with the increase in M_∞.

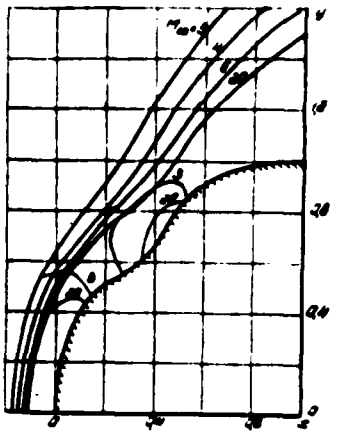

Fig. 16
$m = 0.1$; $k = 8$

Figure 17 gives a comparison of the picture of flow around bodies with m = 0 (sphere), m = 0.1, and 0.2 when k = 8, when $M_\infty = 6$. The picture of flow in the shock layer with deepening of the depression changes when $M_\infty = 6$ in precisely the same way as when $M_\infty = 3$. We note that unlike the case of $M_\infty = 3$, the local zone of subsonic flow in the depression occupies only a part of the shock layer, without reaching the shock wave.

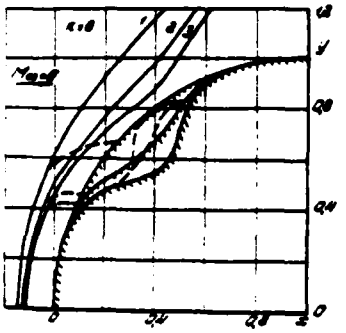

Fig. 17
1. $m = 0$; 2. $m = 0.1$; 3. $m = 0.2$

The regressed shock waves in bodies which have an identical depression depth (m = 0.2), but different depression curvature (for values of the parameter K = 8, 4, 2) are plotted in Fig. 18 (for $M_\infty = 6$). The shock wave approaches the body with the decrease in depression curvature and the shock waves which correspond to bodies with different values of the parameter K can be considered approximately, geometrically similar. We also note that the boundaries of the local subsonic zone in the depression depend weakly on curvature K, while the transverse dimension of this zone significantly increases with the increase in K.

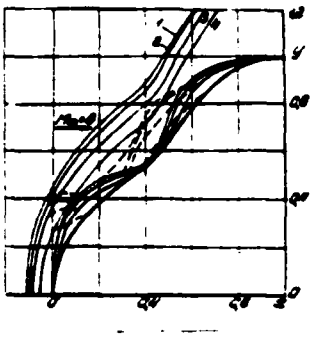

$m = 0.2$

1. K = 8
2. K = 8
3. K = 4
4. K = 2

Fig. 18

We shall dwell on the distribution characteristics of pressure through bodies with a contour (4.1). The distributions of pressure p/p_0 along the surface, depending on the angular coordinate θ, are plotted in Figs. 19 and 20. The characteristic feature of these

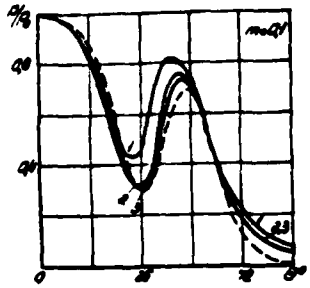

Fig. 19

—— calculation by the establishment method /1. $M_\infty = 3$; 2. $M_\infty = 6$; 3. $M_\infty = 20$/;

---- Newtonian theory

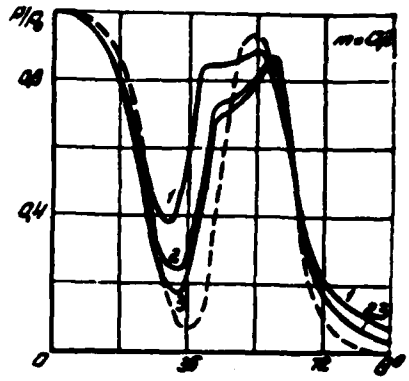

Fig. 20

—— calculation by the establishment method /1. $M_\infty = 3$; 2. $M_\infty = 6$; 3. $M_\infty = 20$/

---- Newtonian theory

distributions is their nonmonotonic character. The increase in pressure in the region $30° \leq \theta \leq 55°$ corresponds to deceleration of gas on part of the surface having negative curvature. The value of the minimum in pressure distribution decreases with the increase in depth or curvature of the depression, while the value of the maximum increases. The maximum value of pressure in the depression differs from pressure in the critical point by only about 10% for a body with the deepest and steepest of the examined depressions ($m = 0.2$, $K = 8$). We note the presence of a small "gap" in the distribution of pressure immediately before pressure reaches the local maximum for this same body. A similar effect was obtained during the calculations of flow around bodies with a complex shape by the S. K. Godunov method in a work [23].

The effect of the M_∞ number on the pressure distribution along the surface is manifested in a decrease in the value of the local pressure minimum. With respect to the local maximum, then for the case $m = 0.1$, its value noticeably decreases, but for the deeper depression $m = 0.2$, it remains approximately constant. The positions of both the minimum and the maximum of pressure for both depressions shift toward the middle with an increase in M_∞.

The calculated distributions of pressure along the body are compared with pressure according to the modified Newton formula in Figs. 19 and 20.

$$p/p_\infty = \sin^2\beta \qquad (4.2)$$

The Newton formula describes the actual distribution of pressure along the body at hypersonic M_∞, particularly when $m = 0.1$, well.

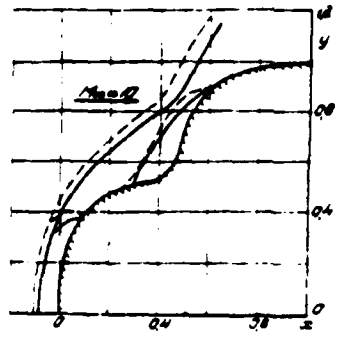

$m = 0.2$; $K = 8$.

Fig. 21

$m = 0.2$; $K = 8$

--- flow-around by a perfect gas ($\gamma = 1.4$);

___ flow-around by equilibrium air ($p_\infty = 0.1$ atm, $T_\infty = 250°$K).

The effect of equilibrium, physico-chemical transformations in the shock layer on the picture of flow-past, is shown by Fig. 21. It appears precisely the same as in the case of flow around convex bodies, and no new qualitative characteristics arise here. We note that the size of the local zone of subsonic flow in the depression also decreases with the decrease in thickness of the shock layer caused by the effect of the real gas. A comparison of the results of calculating flow around bodies (4.1) by equilibrium air and a perfect gas with a specially selected adiabatic exponent shows that the method of approximately calculating the real properties of air during the flow around the facing surfaces of bodies, developed in [17], is also justified for the case of complexly shaped bodies (4.1).

We shall now dwell on the methodological characteristics of the numerical solution to the problem of flow around convexo-concave bodies. A significant aspect here is that one cannot obtain a numerical solution for flow around bodies with a significant depression depth (namely, when $m > 0.05$) without introducing artificial viscosity into the difference scheme (1.3).

When making calculations of the flow past bodies whose curvature does not change sign (Secs. 2 and 3), it was unnecessary to

resort to artificial viscosity and the coefficient σ in (1.3a) was assumed to equal zero. On the other hand, during calculations of the flow around bodies with depressions when $\sigma = 0$, the establishment process diverges. With a certain minimum value $\sigma = \sigma_{min} > 0$ one can obtain a steady state solution, but the distributions of the gasdynamic parameters in the region of the depression will have a sawtoothed character. With a certain $\sigma > \sigma_{min}$, one can smooth these distributions. The results of calculations made in this section (Figs. 13-21) were obtained with values of the artificial viscosity coefficient $\sigma = \sigma_*$. The value of σ increases with the increase in M_∞; when $M_\infty = 3$, $\sigma = 0.25$, when $M_\infty = 8$ $\sigma = 0.5$.

Most of the calculations were made with several values of the parameter σ in order to identify the relationship between the numerical solutions and this value. It proved that the value of σ exerts a noticeable effect on the values of the gasdynamic values, which determine flow in the depression. Thus, the local minimum in the pressure distribution along the body (Figs. 19 and 20) decreases with the increase in σ, while the local maximum drops. The accuracy of making these checks in the region which corresponds to a depression in the body deteriorates with the increase in σ. However, the change in σ within quite broad limits (for example, from 0.25 to 1 when $M_\infty = 3$) has no noticeable effect on the numerical solution outside the depression of the body in precisely the same way as it does on accuracy of making the checks.

With a value $\sigma = \sigma_*$, the accuracy with which the Bernoulli integral is satisfied in the region of the body depression and the condition of entropy constancy comprises approximately 2-4 % when $m = 0.1$, and approximately 5-8 % when $m = 0.2$. In the remainder of the shock layer, the accuracy of making checks is higher and comprises approximately 1-2 %. These data pertain to calculations made on a grid with 11 x 21 points when $\theta_k = 90^\circ$; the accuracy of calculations made on a 9 x 17 grid when $\theta_k = 70^\circ$ is approximately the same. The accuracy of calculations made on the 9 x 17 grid when $\theta_k = 90^\circ$ is somewhat lower.

In conclusion, one should note that the effect of viscosity, as a rule, can be taken into account well within the frameworks of boundary layer theory for convex bodies whose contour curvature does not change sign. Therefore, the calculations made on the basis of the model of a nonviscous gas give the correct pressure distributions on the surface of the streamlined body, as well as the correct values of the other gasdynamic parameters in the entire field behind the closed boundary layer zone. In the examined case of convexo-concave bodies, high positive pressure gradients on the surface, as in Figs. 19 and 20, can lead to boundary layer separation and gas flow in the depression will be significantly viscous. This is specifically indicated by comparing the calculation and experimental data on the flow around convexo-concave bodies in [23]. Therefore, the results of solving the problem of flow around bodies of such shape, evidently, should be viewed as the first approximation to the real case.

Section 5. Nonequilibrium gas flows around surfaces

In works [8-11], the establishment method was applied to calculating the flow around spherical surfaces of varying radii and, specifically, around a plane surface by supersonic, nonequilibrium gas flows. Calculations were made according to the IM program (11 x 21 points).

In [8-10], the investigation was made for free-stream flows which are nonuniform with respect to value and direction; cases of flow engendered by the supersonic spatial source, and a stream flowing in a vacuum from an axisymmetrical nozzle, are examined.

The flow of a compressed gas from a spatial source exists outside a sphere with a radius R_*, in which the velocity of the flow is equal to the velocity of sound. The Mach number M at a distance r from the center of the source can be determined from the equation

$$\left(\frac{R_*}{r}\right)^2 \cdot M\left(\frac{\gamma+1}{2+M^2(\gamma-1)}\right)^{(\gamma+1)/2(\gamma-1)} \qquad (5.1)$$

With hypersonic M , i.e., at great distances from the source, one can use the approximate formula

$$M \approx \left(\frac{\gamma+1}{\gamma-1}\right)^{(\gamma-1)/2} \left(\frac{x}{R_*}\right)^{\gamma-1} \qquad (5.2)$$

The velocity, density and pressure are determined according to the known M with the aid of the formula of the isentropic flow.

The parameters of the gas in the supersonic, freely expanding stream were taken from calculations made by the grid method [15] and the method of characteristics [20]. We note that the flow in such a stream at great distances from the nozzle has the following properties [20]: the flow lines are similar to straight lines, while the distributions of parameters along them satisfy the source law (5.1) or (5.2) with good accuracy; the center of the source is located in the nozzle cross section. However, the radius of the equivalent source R_* changes with the transition from one stream line to the other. In this case, the radius R_* changes weakly in the region which encompasses the axis of symmetry and is bounded by a certain characteristic surface $y = y_*(x)$ (Fig. 22). Intensive gas expansion occurs in the indicated region in the centered rarefaction wave, proceeding from the edge of the nozzle; a sharp decrease in the value of R_* corresponds to it.

Figure 22 plots the geometrical picture of flow around a flat wall by a stream flowing from a nozzle with a uniform flow at the outlet and a Mach number $M_\alpha = 2.5$; the wall is located a distance of 50 r_α from the cross section of the nozzle (r_α is the nozzle radius). In Fig. 22, the dash line plots the picture of flow around a plane by a flow from a source whose radius R_* is equal to the radius of the equivalent source R_* for flow on the stream axis ($R_*/R_\alpha = 0.8$). In the region between the axis and the characteristic $y_*(x)$, the shock waves for both flows around the object differ little from each other. Deviations in the field of the gasdynamic values in the shock layer are somewhat greater, which can be seen by comparing the positions of the sonic lines; to the point, dimensions of

the subsonic regions in both places are approximately equal.

Differences between the two flows around objects become significant about the characteristic $y_*(x)$. In the case of the source, the velocity of the gas behind the shock wave monotonically increases with distance from the axis. In the case of the stream, a sharp decrease in pressure and density in the rarefaction wave above $y_*(x)$ leads to the intensive deviation of the shock wave toward the nozzle and to an increase in the angle between the shock wave and the direction of the free-stream flow.

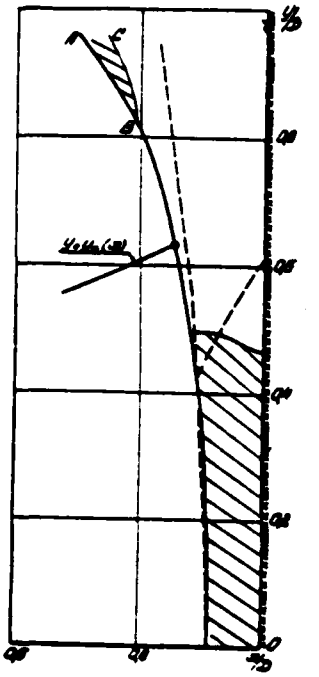

Fig. 22
—— streamline flow
--- stream flow from source

Because of this, velocity behind the shock wave once again begins to decrease and reaches the subsonic values; in this case, a second subsonic zone adjacent to the shock wave (region ABC in Fig. 22) forms in the shock layer.

The presence of this region has no effect on the solution in the subsonic and transonic regions of the shock layer which surround the axis of symmetry. However, when the M_α number increases (or with the increase in γ), the second sonic point B rapidly descends along the shock wave and with a certain value of M_α, one has a closure of the two subsonic regions. A narrow zone of subsonic flow forms in the shock layer, extending along the shock wave.

It was stated in Sec. 1 that the correct statement of the problem of flow around a body with a regressed shock wave on a line which limits the calculated region of flow from above requires that the normal component of gas velocity to this line should exceed the velocity of sound. Unsuccessful efforts were made to obtain a numerical solution with such a property to the problem of flow around

a flat wall by a stream in the examined case. The velocity was subsonic in the calculations that were made in a certain part of the boundary line. Naturally, the question of the validity of such calculations arises.

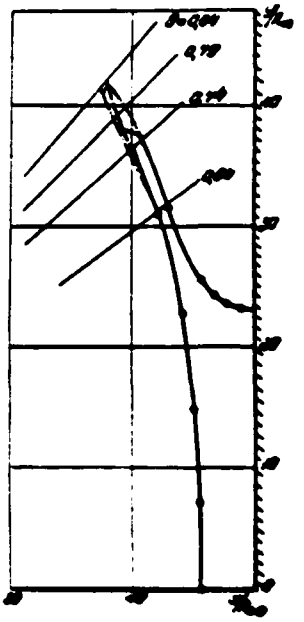

Fig. 23

In order to prove that the solutions obtained in this case correspond to reality, the following numerical experiment was performed. Flow around a plane by a flow from a source whose radius changed depending on angle θ according to an assigned law was calculated. In this case, the flow field was similar to flow in a stream when $M_\alpha = 2.65$. The calculation was made in the spherical coordinate system with its center in the center of the source with positions of the outer ray $\theta_k = 0.64$ and 0.74. The fields of flow in the boundary layer coincided with high accuracy for both cases (Fig. 23). Attempts to obtain a numerical solution when $\theta_k > 0.74$ were unsuccessful.

Calculation was further made for a case when the radius of the source remained constant, beginning with a certain value $\theta = \theta_{const}$. In the calculations, it was assumed that $\theta_{const} = 0.74$ and 0.79 when $\theta_k = 0.84$. In the free-stream flow when $\theta > \theta_{const}$, the intensive expansion of gas ceases and the factors which cause the shock wave to deviate sharply toward the nozzle disappear. Velocity behind the shock wave rapidly reaches supersonic values and the outer ray θ_k wholly lies within the supersonic region.

By comparing the geometrical pictures of flow around a plane in Fig. 23 for all three cases ($\theta_k = 0.74$; $\theta_k = 0.84$; $\theta_{const} = 0.74$; $\theta_k = 0.84$; $\theta_{const} = 0.79$) one can see that up to $\theta = \theta_{const}$, shock waves and the sonic line do not practically differ from each other, and they diverge significantly only when $\theta > \theta_{const}$.

Consequently, the perturbations introduced above into the flow $\theta = \theta_{const}$ are practically not transmitted to the subsonic region. This fact can be explained because, although the velocities are subsonic in a certain region of the boundary line, they are still comparable in value to the speed of sound. Because of this, information through the subsonic corridor adjacent to the shock wave is not practically transmitted upstream. Thus, one can obtain a solution which corresponds to reality without introducing the outer ray into the region of supersonic velocities.

However, such resistance to perturbations does not exist throughout the entire subsonic "corridor." Velocity in the shock wave, having reached a maximum, decreases; with distance from the region of highest velocities, the subsonic flow in the "corridor" becomes more and more sensitive to perturbations arriving from the stream boundary.

Thus, a certain region of high, subsonic velocities exists in the "corridor," weakly transmitting perturbations upstream. It is a unique analog of the supersonic region between two sonic points on the shock wave in the case of flow with two subsonic regions. We note here that a suspended shock wave forms in the stream flowing from the axisymmetrical nozzle into space with counterpressure; flow in the stream is precisely the same as with flow in a vacuum in the region between this wave and the axis. If a flat obstacle is placed in such a stream, then the suspended shock wave can intersect the regressed shock wave before the obstacle at the point where velocity behind the regressed wave is subsonic. Nevertheless, on the basis of the conducted investigations, one can assert that the perturbations introduced by the suspended shock wave have practically no effect on flow in a significant part of the shock layer ahead of the obstacle.

Figures 24 and 25 compare the results of calculating the plane of the stream with the data of experiment [24]. These data pertain to the case of a stream of air ($\gamma = 1.4$), flowing from a nozzle with

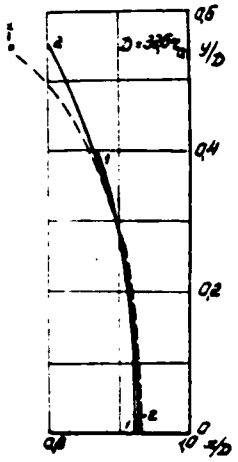

Fig. 24

1. Calculation when $\phi = 0$;
2. calculation when $\phi = 15^{\circ}$;
--- experiment [24]

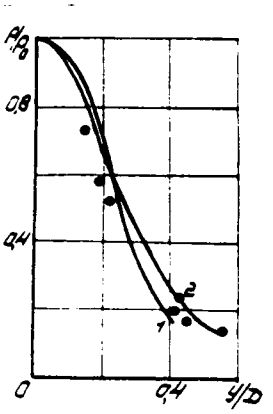

Fig. 25

1. Calculation when $\phi = 0$;
2. calculation when $\phi = 15^{\circ}$;
o - experiment [24]

a Mach number on the section $M_{\alpha} = 5$ for a pressure drop in the nozzle receiver and the surrounding space $p_1/p_1 = 10^4$ (thence $p_0/p_1 = 0.2 \cdot 10^4$). The position of the regressed shock wave ahead of the flat wall located a distance $D = 32.6\ r_{\alpha}$ from the nozzle cross section obtained in the experiment, is plotted by the dash line in Fig. 24. Here, too, the x's mark points of intersection of the regressed wave before the wall with a suspended wave in the stream and a stream boundary. In [24], there are no indications relative to the character of flow at the nozzle outlet (it is only stated that the stream flows from a long, isentropic nozzle). Therefore, the experimental data are compared with the calculation data for the case of a stream flowing from a nozzle with a uniform flow at the outlet ($\phi = 0$) and from a conical nozzle with a coning angle $\phi = 15^{\circ}$.

The experimental and calculated positions of the regressed wave coincide well at distances from the axis of symmetry of $y \leq 0.4D$. When $y > 0.4D$ in the experiment, one observes an extremely sharp deviation of the regressed shock wave toward the nozzle; the numerical solution when $y > 0.4\ D$ for a stream flowing from a nozzle with

$\phi = 0$ could not be obtained.

The coincidence of the calculation and experimental data on determining pressure on the flat wall (Fig. 25) is satisfactory. Checks of accuracy of the obtained solutions showed that the error in satisfying the Bernoulli equation [illegible] ; the scatter of values of the entropy function on different flow lines comprised 0.5 - 3%. The results pertained to the case of a stream; in the case of the source, errors [illegible] and [illegible] did not exceed 0.5%.

A work [11] examined flow around a sphere parallel but not equal in value to a supersonic flow, which can be viewed as two coaxial streams which have a transition zone between them. Calculations were made both for a case when velocity V_{∞_1} of the internal stream is greater than the velocity V_{∞_2} of the outside stream, and for the case when $V_{\infty_1} < V_{\infty_2}$. The transitional zone occupied a region [illegible] . The velocity profile V_∞ of the transition zone was assigned by the formula

$$\frac{V_{\infty_1} - V_\infty}{V_{\infty_1} - V_{\infty_2}} = \left[1 - \left(\frac{y - R_1}{h}\right)^{3/2}\right]^2 \quad \text{when} \quad V_{\infty_1} > V_{\infty_2} \tag{5.3}$$

$$\frac{V_{\infty_2} - V_\infty}{V_{\infty_2} - V_{\infty_1}} = \left[1 - \left(\frac{y - R_1}{h}\right)^{3/2}\right]^2 \quad \text{when} \quad V_{\infty_2} > V_{\infty_1} \tag{5.4}$$

Static pressure and total enthalpy throughout the entire flow were assumed to be constant.

The radius of the outside stream is considered to be sufficiently great such that the outer boundary of the stream has no effect on the calculated region of flow. Most calculations are made when $R_1 = 0.4$, $h = 0.2$.

The geometrical pictures of flow around a sphere by coaxial streams are plotted in Figs. 27 and 28. The Mach number of the internal stream in the cases $M_{\infty_1} = 3$ is presented in Figs. 26 and 27. In Fig. 26, velocity of the outside stream is less than that of the inside stream ($M_{\infty_2} = 2.5$ and 2), while Fig. 27 shows the

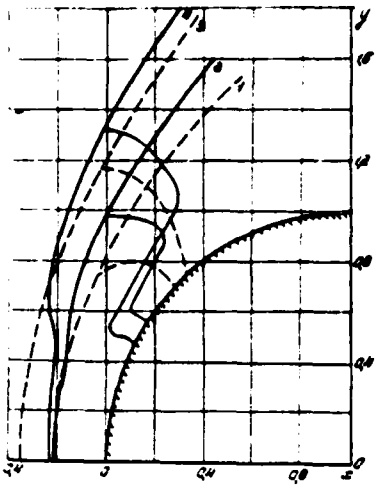

Fig. 26

1. M_∞ = 3, 2. $M_{\infty 1}$ = 3, $M_{\infty 2}$ = 2,5, 3. M_∞ = 2, 4. $M_{\infty 1}$ = 3, $M_{\infty 2}$ = 2,0

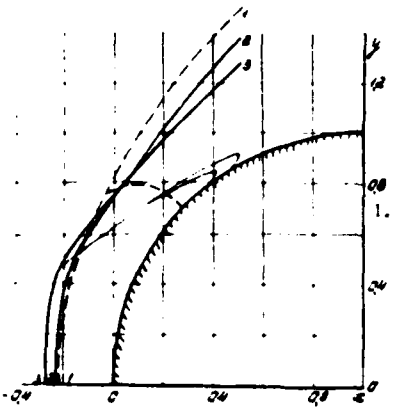

Fig. 27

1. M_∞ = 3, 2. $M_{\infty 1}$ = 3; M_∞ = 3,5, 3. $M_{\infty 1}$ = 3; $M_{\infty 2}$ = 4

reverse case ($M_{\infty 2}$ = 3.5 and 4). The examined flows are characterized by a more complex shape of the shock wave and the sonic line in comparison with the flow of a uniform flow around a sphere. We note that when $M_{\infty 2} < M_{\infty 1}$, one has a significant increase in part of the region of effect adjacent to the body, but when $M_{\infty 2} > M_{\infty 1}$, one has an increase in the part of the region of effect adjacent to the shock wave. A region of the shock wave which contains the inflection points corresponds to the transition zone in the free-stream flow (5.3).

The gas parameters behind the shock wave change very sharply here. Calculations show that when $M_{\infty 1}$ is small and $M_{\infty 2} > M_{\infty 1}$, one observes the appearance of a local supersonic zone in this region adjacent to the shock wave (for example, when $M_{\infty 1}$ = 1.3, $M_{\infty 2}$ = 1.5). When $M_{\infty 1}$ decreases, this zone blends with the basic supersonic region (for example, when $M_{\infty 1}$ = 1.1, $M_{\infty 2}$ = 1.5).

We note that regression of the shock wave from the sphere on the axis of symmetry during flow passed by coaxial streams with Mach numbers $M_{\infty 1}$ and $M_{\infty 2}$ increases in comparison with regression ahead of the sphere streamlined by a uniform flow with $M_\infty = M_{\infty 1}$

both with a decrease and an increase in M_{∞_2} by comparison with M_∞ (Figs. 26 and 27). The increase in M_{∞_2} in comparison with M_∞ leads to a decrease in pressure on the sphere and, on the contrary, a decrease in M_{∞_2} leads to an increase in pressure on the body.

In the calculations that were performed, the accuracy of satisfying the Bernoulli equation was, as a rule, .6-1.2% . The scatter of values of the entropy function on different flow lines was within limits of 0.5 - 4%. The accuracy of the calculations increases with the decrease in the difference of velocities of the internal and external streams with a fixed width of the transition zone. Accuracy also increases with the increase in the width of this zone with fixed stream velocities.

Section 6. Solving the direct problem for a Laval nozzle

The problem of flow in a Laval nozzle of assigned shape was solved in a work [7] with the aid of the establishment method.

Let $y = G(x)$ be the contour equation of the nozzle, and F be the length of the nozzle. We insert the normed variables

$$\xi = x/F \quad , \quad \eta = y/G(x) \quad . \tag{6.1}$$

The outlet cross section ($\xi = 1$) is arranged such that condition $u > c$ is satisfied everywhere on it; then when $\xi = 1$, one need not impose boundary conditions; relative to nozzle intake ($\xi = 0$), more shall be stated below. Let the initial condition of a gas be assigned at a moment $t = 0$. t_∞ signifies a finite moment of time and, consequently, the region of interest to us is such:

$$0 \leq t \leq t_\infty \quad , \quad 0 \leq \xi \leq 1, \; 0 \leq \eta \leq 1.$$

We shall briefly describe the algorithm of calculations with direct and inverse acceleration when solving a system of differential equations similar to (1.4). For the sake of simplicity, we shall assume that only one point ξ_k exists such that for all

$\xi_m < \xi_*$ $(m = 0,1,\ldots,k-1)$ inequality $u < c$ is satisfied. This ensures stability of trial run (Sec. 1), but when $\xi_m > \xi_*$, $u > c$. With the aid of an auxiliary difference scheme described in [5], we shall determine the values of the gasdynamic parameter u and π when $\xi = \xi_k$ on a time layer $t = t^{n+1}$. We shall write the trial and error relationship in the following form when $\xi = \xi_k$

$$(\mu_u)^{n+1}_{1,\ell}\, u + (\mu_\theta)^{n+1}_{1,\ell}\, \theta + (\mu_\pi)^{n+1}_{1,\ell}\, \pi + (g)^{n+1}_{1,\ell} \qquad (6.2)$$

(the index "1" pertains to line $r = r_1$). We shall assume $\mu_\theta = 0$, $\mu_u = -0.8$, $\mu_\pi = 0.8$; when $g = -0.8u + 0.8\pi$.

Further, with the aid of recurrent relationship similar to (1.7), we shall determine the trial and error coefficients when $m = k-1, k-2, \ldots 0$, i.e., we shall perfect the direct trial and error run in the direction toward the nozzle intake. Having determined the gasdynamic parameters when $m = 0$ (see below), we can successively find their values when $m = 1,2,\ldots, k$, i.e., complete the inverse trial run. When $m = k+1, k+2, \ldots M$, the inverse trial run is accomplished using only the system of difference equations similar to (1.4), without using the trial and error relationship.

Calculations are made for all θ_ℓ $(\ell = 0,1,\ldots,L)$. During calculations on the nozzle contour ($l = L$), naturally, the boundary condition of non-flow is used. By transferring from one time layer to another, we find the flow field in the entire region.

Most of the calculations were carried out with a difference grid having 7 x 64 points (7 in the θ direction, and 64 in the ξ direction).

Figure 28 gives certain results of calculations which pertain to the steady state flow regime. The nozzle 1, shown in Fig. 28, was obtained as the result of solving the inverse steady state problem in the work of U. G. Pirumov [19]. All linear dimensions are related to the radius of the nozzle throat. The figure shows

I - nozzle from a work [19];

II - nozzle with a contour (6.3);

—— distributions of parameters on the side of the nozzle and the shape of the sonic line;

--- distributions of parameters on the axis of the nozzle;

° - according to the results of a work [19].

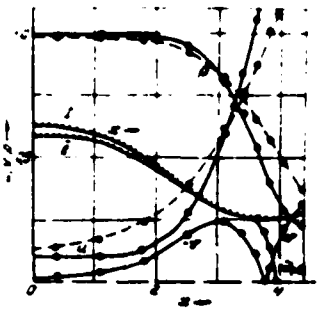

Fig. 28

the nozzle region close to the outlet, and for convenience, the origin of calculation is shifted along the x axis in comparison with the equation presented in the calculation (for the given nozzle, the distance from the intake cross section to the throat $\lambda = 9.897$).

Figure 28 gives the position of sonic lines and the distributions of parameters along the axis and the contour. Pressure is related to the value p_0, velocity to the value $\sqrt{p_0/\rho_0}$, where p_0, ρ_0 -- total pressure and density; $\gamma = 1.4 = \text{const}$.

Of the flow characteristics, we note a slight, approximately 0.1 - 0.4 of p_0 increase in pressure on the side (in comparison with its value when $x = 0$), which exists before the beginning of the intensive acceleration of gas. It is almost unnoticeable in Fig. 28 due to the smallness of scale.

The transition surface through the velocity of sound significantly differs from the rectilinear one in the regime of steady state flow. The sonic line extremely rapidly (in comparison with flow on the whole) acquires a shape similar to the stationary one.

The difference between the results obtained during solution of the direct, unsteady problem and the data [19] in the vicinity of the throat comprises a value on the order of 1%. This difference is basically due to certain inaccuracies in assigning the nozzle

contour. We still note that already when $x > 0.6$, flow noticeably differs from one-dimensional flow (particularly in the vicinity of the critical cross section).

When solving the direct, unsteady problem for the nozzle depicted in Fig. 28, the initial condition of the gas was determined from a calculation made by a method [19]. In the process of solution, steady state values of all gasdynamic parameters were maintained at the intake ($\xi = 0$). Inasmuch as the basic goal of the calculation of flow in the given contour was a comparison with the data of [19], the indicated method seems the natural one.

The results of a calculation of flow in a nozzle whose contour was assigned by the equation

$$y = G(x) \begin{cases} 2.32 & \text{when } 0 \leq x \leq 71.825 \\ 1.86 + 0.86 \cos \frac{\pi}{3.2}(x - 71.825) & \text{when } 71.825 \leq x \leq 74.825. \end{cases} \tag{6.3}$$

were also cited in [7]. Figure 28 shows this contour. The initial state of the gas in this case was determined from the one-dimensional theory with the additional assumption of a linear law of change of the angle of inclination of the velocity vector between the contour and the axis in cross section x = const. Steady state parameter values were maintained in the intake to the nozzle ($\xi = 0$). Such conditions when $\xi = 0$ are essentially equivalent to conditions at infinity, inasmuch as the length of the subsonic part was selected such that perturbations over time $t = t_\infty$ did not reach from the intake to the region of the contour shown in Fig. 28, which is of interest to us. In a known sense, the obtained solution simulates (with an accuracy up to the initial data when t = 0) the operation of a unique wind tunnel.

We note still another statement of the examined problem, based on the model of a tank-type installation. A quite large reservoir filled with gas is attached in one way or another to the investigated contour. If $G >> g$, where G is the mass of the gas contained in the

container and g is the mass of the gas which passes through the nozzle over a time t_∞, necessary for entry into the steady state regime, then as the result of the calculation when $t = t_\infty$, we obtain the steady state solution. In this case, the problem is completely closed and no additional conditions except the boundary conditions of non-flows are required.

We note in conclusion that the method of establishment was used in a work [12] for calculating unsteady flow in a plane, supersonic stream interacting with external, acoustical waves of assigned frequency and amplitude. This problem was examined in connection with the investigation of the phenomenon of sonic radiation and a discrete frequency by supersonic streams flowing into a flooded space. The investigation of the relationship between solutions which describe the perturbed flow in the stream and the amplitudes of the external acoustical waves given in [12] made it possible to draw certain conclusions about the mechanism of limiting pulsations of the stream which emits sound at a discrete frequency, leading to the establishment of self-excited vibrations.

REFERENCES

1. Бабенко К.И., Воскресенский Г.П. Численный метод расчета пространственного обтекания тел сверхзвуковым потоком газа. ЖВМиМФ, т. 1, № 6, 1961.

2. Бабенко К.И., Воскресенский Г.П., Любимов А.Н., Русанов В.В. Пространственное обтекание гладких тел идеальным газом. "Наука", М., 1964.

3. Бабенко К.И., Русанов В.В. Разностные методы решения пространственных задач газовой динамики. Труды II Всесоюзного съезда по механике, обз. доклады, вып. 2, "Наука", М., 1968.

4. Любимов А.Н., Русанов В.В. Течение газа около тупых тел. "Наука", М., 1970.

5. Дьяконов Ю.Н., Пчелкина Л.В., Самойлерова И.Д., Усова В.И. К расчету пространственных течений вязкого газа методом сеток. В об. "Вычислительные методы и программирование", вып. XV, изд. МГУ, 1970.

6. Дьяконов Ю.Н., Пчелкина Л.В., Самойлерова И.Д. Сверхзвуковое обтекание затупленных тел. Изд. МГУ, 1971.

7. Дьяконов Ю.Н., Пчелкина Л.В. О прямой задаче для сопла Лаваля. ДАН СССР, т. 191, № 2, 1970.

8. Любимов М.Г. Исследование течений газа при сверхзвуковом обтекании затупленных тел и в сверхзвуковых струях. Кандидатская диссертация, МГУ, 1971.

9. Лебедев М.Г., Савинов К.Г. Соударение неравномерных сверхзвуковых потоков газа с преградами. III Всесоюзный съезд по механике. Аннотации докладов. М., 1968.

10. Лебедев М.Г., Савинов К.Г. Удар неравномерного сверхзвукового потока газа в плоскую преграду. Изв. АН СССР, МЖГ, № 3, 1968.

11. Савинов К.Г. Обтекание сферы двумя соосными сверхзвуковыми струями. Изв. АН СССР, МЖГ, № 4, 1970.

12. Лебедев М.Г., Теленин Г.Ф. Исследование взаимодействия сверхзвуковой струи с акустическим полем. Изв. АН СССР, МЖГ, № 4, 1970.

13. Дьяконов Ю.Н., Кокошинская Н.С., Лукашин В.М., Пчелкина Л.Д., Сандомирская Н.Д. Пространственное обтекание затупленных тел сложной формы. В сб. "Вычислительные методы и программирование", вып. XV, изд. МГУ, 1970.

14. Дьяконов Ю.Н., Пчелкина Л.В., Сандомирская Н.Д. О расчете сверхзвукового обтекания тел под большими углами атаки. В сб. "Вычислительные методы и программирование", вып. XIX, изд. МГУ, 1972.

15. Дьяконов Ю.Н., Усков В.Н. Расчет сверхзвуковых струй идеального газа методом сеток. В сб. "Аэродинамика больших скоростей". Труды Института механики МГУ, № 5, 1970.

16. Гилинский С.М., Лебедев М.Г. Исследование обтекания плоских и осесимметричных тел с отошедшей ударной волной потоком с малой сверхзвуковой скоростью. Изв. АН СССР, Механика, № 1, 1965.

17. Лебедев М.Г., Миносцев В.Б., Теленин Г.Ф., Тишков Г.П. Приближенный метод учета реальности газа при гиперзвуковом обтекании сегментальных тел. Изв. АН СССР, МЖГ, № 2, 1969.

18. Гилинский С.М., Теленин Г.Ф., Тишков Г.П. Метод расчета сверхзвукового обтекания затупленных тел с отошедшей ударной волной. Изв. АН СССР, ОТН, Механика и машиностроение, № 4, 1964.

19. Пирумов У.Г. Расчет течения в сопле Лаваля. Докл. АН СССР, т. 178, № 2, 1967.

20. Авдеенкова Г.П., Ашратов Э.А. Истечение сверхзвуковой струи в вакуум. В сб. "Вычислительные методы и программирование", изд. МГУ, вып. 7, 1967.

21. Rusanov V.V. A three - dimensional supersonic gas flow past smooth bodies. Proc.II Internat. Congr. Appl. Mech., 1964, 774 - 778.

22. Voglie - Laurin R. Transonic rotational flow over a convex corner. Journ. Fluid Mech., 1960, pt 2, N 1.

23. Taylor T.D., Masson B.S. Application of the unsteady numerical method of Godunov to computation of supersonic flows past bell - shaped bodies. Journ. Comput.Physics, 1970, vol.5, N 3.

24. Seiff L.S. Interaction of highly underexpanded jets with simulated lunar surfaces. NASA TN D - 1095,1961.

A DIFFERENCE SCHEME OF THE THIRD ORDER OF ACCURACY FOR CALCULATING TWO-DIMENSIONAL FLOWS WITH CONTACT SEPARATION

V. V. Yeremin, Yu. M. Lipnitskiy

The presently employed difference methods of through calculation basically have the first or second order of approximation. Difficulties of increasing the order of the difference schemes consist in the necessity of using a significantly larger number of points of the initial field than in schemes of the first or second order, which has a significant effect on calculation time. This has an effect particularly when the order of approximation is increased for two-dimensional schemes . The increased requirements of the accuracy of determining the gasdynamics of flows, on the one hand, and the increase in the speed and memory of the computer, on the other, advance the problem of developing and adopting methods of increased accuracy for solving complex gasdynamic problems. Works [1,2,3] have been devoted to the development of such schemes. These works have suggested difference schemes of increased accuracy for solving one-dimensional gasdynamic problems. The fact that the schemes of a higher order of accuracy produce significantly less oscillation near the separation and significantly reduce the zone of its "blurring" is a significant result of these works. The numerical results for two-dimensional problems of gasdynamics, obtained with the aid of third order devices, have not yet been published, although such difference schemes based on a 25 point pattern have been constructed in works [2, 3].

This article suggests a quite compact device of the third order of approximation for solving two-dimensional problems of gasdynamics based on a 16 point pattern and calculation examples are given in it.

We shall write a system of gasdynamic equations for which the difference scheme is constructed in the divergent form

$$\frac{\partial f}{\partial t} + \frac{\partial F(f)}{\partial x} + \frac{\partial G(f)}{\partial y} + H(f, y) = 0 \quad . \tag{1}$$

where

$$f = \begin{Vmatrix} \rho \\ \rho u \\ \rho v \\ \ell \end{Vmatrix} , \quad F = \begin{Vmatrix} \rho u \\ \rho u^2 + p \\ \rho uv \\ (\ell + p)u \end{Vmatrix} , \quad G = \begin{Vmatrix} \rho v \\ \rho uv \\ \rho v^2 + p \\ (\ell + p)v \end{Vmatrix} , \quad H = \frac{v}{y} \begin{Vmatrix} \rho v \\ \rho uv \\ \rho v^2 \\ (\ell + p)v \end{Vmatrix}$$

The symbols for the gasdynamic functions are the standard ones. System (1) is closed by the equation for specific energy, which has the following form for a perfect gas:

$$\ell = \frac{\rho u^2}{2} + \frac{\rho v^2}{2} + \frac{p}{\gamma - 1} \quad .$$

We insert a difference grid with steps Δx, Δy, Δt in a space (x, y, t). In addition to the main difference grid, we insert an auxiliary one (Fig. 1), where $h = \frac{\Delta x}{2}$, $m = \frac{\Delta y}{2}$, $\Delta t = \Delta \tau$.
We shall use both integral and half-integral values of the spatial indices k and ℓ, having designated values of functions at nodes of the basic grid $f_{k,\ell}$, and at nodes of the auxiliary grid $f_{k,\ell}^{(0)}$.
The solution to the system (1) on the step shall be sought as the result of the following iteration process:

$$\{f_{k,\ell}^{n}\} = f_{k,\ell}^{(0)} = f_{k,\ell}^{(1)} = f_{k,\ell}^{(2)} = f_{k,\ell}^{(3)} = \{f_{k,\ell}^{n+1}\}$$

In order to calculate each $f_{k,\ell}^{(s)}$, we shall use values

$$f_{k,\ell}^{(0)}, f_{k,\ell}^{(1)}, \ldots, f_{k,\ell}^{(s-1)} \quad .$$

We insert the symbols for the averaging operators and for taking the difference according to x and y :

$$\begin{aligned} \mu_x f_{k,\ell} &= \frac{1}{4}(f_{k-1/2,\ell-1/2} + f_{k-1/2,\ell+1/2} + f_{k+1/2,\ell-1/2} + f_{k+1/2,\ell+1/2}) \\ \delta_x f_{k,\ell} &= \frac{1}{2}((f_{k+1/2,\ell-1/2} - f_{k-1/2,\ell-1/2}) + (f_{k+1/2,\ell+1/2} - f_{k-1/2,\ell+1/2})) \\ \delta_y f_{k,\ell} &= \frac{1}{2}((f_{k+1/2,\ell+1/2} - f_{k+1/2,\ell-1/2}) + (f_{k-1/2,\ell+1/2} - f_{k-1/2,\ell-1/2})) \quad . \end{aligned} \tag{2}$$

We shall require that the sought difference scheme be a natural

continuation of schemes of the first and second orders, i.e., that the first step

$$f_{\alpha,\ell}^{(1)} = \mu f_{\alpha,\ell}^{(0)} - \frac{\tau}{2h}\delta_x F_{\alpha,\ell}^{(0)} - \frac{\tau}{4m}\delta_y G_{\alpha,\ell}^{(0)} - \tau\mu H_{\alpha,\ell}^{(0)} \quad , \tag{3}$$

and the second step

$$f_{\alpha+1/2,\beta+1/2}^{(2)} = f_{\alpha+1/2,\beta+1/2}^{(0)} - \frac{\tau}{2h}\delta_x F_{\alpha+1/2,\beta+1/2}^{(1)} - \frac{\tau}{2m}\delta_y G_{\alpha+1/2,\beta+1/2}^{(1)} - 2\tau\mu H_{\alpha+1/2,\beta+1/2}^{(1)} \tag{4}$$

$f_{\alpha,\ell}^{n+1} - f_{\alpha,\ell}^{(2)}$ shall be sought in the form:

$$\begin{aligned} f_{\alpha,\ell}^{(2)} &= \alpha_1\mu f_{\alpha,\ell}^{(0)} + \alpha_2 f_{\alpha,\beta}^{(1)} + \alpha_3\left(f_{\alpha+1,\ell+1}^{(1)} + f_{\alpha+1,\beta-1}^{(1)} + \right. \\ &+ \left. f_{\alpha-1,\beta-1}^{(1)} + f_{\alpha-1,\beta+1}^{(1)}\right) + \alpha_4\tau\mu\left(H_{\alpha+1,\ell}^{(0)} + H_{\alpha,\beta-1}^{(0)} + H_{\alpha-1,\ell}^{(0)} + H_{\alpha,\beta+1}^{(0)}\right) + \\ &+ \alpha_5\left[\frac{\tau}{h}\delta_x\left(F_{\alpha,\beta-1}^{(0)} + F_{\alpha,\beta+1}^{(0)}\right) + \frac{\tau}{m}\delta_y\left(G_{\alpha+1,\ell}^{(0)} + G_{\alpha-1,\ell}^{(0)}\right)\right] + \\ &+ \alpha_6\left[\frac{\tau}{h}\delta_x F_{\alpha,\beta}^{(1)} + \frac{\tau}{m}\delta_y G_{\alpha,\beta}^{(1)}\right] + \alpha_7\tau\mu H_{\alpha,\beta}^{(1)} + \alpha_8\tau\mu H_{\alpha,\ell}^{(0)} \quad . \end{aligned} \tag{5}$$

The unknown coefficients of formula (5) need to be selected such that the expansion

$$f_{\alpha,\ell}^{n+1} = f_{\alpha,\beta}^{n} + \frac{\partial f}{\partial t}\Delta t + \frac{\partial^2 f}{\partial t^2}\frac{\Delta t^2}{2} + \frac{\partial^3 f}{\partial t^3}\frac{\Delta t^3}{6} + \ldots \quad ,$$

where the time derivatives are expressed with the aid of equation (1) through functions, and their derivatives according to the spatial coordinates coincide with the expansion $f_{\alpha,\ell}^{(2)}$ in powers of Δt up to terms of the order Δt^3, inclusively.

Making the expansions is an extremely laborious task because of the nonlinear character of the relationship F(f), G(f) and H(f). Omitting these cumbersome intermediate calculations, we give the final result:

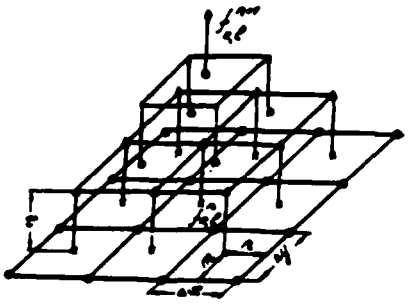

Fig. 1

$$\alpha_1 = -\frac{1}{4} \quad , \quad \alpha_2 = \frac{3}{2} \quad , \quad \alpha_3 = -\frac{1}{16} \quad , \quad \alpha_4 = \frac{1}{4} \quad ,$$

$$\alpha_5 = \frac{1}{16} \quad , \quad \alpha_6 = -\frac{9}{16} \quad , \quad \alpha_7 = -\frac{9}{4} \quad , \quad \alpha_8 = -\frac{1}{2} \quad .$$

i.e.,

$$f_{i,j}^{(3)} = -\frac{1}{4}\mu f_{i,j}^{(0)} + \frac{3}{2} f_{i,j}^{(1)} - \frac{1}{16}\left(f_{i+1,j+1}^{(1)} + f_{i+1,j-1}^{(1)} + f_{i-1,j-1}^{(1)} + f_{i-1,j+1}^{(1)}\right) + \frac{1}{4}\mu\left[H_{i+1,j}^{(0)} + H_{i,j-1}^{(0)} + H_{i-1}^{(0)} + H_{i,j+1}^{(0)}\right] + \frac{\tau}{16h}\delta_x\left(f_{i,j-1}^{(0)} + f_{i,j+1}^{(0)}\right) + \frac{\tau}{16m}\delta_y\left(G_{i+1,j}^{(0)} + G_{i-1,j}^{(0)}\right) - \frac{9}{16}\left[\frac{\tau}{h}\delta_x f_{i,j}^{(2)} + \frac{\tau}{m}\delta_y G_{i,j}^{(2)}\right] - \frac{9}{4}\tau\mu H_{i,j}^{(2)} - \frac{1}{2}\tau\mu H_{i,j}^{(0)}.$$

There can be infinitely many schemes of the third order based on the 16 point pattern, inasmuch as the equation system for determining the scheme coefficients has ten equations with 16 unknowns. Of all the solutions to this system, of the most practical value are schemes which satisfy (3) and (4) and have the least number of components in the right-hand side. The form (5) was chosen in accordance with these conditions.

We shall limit ourselves to an examination of a linear, differential equation of the following type during the investigation of stability of the suggested difference scheme :

$$\frac{\partial f}{\partial t} + \frac{\partial f}{\partial x} + \frac{\partial f}{\partial y} = 0, \quad f = f(x, y, t).$$

The difference scheme for this equation is written in the following way:

$$f_{i,j}^{(3)} = -\frac{1}{4}\mu f_{i,j}^{(0)} + \frac{3}{2} f_{i,j}^{(1)} - \frac{1}{16}\left[f_{i+1,j+1}^{(1)} + f_{i+1,j-1}^{(1)} + f_{i-1,j-1}^{(1)} + f_{i-1,j+1}^{(1)}\right] + \frac{\tau}{16h}\delta_x\left(f_{i,j-1}^{(0)} + f_{i,j+1}^{(0)}\right) + \frac{\tau}{16m}\delta_y\left(f_{i+1,j}^{(0)} + f_{i-1,j}^{(0)}\right) - \frac{9}{16}\left[\frac{\tau}{h}\delta_x f_{i,j}^{(2)} + \frac{\tau}{m}\delta_y f_{i,j}^{(2)}\right].$$

Having expressed values $f_{i,j}^{(3)}$ by the values $f_{i,j}^{(0)}$, and by examining a solution of the type $f_{i,j}^{n} = \lambda^{n} e^{i(\varphi_1 i + \varphi_2 j)}$ for determining the region of stability of the difference scheme, we obtain an inequality: $\lambda^{n} \leq 1$, where

$$\lambda = \frac{5}{4}\cos\frac{\alpha}{2}\cos\frac{\beta}{2} - \frac{1}{4}\cos\frac{\alpha}{2}\cos\frac{\beta}{2}\cos\alpha\cdot\cos\beta - \frac{15}{4}i\left(\omega_1\sin\frac{\alpha}{2}\cdot\right.$$

$$\left.\cos\frac{\beta}{2} + \omega_2\sin\frac{\beta}{2}\cos\frac{\alpha}{2}\right) + \frac{i\omega_1}{4}\cdot\sin\frac{\alpha}{2}\cos\frac{\beta}{2}\cos\alpha\cdot\cos\beta + \frac{1}{4}i\omega_2\cdot$$

$$\cdot\sin\frac{\beta}{2}\cos\frac{\alpha}{2}\cos\alpha\cdot\cos\beta + \frac{i\omega_1}{2}\sin\frac{\alpha}{2}\cos\frac{\beta}{2}\cos\beta + \frac{i\omega_2}{2}\cdot$$

$$\cdot\sin\frac{\beta}{2}\cos\frac{\alpha}{2}\cos\alpha - \frac{9}{16}\omega_1^2\sin\frac{\alpha}{2}\sin\alpha\left(\cos\frac{3}{2}\beta + 3\cos\frac{\beta}{2}\right) - \frac{9}{4}\omega_1\omega_2\cdot$$

$$\cdot\cos\frac{\alpha}{2}\cos\frac{\beta}{2}\sin\alpha\cdot\sin\beta - \frac{9}{16}\omega_1^2\sin\frac{\beta}{2}\sin\beta\left(\cos\frac{3}{2}\alpha + 3\cos\frac{\alpha}{2}\right) -$$

$$-\frac{9}{32}\omega_1^3 i\left(\cos\frac{3}{2}\beta + 3\cos\frac{\beta}{2}\right)\left(\sin\frac{3}{2}\alpha - 3\sin\frac{\alpha}{2}\right) +$$

$$+\frac{27}{8}\omega_1^2\omega_2\cdot\sin\frac{\alpha}{2}\cos\frac{\beta}{2}\sin\alpha\cdot\sin\beta +$$

$$+\frac{27}{8}\omega_1\omega_2^2 i\sin\frac{\beta}{2}\cos\frac{\alpha}{2}\sin\alpha\sin\beta -$$

$$-\frac{9}{32}\omega_2^3 i\left(\sin\frac{3}{2}\beta - 3\sin\frac{\beta}{2}\right)\left(\cos\frac{3}{2}\alpha + 3\cos\frac{\alpha}{2}\right),$$

$$\omega_1 = \frac{\tau}{h},\quad \omega_2 = \frac{\tau}{m},\quad \alpha = \varphi h,\quad \beta = \psi m.$$

The analytical investigation of this inequality is extremely difficult, and therefore the region of its solution was determined numerically. With fixed ω_1 and ω_2, max $|\lambda|$ was sought according to α and β.

The relationship between max $|\lambda|$ and ω_1 and ω_2 was constructed as the result of this. The investigation of this relationship showed that the scheme is stable when $\omega_1^2 + \omega_2^2 < R^2$, where R = 1/3.

As an example, Figs. 2-10 give the results of calculations of flow around a flat tip by uniform and nonuniform supersonic flows of a perfect gas. The general picture of flow in the case of a homogeneous free-stream flow with a number $M_\infty = 3$, $\gamma = 1.4$ is shown in Fig. 2. It gives the horizontal lines which are designated by the indices 1, 2, 3, 4, and the distributions of the gasdynamic functions along which lines are drawn in Figs. 3-6. The presented values of pressure p, density ρ, and the projections of the velocity vectors

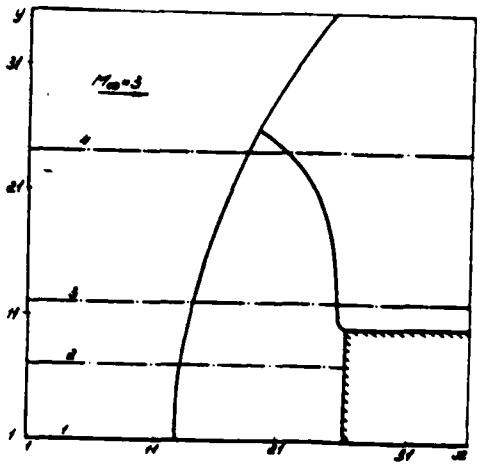

Fig. 2

u, v are respectively related to the doubled velocity head $\rho_\infty V_\infty^2$, the density head ρ_∞, and the velocity head V_∞ of the free-stream flow.

Figures 3 and 4 clearly show regions of unperturbed flow and the flow between the shock wave and the body, and the jump is "blurred" over 2-3 points of the difference scheme. Errors in satisfying the Hugoniot conditions did not exceed 1%.

A characteristic region of rarefaction appears in the distribution of the gasdynamic parameters in Figs. 5 and 6, inasmuch as the third and fourth rays (Fig. 2) intersect the fan of the rarefaction waves proceeding from the body contour break point.

From the viewpoint of investigating the possibilities of the scheme, the examples of calculating flow around a body by a nonhomogeneous, supersonic flow with contact separation is most interesting. The corresponding picture of flow is shown in Fig. 7, where the dash line depicts contact separation, while pressure and density in the free-stream are constant and the velocity value changes upon transferring through it two times ($M_\infty = 3$, $M_\infty = 0$, $\gamma = 1.4$). Contact separation in the examined case falls on the shock wave below the

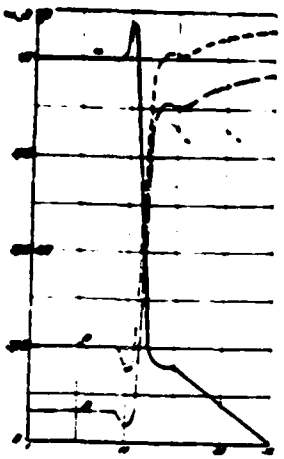

Fig. 3

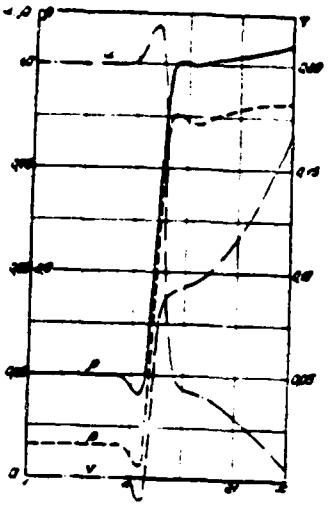

Fig. 4

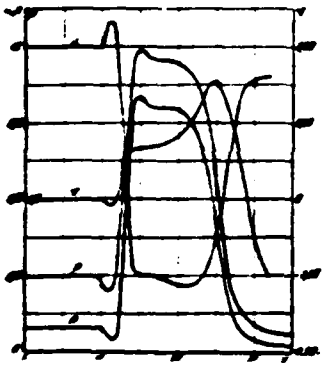

Fig. 5

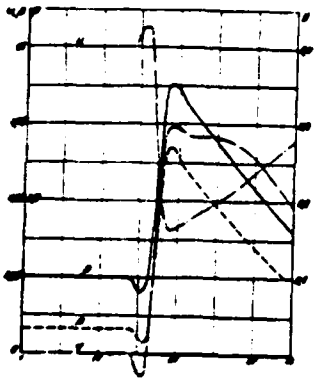

Fig. 6

sonic line, which corresponds to flow with a number $M_\infty = 3$ (Figs. 2, 7). This leads to a significant restructuring of the flow picture and to the formation of a trinary point on the shock wave (the sonic line and contact separation on the shock wave have a common point). In connection with the decrease in the vertical size of the region of effect, shock wave regression increases and the sonic line deforms significantly. The distributions of pressure and the longitudinal velocity component along the cross sections 1, 2, 3 and 4 (Fig. 7) are shown in Figs. 8-9. Pressure remains constant in cross section 1, being slightly perturbed in the contact separation. The second cross section intersects the shock wave at a small angle, which leads to "blurring" of the shock wave over a large num-

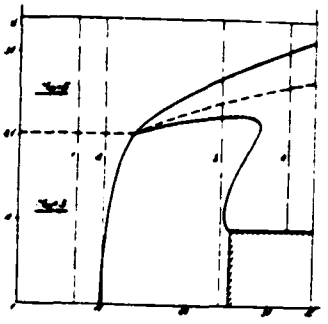

Fig. 7

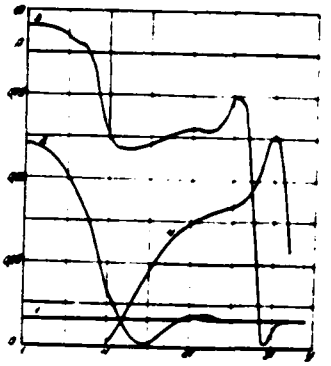

Fig. 8

ber of grid points.

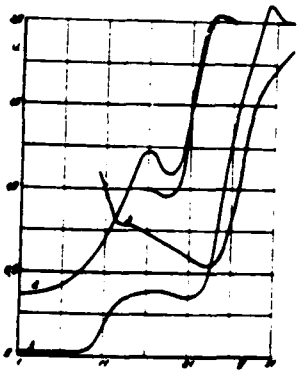

Fig. 9

The flow is still not perturbed in the vicinity of the contact discontinuity, and its pressure change is slight. The contact discontinuity is situated in the region behind the shock wave on rays 3 and 4 and the characteristic pressure buildup behind it, associated with the increase in pressure after the shock wave, proportional to the square of the M number is noticeable. The change in the longitudinal velocity component in cross sections 1, 2, 3 and 4 makes it possible to note precisely the same characteristic flow regions.

The suggested difference scheme makes it possible to make calculations for flows with contact discontinuity even in the case when the velocity value during passage through it changes from supersonic to subsonic. Figure 11 shows an example of such calculation. In Fig. 11, the dot-dash line shows contact discontinuity and the velocity value during transit through it changes six times

$$(M_{\infty} = 3, \quad M_{\infty} = 0.3, \quad \gamma = 1.4)$$

The solid line depicts the shock wave and the dash line shows the sonic line.

Fig. 10

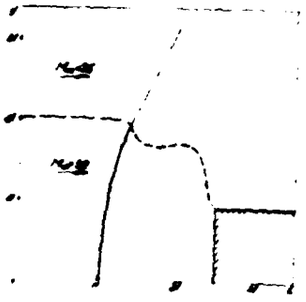

Fig. 11

Calculation accuracy is controlled by checking the Bernoulli relationship, which is an integral of the differential, but not the difference equations. The value of the Bernoulli integral

$$6 \cdot \frac{\gamma}{\gamma-1}\frac{p}{\rho} \cdot \ldots \cdot$$

for a homogeneous flow differed from the value calculated according to the parameters of the free-stream flow by no more than 0.5%. On the contact discontinuity, the value of Bernoulli integral constants changes in jump fashion, according to whose "blurring" value one can judge the quality of function of the difference scheme.

When constructing the difference system in the work, contact separations in all regions of flow (Figs. 1, 2, 3, 4) were "blurred" on no more than 4-5 points, which makes it possible to determine the discontinuity line, not only by plotting the streamline, but also according to values of the Bernoulli integral (Fig. 10).

The authors consider it their duty to thank V. B. Balakin for his useful discussions and the attention he gave to the work.

REFERENCES

1. Балакин Ю.Б. О методах типа Рунге-Кутта для газовой динамики. ЖВМиМФ, т. 10, № 6, 1970.

2. S.Z. Burstein. Third order difference methods for Hyperbolic Equations, Journal of computational Physics, N 5, 1970.

3. V.V.Rusanov, On Difference schemes of Third Order Accuracy of Nonlinear Hyperbolic Systems, Journal of computational Physics, N 5, 1970.

INVESTIGATION OF SUPERSONIC FLOW AROUND A SPHERE BY A FLOW OF AIR WITH A HIGH STATIC TEMPERATURE

Ye. G. Shapiro

The investigation of supersonic flows near blunt bodies has been made in many works [1]. Approximate laws of similarity have been established for such flows, and the necessity of taking the physico-chemical processes in the boundary layer into account has been shown for hypersonic flows.

It has been assumed in most of these works that the gas ahead of the wave has a temperature T_∞ = 200 - 300° K, and primary emphasis has been placed on investigating the hypersonic flows. However, in certain cases associated with experiments, one has had to deal with a flow of gas with a high static temperature and a low Mach number [$Mach_\infty < 6$] even at high velocities. This work is devoted to the numerical investigation of such flows.

Statement of the problem. Supersonic flow of air past a sphere is examined. The equations of motion

$$\nabla\rho\vec{v}=0\ ,\quad (\vec{v}\nabla)\vec{v}+\rho^{-1}\nabla p=0\ ,$$
$$\rho\vec{v}\nabla\left(h+\frac{1}{2}v^2\right)=0\ ,\quad h=h(p,T)\ ,\quad \rho=\rho(p,T) \qquad (1)$$

are written in the spherical system of coordinates whose center coincides with the center of the sphere and an axis running along the flow axis. As sought functions, we choose the radial function u and the circular function v of the velocity component, as well as pressure and temperature p, T.

The non-dimensional variables are inserted according to formulas

$$u^*=u/u_\infty\ ,\quad v^*=v/u_\infty\ ,\quad p^*=p/\rho_\infty u_\infty^2\ ,$$
$$T^*=T/T_\infty\ ,\quad r^*=r/R_0\ . \qquad (2)$$

As usual, the non-flow condition on the body and the laws of conservation on the shock wave were taken as the boundary conditions. Functions h and ρ were calculated according to the A. N. Krayko approximation formulas [2] not only in the boundary layer, but also ahead of the shock wave front, inasmuch as $T_\infty \geq 2000^\circ$ K in most calculations, and at such temperatures as is known, physico-chemical processes already occur in the air.

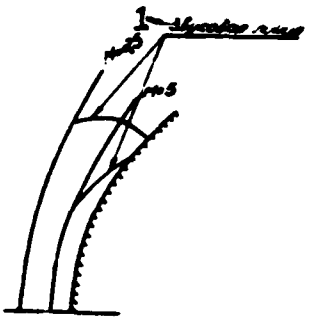

Fig. 1
1 - sonic line

The problem was solved by the G. F. Telenin method. The following was taken for the independent variable

$$\xi = \frac{r - r_0}{r_1 - r_0} \qquad (3)$$

where r_1 is the shock wave contour, r_0 -- contour of the body. The gasdynamic parameters were approximated by Lagrangian polynomials according to a five-ray method ($\vartheta_1 = 0$; $\vartheta_2 = 0.257$; $\vartheta_3 = 0.538$; $\vartheta_4 = 0.725$; $\vartheta_5 = 0.800$).

2. Relationship between the position of the shock wave and the Mach number, temperature, and pressure of the free-stream flow.

The calculations that were made ($p_\infty = 1$ atm.; $T_\infty = 3000^\circ$K; $1.5 \leq M_\infty \leq 8$) showed that the shock wave monotonically approaches the body in precisely the same way as in the case of standard external conditions when the Mach number increases, while the sonic line is displaced toward the axis of symmetry (Figs. 1 and 2).

Already in the first works devoted to hypersonic flows around blunt bodies, it was shown that the gas behind the shock wave cannot be considered a perfect gas. At high Mach numbers, temperature behind the shock wave becomes sufficient for physico-chemical processes to develop in the shock layer, in connection with which regression

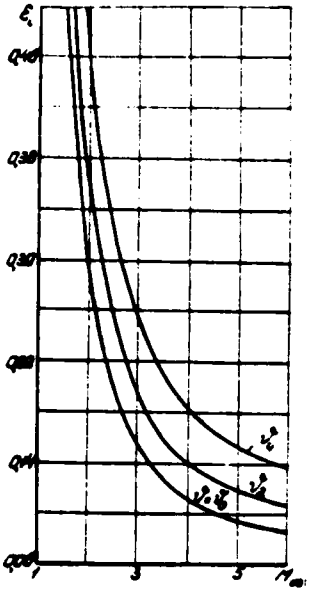

Fig. 2

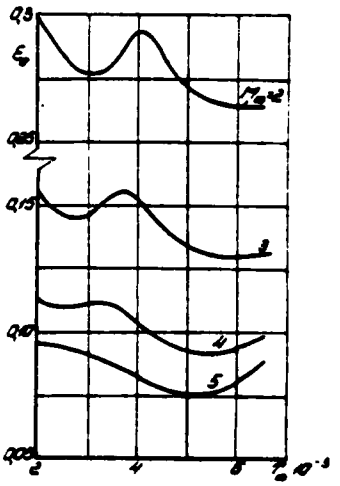

Fig. 3

of the shock wave ε from M_∞ is more complex in comparison with the case of a perfect gas. The position of the shock wave in the perfect gas is determined by M_∞ and by the heat capacity relationship γ and does not depend on pressure and temperature ahead of its front. Inasmuch as the increase in temperature in the equilibrium gas is accompanied by physico-chemical processes, the increase in temperature ahead of ths shock wave front with a fixed M_∞ causes physico-chemical processes in the shock layer, and the position of the shock wave will depend upon T_∞, monotonically (Fig. 3). For an illustration, we shall examine the process of dissociation of N_2 and O_2 molecules in the shock layer. Figure 4, a,b shows concentrations with molecules of O_2 (curve 1) and N_2 (curve 2) related to standard atmospheric conditions taken from tables [3] according to conditions behind the direct shock wave for $M_\infty = 2$ and 4, depending upon T_∞. Here, too, the dash line plots the corresponding values ε_0 (T_∞). The initial segment of the curve ε_0 (T_∞) when $M_\infty = 2$ corresponds to the beginning of the process of oxygen dissociation; for $M_\infty = 4$ with precisely the same T_∞, we have an already developed process of O_2 dissociation. When the O_2 dissociation process culminates, regression of the shock wave on the ε_0 axis acquires its maximum value in both cases. The process of N_2

dissociation is still not complete in both cases, and therefore there is no second maximum on the $\varepsilon_0(T_\infty)$ curves. Higher temperatures in the shock layer correspond to high Mach numbers ahead of the shock wave with identical external conditions, and therefore the higher degrees of molecular dissociation and the associated maxima and minima of curves $\varepsilon_0(T_\infty)$ are displaced toward the low temperatures when the Mach number increases (Fig. 3). On the other hand, the increase in M_∞ is accompanied by an increase in pressure behind the wave, while the pressure increase reduces the degree of dissociation at precisely the same temperatures. Therefore, the curves in Fig. 3 become smoother at the high Mach numbers.

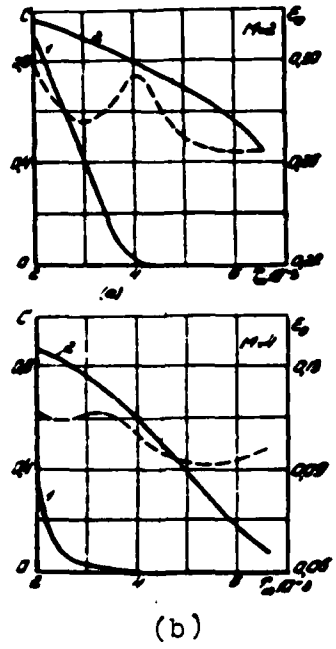

(b)

Fig. 4

Pressure ahead of the shock wave front has a significant effect on the position of the shock wave in the equilibrium gas. Figure 5 shows the relationship between regression of the shock wave along the five rays $\vartheta_1 = 0$, 0.287, 0.538, 0.725, 0.8 when $M_\infty = 3$, $T_\infty = 6000^\circ$ K with pressure of the free-stream flow. The relationship between ε_1 and p_∞ has precisely the same complex, nonmonotonic character as with T_∞. Here, the nonmonotonic nature of the behavior of ε is already not associated with changes of temperature in the shock layer, which are relatively small, but with changes in pressure in it and the maximum $\varepsilon(p_\infty)$ is due to culmination of the nitrogen dissociation process.

The shape of the shock wave changes weakly with a change in p_∞ and with the change in T_∞. Only its position relative to the sphere changes. When the Mach number of the free-stream flow decreases, the shock wave not only regresses from the body, but straightens (the radius of curvature of the shock wave increases on

the axis).

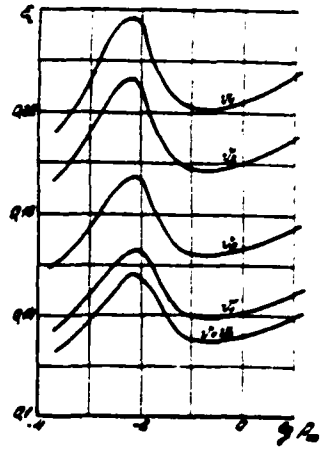

Fig. 5
$M = 3$, $T_\infty = 6000^\circ$ K

3. Certain properties of similarity of equilibrium flows near the sphere. Flow around a body of assigned form by a perfect gas is totally determined by two parameters -- M_∞ and γ -- and equilibrium flow is determined by the Mach number, the equation of state, temperature T_∞, and pressure p_∞. However, analysis of calculation results showed [4,5] that in the case of an equilibrium gas, the number of parameters can be reduced. An approximate formula was given in a work [4]

$$\varepsilon_0 \cdot 0.8 \approx , \qquad (4)$$

reflecting the relationship between regression of the shock wave on the axis with compression in the shock wave $\varepsilon = \rho_\infty/\rho_1|_{y=0}$. Here, too, a formula is given for the dimensionless velocity of flow in the critical point $\frac{\partial u}{\partial x}\frac{\rho_\infty}{p_\infty}$. These results are extended to ellipsoids in a work [6], which showed that the value of the parameter ε uniformly determines flow rate.

Approximating relationships for ε are suggested in a work [7], as are flow rates for blunt bodies of any shape. In all of these works, the number of determinative parameters is reduced to one. However, as was indicated in [5], one can achieve greater accuracy, particularly if one is dealing not with too high Mach numbers, if one leaves out two parameters -- the compression coefficient and the Mach number of the free-stream flow. Such a refinement was made in a work [8], which gives the results of calculating flow around a sphere by a perfect gas in a broad range of numbers M_∞ = 1.5 - 1000, γ = 1.05 - 1.6. On the basis of analyzing calculations in [8], similarity criteria were suggested as follows:

$$N_1 = \varkappa + 0{,}07/M_\infty^2 \tag{5}$$

$$N_2 = \sqrt{2\varkappa(\varkappa + 2p_1)} \cdot 1/M_\infty \tag{6}$$

$$N_3 = \varkappa + 0{,}1/M_\infty \tag{7}$$

$$N_4 = (1+\varkappa)\sin\sqrt{\varkappa}\left\{1+0{,}67\left[(1+\varepsilon_0)\sin\sqrt{\varkappa}\right]^2\right\} \tag{8}$$

which make it possible to present the results in the form of analytical relationships:

$$\varepsilon_0 = N_1(0{,}76 + 1{,}05\,N_1^2) \tag{9}$$

$$\frac{\rho_0}{\rho_\infty u_\infty}\frac{dv_0}{dx} = 0{,}88\,N_2(1 - 0{,}15\,N_2^2) \tag{10}$$

$$r_1 = 0{,}554 \cdot N_3(0{,}6 - 0{,}366\,N_3^2) \tag{11}$$

$$r_2 = 1{,}05\,N_4 \tag{12}$$

Here, r_1 and r_2 are distances from the axis of symmetry to the sonic points on the surface of the body and the shock wave. The compression coefficient $\varkappa$ enters into the similarity criterion as the basic parameter. Furthermore, values M_∞ and $p_1 = p_\infty/\rho_\infty u_\infty^2$ are used.

The authors of a work [8] pointed out that the error of the formula for ε_0 did not exceed 4.5% for r_1 = 0.8%, and 10% for r_2 (when $M_\infty \geq 2$ - 6.6%). Formula (10) was least successful for the rate of flow -- the error of the formula reached 24%.

Formula (9) at high M_∞ is quite similar to relationship (4). However, at small Mach numbers (9) gives more accurate results. Thus, for $M_\infty = 2$, $\gamma = 1.4$, formula (9) gives 1.5% error, while formula (4) gives 15% error.

A check of the suitability of the formulas (5-12) was made in this work for the examined case of flow around a sphere by equilibrium air with a high static temperature. Figures 6, 7 and 8 give the curves calculated according to the formulas for ε_0, r_1 and r_2, In Figures 6-9, the following symbols are used: light circles and light triangles -- M_∞ = 2, 4, respectively, dark circles and triangles -- M_∞ = 3, 5 (various values of the similarity cri-

teria for identical M_∞ were obtained as the result of different T_∞), the rectangles note data which correspond to the fractional values of the number $1.5 < M_\infty < 6$ when p_∞ = 1 atm, $T_\infty = 2000^\circ$ K.. It is evident that formulas (9), (11) and (12) determine the position of the shock wave and the sonic points in the examined class of flows quite well.

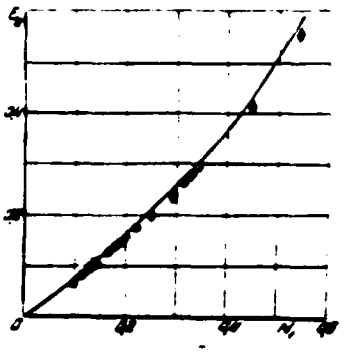

Fig. 6

Formulas (6) and (10) produced the greatest error. In addition to the basic determinative parameter $\varkappa$, they also include the Mach number of the free-stream flow and the dimensionless pressure behind the shock wave $\varkappa = p_2/p_\infty$. In the literature devoted to hypersonic flow around blunt bodies, there are indications that the velocity gradient in the critical point depends solely on compression $\varkappa$ for an equilibrium gas [4, 6]. For the case of flow past a sphere by an equilibrium gas, the following relationship is suggested in [4]

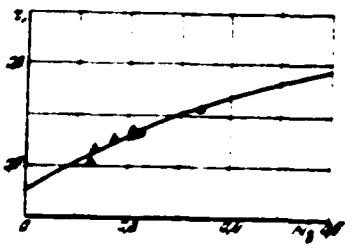

Fig. 7

$$\frac{R_0}{u_{max}}\frac{dv_0}{ds} = (1{,}6 \cdot 1{,}5\,\varkappa)\sqrt{\varkappa} \quad . \tag{13}$$

In both of these works, velocities were related to the maximum velocity u_{max}. Furthermore, it was noted that when a perfect gas flows past bodies, the parameter $\varkappa$ must be replaced by the value $(\gamma-1)/\gamma$.

In a work [7], velocities were related to u_∞ and a universal formulas was suggested for dimensionless flow rate which is suitable for both the equilibrium and the perfect gas

$$\frac{R_0}{u_\infty}\frac{dv_0}{ds} = \sqrt{2\mu(\varkappa)\varkappa} \quad . \tag{14}$$

where $\mu(\varkappa)$ weakly depends on the shape of the body. For the Heiz solution [9], $\mu = 4/3$.

The necessity of replacing ε with the value $(\gamma-1)/(\gamma+1)$ with the examined flow of a perfect gas is explained in the following way. We shall assume that the velocity of flow is determined by compression and the relationship has the form

$$\frac{R_0}{u_\infty}\frac{dv_0}{ds} = a\sqrt{\varepsilon} \quad . \qquad (15)$$

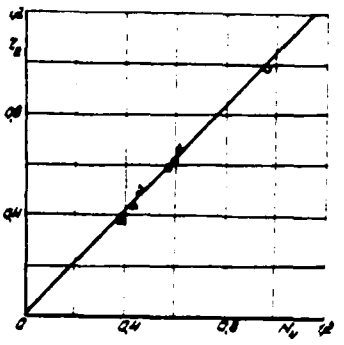

Figure 8

where $a = const$. Considering that this relationship is conserved for the perfect gas, we proceed to a different velocity scale u_{max}. Inasmuch as,

$$\frac{u^2_{max}}{u^2_\infty} = 1 + \frac{2}{\gamma-1}\frac{1}{M^2_\infty} \quad ,$$

and compression in the direct discontinuity is

$$\varepsilon = \frac{2 + M^2_\infty(\gamma-1)}{M^2_\infty(\gamma+1)} \quad ,$$

then for non-dimensional flow rate we obtain

$$\frac{R_0}{u_{max}}\frac{dv_0}{ds} = a\sqrt{\frac{\gamma-1}{\gamma+1}} \quad . \qquad (16)$$

Thus, the selection of u_{max} as the velocity scale led to relationships of the type (16) and precisely this kind of relationship was obtained on the basis of analyzing the calculation of flow around blunt bodies by a perfect gas. The calculation of equilibrium flow detected relationships of the type (13) although u_{max} was taken as the velocity scale. The fact of the matter is that such flows with high velocities corresponded to equilibrium flows when the kinetic energy of the gas was much greater than the thermal energy, $u^2_{max} \approx u^2_\infty$ and, therefore, the relationship of the type (13) practically coincides with relationships (15). When the M_∞ number is not too great or when the free-stream flow has a high temperature, the difference between u_{max} and u_∞ becomes significant, and the correct choice of the velocity scales becomes important. Great deviations of the empirical formula (10) from the results of calculation, and the presence of additional parameters M_∞ and $p_\infty/\rho_\infty u^2_{max}$ in it, are evidently associated with the unsuccessful selection of the velocity scale.

The calculations made in this work confirmed the assumption that flow rate in the critical point is a uniform function of compression. The data which correspond to the entire investigated range of Mach , numbers, temperatures and pressure were approximated well by the relationship $\frac{R_0}{u_\infty}\cdot\frac{dv_e}{ds}=(1{,}72-0{,}8\sqrt{\varepsilon})\sqrt{\varepsilon}$.

(17)

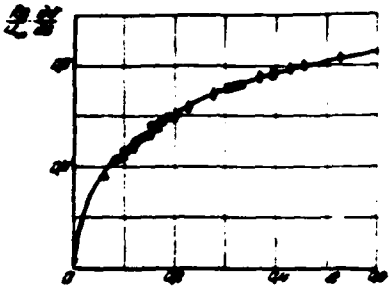

Fig. 9

We note that all formulas (10), (13), (14) and (17) produce similar results with high compression values when $\varepsilon \ll 1$ and $M_\infty \gg 1$. They are all described by a relationship of the type (15) where the coefficient α changes within limits from 1.6 to 1.76.

The velocity gradient in the critical point can be approximated by the following relationship

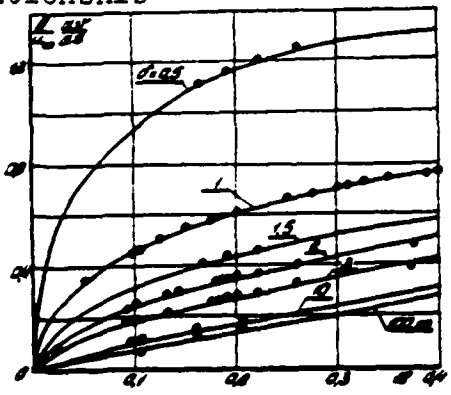

$$\frac{R_0}{u_\infty}\cdot\frac{dv_e}{ds}=\sqrt{\varepsilon}\left[\frac{1{,}72}{\beta^{0{,}3}}+\left(0{,}7-\frac{1{,}5}{\beta^{1{,}25}}\right)\sqrt{\varepsilon}\right] \qquad (18)$$

Figure 10

for an ellipsoid of rotation with a semi-axis ratio of $\beta=\frac{a}{c}$.

Figure 10 shows curves calculated according to formula (18), which plot the results of calculating the flow around ellipsoids according to the data of works [6,10,11].

4. Modeling equilibrium flow of a perfect gas. A work [5] suggested modeling equilibrium flow at the forward part of a blunt body by flow of a perfect gas with an adiabatic exponent

$$\gamma_{ef}=\frac{M_\infty^2(1+\varepsilon)-2}{M_\infty^2(1-\varepsilon)} \qquad (19)$$

The possibility of such modeling for the flow around a sphere by a gas with a high static temperature was tested in this work.

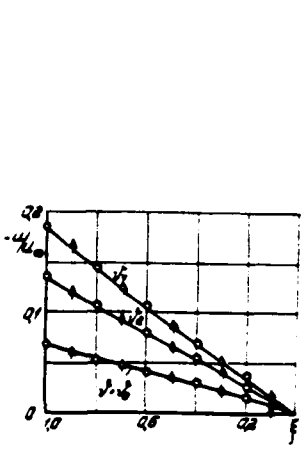

Fig. 11

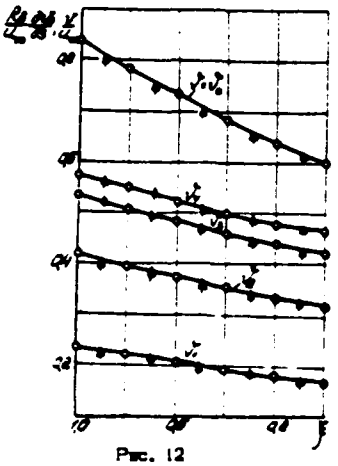

Рис. 12

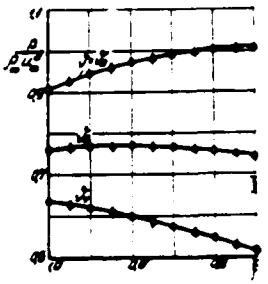

Fig. 13

Figs. 11 - 13. • - T_∞ = 2300°K
• - T_∞ = 4000° K
•• - P_∞ = 0,3 · 10^{-1} атм

Figures 11-13 give the distributions of the velocities and pressures for a perfect gas $M_\infty = 3$, $\gamma = 1.18$ according to the ξ coordinate on different ray $\vartheta \cdot \vartheta_i$. The symbols on these curves plot points which correspond to values of precisely the same parameters for flow around the sphere $M_\infty = 3$, $P_\infty = 1$ атм, $T_\infty = 2300°K$, $M_\infty = 3$, $P_\infty = 1$ атм, $T_\infty = 4000°$ and $P_\infty = 0.3 \cdot 10^{-1}$ атм, $T_\infty = 6000°$ K.

Compression is identical in all the examined cases: ε = 0.1845. Differences in the fields of velocities, pressures and in values $\varepsilon(\vartheta)$ do not exceed 3%. The temperature field for the examined cases (curves 0 - γ = 1.18, 1 - T_∞ = 2300°K, 2 - T_∞ = 4000°K, 3 - P_∞ = 0,3 · 10^{-1} атм) are presented for the zero ray in Figure 14 for the last ray in Figure 15. As is evident, the temperature difference is more significant and reaches 14%. The fact of the matter is that in a real gas enthalpy will already not be proportional to temperature and, therefore, even in a case wher enthalpy in the real and simulated flows is identical, the distribution of temperature in the shock layer will generally be different. In the case examined here, which is flow of high temperature air around a sphere, gas ahead of the shock wave cannot be considered a perfect gas. Totalenthalpy of the real flow $H = \frac{1}{2} + \frac{h^*(P_\infty, T_\infty)}{a_\infty^2}$ need not be equal to total entropy of the simulated flow $H = \frac{1}{2} + \frac{1}{(\gamma_\infty - 1) M_\infty^2}$ with identical Mach numbers M_∞ and compression ε but different p_∞ C_∞. Enthalpies behind the shock wave in these flows $\frac{h^*(P^*, T^*)}{a_\infty^2}$ and $T \cdot \frac{1}{M_\infty^2 (\gamma_\infty - 1)}$ will not be equal. Thus arises

the impossibility of directly simulating temperature distribution. All the same, despite this, one can obtain a temperature distribution in the shock layer for the real gas from the model solution. At the same time, by knowing T_∞, P_∞, and M_∞, it is easy to find the total enthalpy of the free-stream flow of the real gas H^*_∞. Having taken the velocity distribution from the model solution, we find enthalpy in the shock layer $h^*(p^*, T^*) = H^*_\infty - \frac{v^2}{2}$. Now, inasmuch as the distribution of pressures is also known to us, it is not difficult to find temperature.

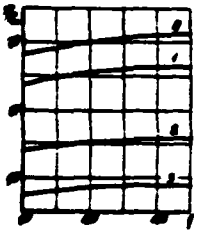

Figure 14

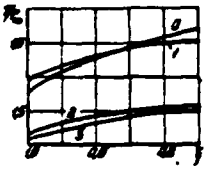

Figure 15

REFERENCES

1. Рождественский Г.С., Тишкин Г.Ф. Сборник Численные методы в газовой динамике, изд. МГУ, М., стр. 93 – 113, 1968.

2. Крайко А.Н. Аналитическое представление термодинамических функций воздуха. Изв. журнал, т. IV, вып. 3, 1964.

3. Предводителев А.С. и др. Таблицы термодинамических функций воздуха. М., 1962.

4. Тишкин Г.Ф., Тишкин Г.Л. Исследование сверхзвукового обтекания сферы воздухом в установках газом при термодинамическом равновесии. ДАН СССР, т. 159, № 1, 1964.

5. Либерман М.Г. и др. Приближенный метод учета влияния реальных газов при гиперзвуковом обтекании затупленных тел. Изв. АН СССР МЖГ, № 2, 1968.

6. Гилинский С.М., Макарова И.Е. Расчет сверхзвукового обтекания затупленных тел потоком воздуха с учетом равновесных физико-химических превращений. Изв. АН СССР, МЖГ, № 1, 1966.

7. Стулов В.П. О законе подобия при сверхзвуковом обтекании затупленных тел. Изв. АН СССР, МЖГ, № 4, 1968.

8. Баскин А.П. и др. Обтекание сферы сверхзвуковым потоком совершенного газа. Уч. записки ЦАГИ, т. II, № 3, 1971.

9. Хейз У.Д., Пробстин Р.Ф. Теория гиперзвуковых течений. Изд. И.Л., М., 1962.

10. Белоцерковский О.М. Расчет обтекания осесимметричных тел с отошедшей ударной волной. ВЦ АН СССР, М., 1961.

11. Белоцерковский О.М. Обтекание затупленных тел сверхзвуковым потоком газа. ВЦ АН СССР, М., 1967.

BOUNDARIES OF APPLICABILITY OF THE LAW OF BINARY SIMILARITY DURING THE FLOW OF A DISSOCIATING GAS AROUND BODIES

by

T. P. Stulov

When investigating non-equilibrium flow around blunt bodies, the law of binary similarity plays an important role [1]. According to the law of binary similarity, non-equilibrium flows of a given gas assigned condition v_∞, T_∞ near geometrically similar bodies are similar, if the condition, $p_\infty R_0$ = const is satisfied for these flows, where p_∞ is pressure in the free-stream flow, R_0 is the characteristic size of the body. The applicability of the binary similarity in the dissociating gas is limited due to taking recombination, which proceeds in the trinary collisions, into account [1]. Inasmuch as the importance of the recombination terms increases proportional to the approach to equilibrium, then it is clear that one should in fact anticipate great deviations from the rule of binary similarity in precisely this region. In the practical regard, it is extremely important to determine the region in the plane of variables (p_∞, R_0) in which the binary similarity law is valid with the assigned accuracy.

Violation of binary similarity during flow around a blunt body primarily has an effect on the distribution parameters in the vicinity of the critical point, for in the critical point itself the composition of gas always corresponds to local thermodynamic equilibrium. With the increase in the parameters $p_\infty R_0$, the region of quasiuniform in the shock layer increases and finally encompasses the entire shock layer with the exception of a narrow relaxation zone behind the curvilinear shock wave. One can take the following condition as the criterion for describing the region of validity of the binary similarity law for the shock layer in general; the law of binary similarity is valid when the length of the relaxation zone behind the direct shock wave exceeds a certain proportion of the

length of regression of the shock wave ahead of the body under precisely the same conditions, i.e.,

$$l > k\varepsilon. \tag{1}$$

Choice of the arbitrary parameter k insures satisfying the law of binary similarity in the sought region with the accuracy assigned in advance. Obviously, one can only find the value of k empirically, on the basis of numerical solutions to the problem.

Equality $l = k\varepsilon$ gives the boundary of the region in the plane (p_∞, R_0). An explicit formula will be obtained below for this boundary and numerical estimates will be given for specific cases.

In order to establish the relationship between regression of the shockwave ε and the length of the relaxation zone behind the direct shock l, we shall use the approximate law of flow similarity at the leading surface of the body examined [2]. Formula (5) of this work

$$\int_0^\infty \frac{\rho(x)}{\rho_\infty} e^{-\frac{x}{\varepsilon}} dx = AR_0 \tag{2}$$

establishes the relationship between ε and the distribution of density behind the direct shock wave $\rho(x)$ under precisely the same conditions. Formula (2) was obtained with the following assumptions: 1) the flow of the mass of gas changes along the critical stream line according to a linear law; 2) the ratio of regression of the shock wave to the radius of curvature of the body R_0 is proportional (with a coefficient A) to the integral compression of gas on the flow axis.

In order to determine the density profile $\rho(x)$, we obtain an approximate solution to the problem of flow behind the front of the direct shock wave in the dissociating gas. We shall examine the relaxation zone behind the direct shock wave in a mixture of gases M_2 and X formed by the dissociation of component M_2 into atoms. The equation for the change of the atomic component is written as follows:

$$\rho v \frac{d\gamma(M)}{dx} = 2\rho^2 k_d \left[\gamma(M_2) - \frac{\gamma^2(M)}{K_p(T)} \right]. \tag{3}$$

where

$$K_d = K_0(T)[k_1(M_2)\gamma(M_2) + k_2(M)\gamma(M) + K_3(X)\gamma(X)], \quad \gamma(N) = n(N)/\rho .$$

By excluding the value $\gamma(M_2)$ from the brackets in the right hand part of equation (3), with the aid of the material balance equation

$$m(M_2)\gamma(M_2) + m(M)\gamma(M) + m(X)\gamma(X) = 1 , \tag{4}$$

and density ρ with the aid of the equation of state, we obtain the equation for determining $\gamma(M)$

$$\frac{d\gamma(M)}{dx} = \frac{2\rho^2 k_d}{\rho v[\lambda + \gamma(X) + \frac{1}{2}\gamma(M)]}\left\{\lambda(\lambda + \gamma(X)) - \frac{\gamma(X)}{2}\gamma(M) - \left[\frac{1}{4} + \frac{\rho}{K_p(T)}\right]\gamma^2(M)\right\} , \tag{5}$$

where

$$\lambda = \frac{1 - m(X)\gamma(X)}{2\,m(M)} , \quad K_p(T) = RTK_0(T) .$$

Thus, if one ignores the relationship between the multiplier before the parenthesis in the right hand part of (5) and $\gamma(M)$, then the rate of dissociation becomes a quadratic function of the concentration of the atomic component. We designate

$$l_1 = \frac{\rho v[\lambda + \gamma(X) + \frac{1}{2}\gamma(M)]}{2\rho^2 k_d} , \quad a_1 = \lambda(\lambda + \gamma(X)) ,$$
$$a_2 = \frac{1}{2}\gamma(X) , \quad a_3 = \frac{1}{4} + \frac{\rho}{K_p(T)} . \tag{6}$$

In order to solve equation (5) with the initial condition

$$\gamma(M) = 0 \quad \text{when} \quad x = 0 \tag{7}$$

we shall consider that the coefficient l_1 and a_3 in the relaxation zone are constant. Below, when making the calculations, we shall use certain average values of these components. The solution to equation (5) has the form

$$\gamma(M) = -\frac{z + a_2}{2a_3} + \frac{z/a_3}{\frac{(z-a_2)^2}{4a_1a_3}\exp\left(-\frac{zx}{l_1}\right) + 1} , \quad z = \sqrt{a_2^2 + 4a_1a_3} . \tag{8}$$

Solution (8) takes a particularly simple form in the case of dissociation of a pure gas, i.e., when $\gamma(X) = 0$

$$\gamma(M) = \frac{2\lambda}{\sqrt{1 + 4\rho/K_p}}\left[\frac{2}{\exp\left(-\frac{zx}{l_1}\right) + 1} - 1\right] , \quad z = \lambda\sqrt{1 + 4\rho/K_p} . \tag{9}$$

It follows from the solution (8) that one should view the value $\ell \cdot \ell_1/\varepsilon$ as the length of relaxation in the dissociating gas, and not simply ℓ_1. In order to obtain the explicit relationship between ℓ and p_∞, we shall assume that the following approximate equalities are valid:

$$\frac{p}{p_\infty} = \frac{\rho_\infty \cdot 1}{\gamma_\infty - 1}, \quad \frac{\rho}{\rho_\infty} = \gamma_\infty M_\infty^2 \tag{10}$$

by substituting (10) in the expression for $\ell \cdot \ell_1/\varepsilon$ we obtain

$$\ell = \frac{\delta(T)}{\rho_\infty \sqrt{1 + a p_\infty}}$$

$$a = \frac{\lambda(\lambda + f(x))}{(\lambda + f(x)/2)^2} \frac{4\gamma_\infty M_\infty^2}{\kappa_p(T)} \tag{11}$$

$$\delta(T) = \varepsilon_\infty \frac{\gamma_\infty - 1}{\gamma_\infty + 1} \frac{1}{\gamma_\infty M_\infty^2} \frac{RT}{m k_d(T)} \left[1 + \frac{f(M) - 2\lambda}{2(2\lambda + f(x))} \right]$$

Thus, the length of relaxation in the dissociating gas is inversely proportional not to p_∞, as with the purely binary processes, but to the value $p_\infty \sqrt{1 + a p_\infty}$. The second factor arises due to the relationship between the equilibrium degree of dissociation and the characteristic pressure. We recall that temperature should be taken in a certain average point of the relaxation zone for calculating a and b.

The distribution of $\rho(x)$ necessary for substitution in equation (2) should be found from the algebraic equations of mass, momentum, and energy conservation using solution (8). In this case, the relationship between $\rho(x)$ and $\exp(-x/\ell)$ would be non-linear, as in formula (8). However, in order to obtain the criterion curve (1), it is more simple to use the linear relationship between $\rho(x)$ $\exp(-x/\ell)$. Such a replacement somewhat changes the value of the integral (2), but it significantly simplifies the calculations. Thus, assuming

$$(\rho - \rho_0)/(\rho_1 - \rho_0) = \exp(-x/\ell) \tag{12}$$

and by substituting this formula in (2) we obtain the relationship between the length of relaxations ℓ and shock wave regression ε

$$\rho_f \varepsilon \cdot (\rho_f - \rho_\ell)\frac{\ell_\ell}{\ell - \ell_\ell} = AR_0\rho_\infty \quad . \tag{13}$$

Here $\rho_f \cdot \rho_\ell$ - density of gas at the beginning and end of the relaxation zone, respectively. Values $\varepsilon_\ell \cdot AR_0\rho_\infty/\rho_\ell$ and $\varepsilon_f \cdot AR_0\rho_\infty/\rho_f$ are equal to regression of the shock wave in the equilibrium and the frozen flows. By using these symbols, we obtain

$$\frac{\ell}{\varepsilon} = \frac{1 - \varepsilon/\varepsilon_\ell}{\varepsilon/\varepsilon_f - 1} \quad . \tag{14}$$

By excluding ε from (14) with the aid of the criterion equality $\ell \cdot k\varepsilon$, we obtain

$$k \cdot \frac{1 - \ell/k\varepsilon_\ell}{\ell/k\varepsilon_f - 1} \quad . \tag{15}$$

We shall insert the dimensionless values of shock wave regression $\varepsilon_{0f} \cdot \varepsilon_f/R_0$ and $\varepsilon_{0\ell} \cdot \varepsilon_\ell/R_0$. By substituting these formulas and expressions [11] for ℓ in formula (15) we obtain the boundary equation of the region of validity of the binary similarity law in the following form:

$$\rho_\infty R_0\sqrt{1 + \sigma\rho_\infty} \cdot \frac{\theta(T)}{T_0 k}\left[\frac{1}{\varepsilon_{0f}} \cdot \frac{1}{k\varepsilon_{0\ell}(\rho_\infty)}\right] \quad . \tag{16}$$

where it is taken into account that the position of the shock wave in the equilibrium flow depends on pressure in the free-stream flow, although quite weakly [3].

If the curve (16) is plotted in the Cartesian coordinate system (ρ_∞, R_0), then the region of applicability of the binary similarity law will lie on the left side of the curve, i.e., in the direction of decrease of the derivative $\rho_\infty R_0$ during motion from the curve, inasmuch as the condition $\ell > k\varepsilon$ is satisfied in this region. Inasmuch as the relationship $\varepsilon_{0\ell}(\rho_\infty)$ is weak, then with sufficiently small p_∞, when $\sigma\rho_\infty$ is small in comparison with unity, curve (16) is similar to a hyperbola $\rho_\infty R_0 \cdot c_0$. With the increase in p_∞, curve (16) intersects the hyperbola with a decreasing constant c (the decrease in c occurs according to the law $c_0/\sqrt{1 + \sigma\rho_\infty}$) and when $\rho_\infty \to \infty$ we have $R_0 \cdot c_0/\rho_\infty^{1/2}$ i.e., R_0 stripes to 0 more rapidly than for the hyperbola. Thence follows the important conclusion that with any value p_∞ R_0, the region of validity of binary similarity law is limited with respect to the high pressure values in the free-stream flow.

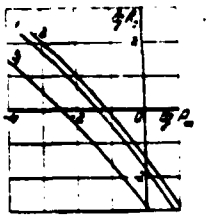

Figure 1

Examples of curves (16) for the case of air are shown in Figure 1 in the logarthmic coordinate system (R_0 in CM , p_∞ in atm). Curves 1 and 2 relate to conditions in the free-stream flow $M_\infty = 13$, $T_\infty = 250°K$, when the dissociation reaction of O_2 predominates. For the curve 1 , $k = 1$, $k = 0.5$ for curve 2. It is evident that the change in k leads to a small, nearly parallel shift of the curve. Curve 3 was plotted for a case $M_\infty = 25$, $T_\infty = 250°K$ ($k = 1$), when nitrogen dissociation is the predominant reaction. Inasmuch as the characteristic length of relaxation in air monotonically decreases with the increase in temperature, then the boundary curves (16) when $13 < M_\infty < 25$ should be situated between curves 1 and 3 (1).

Curve (16) can be viewed in precisely the same way as the arbitrary boundary between the equilibrium and nonequilibrium flows, if one terms a flow to be equilibrium flow in which the length of the relaxation zone does not exceed a certain small proportion of shock wave regression. Inasmuch as $\varepsilon_{ij} \sim \varepsilon_{ot}$, then with small k equation (16) can be somewhat simplified and rewritten in the following form:

$$R_0 \rho_\infty \sqrt{1 + a\rho_\infty} = \frac{\delta(\tau)}{k\varepsilon_{ot}(\rho_\infty)} \qquad (17)$$

REFERENCES

1. Стулов В.П., Теленин Г.Ф. Нерановесное обтекание сферы сверхзвуковым потоком воздуха. Изв. АН СССР, Механика, № 1, 1965.

2. Стулов В.П. О законе подобия при сверхзвуковом обтекании затупленных тел. Изв. АН СССР, Механика жидкости и газа, № 4, 1969.

3. Теленин Г.Ф., Тиняков Г.П. Исследование сверхзвукового обтекания сферы воздуха и углекислым газом при термохимическом равновесии. ДАН СССР, т. 159, стр. 30, 1964.

4. Hall J.G., Eschenroeder A.Q., Marrone P.V. Blunt-nose airflows with coupled non-equilibrium processes. J.Aero.Sci. v.29, 1038,1962.

CONDITIONS ON THE INCIDENT AND REFLECTED SHOCK WAVES IN AN EQUILIBRIUM GAS

by

V. N. Mirskiy

Basic Equations

An equilibrium flow of a gas mixture in shock tubes behind the incident and reflected shock waves is examined. The flow is described by a system of equations which express the laws of conservation of the mass flow, momentum, total energy, and the equations of state. We shall write the equations form a plane, incident wave in the system of coordinates associated with the wave.

$$\rho_1 D_1 = \rho_0 D_0$$

$$\frac{P_1}{\rho_0 D_0^2} + \frac{1}{\rho_1 / \rho_0} = \frac{P_0}{\rho_0 D_0^2} + 1 \qquad (1)$$

$$\frac{h_1}{D_0^2} + \frac{1}{2}\frac{1}{(\rho_1/\rho_0)^2} = \frac{h_0}{D_0^2} + \frac{1}{2}$$

$$h_1 = h_1(P_1, T_1)$$

$$\rho_1 = \rho_1(P_1, T_1) \quad .$$

where P_0, ρ_0, h_0, T_0 - gas parameters ahead of the wave, $\rho_1, \rho_1, h_1, D_1, T_1$ - parameters behind the incident wave subject to determination.

In order to establish gas parameters behind the reflected shock wave and to calculate its velocity D_2, we proceed to a coordinate system which moves with the reflected wave and shall write the laws of conservation for it, taking into account that the gas behind the reflected wave should be at rest relative to the tube end. We immediately note that gas velocity ahead of the reflected wave will be an unknown value relative to the incident wave, unlike the equation of the incident wave. The equations have the following form:

$$
\begin{aligned}
&\rho_2 D_2 = \rho_1 (V_1 + D_2) \\
&p_2 + \rho_2 D_2^2 = p_1 + \rho_1 (V_1 + D_2)^2 \\
&h_2 + \frac{D_2^2}{2} = h_1 + \frac{(V_1 + D_2)^2}{2} \\
&h_2 = h_2 (T_2, P_2) \\
&\rho_2 = \rho_2 (T_2, P_2)
\end{aligned}
\tag{2}
$$

where D_2 is the velocity of gas behind the reflected shock wave, $V_1 = V_o$ --velocity ahead of the reflected shock wave relative to the sides of the tube, a value known from solving problem (1), $(V_1 + D_2)$--gas velocity ahead of the reflected wave in the laboratory coordinate system.

We obtain the following equation system after simple transformations of equation (2):

$$
\begin{aligned}
&\frac{p_2}{\rho_1 V_1^2} + \frac{\rho_2/\rho_1}{(\rho_2/\rho_1 - 1)^2} = \frac{p_1}{\rho_1 V_1^2} + \frac{(\rho_2/\rho_1)^2}{(\rho_2/\rho_1 - 1)^2} \\
&\frac{h_2}{V_1^2} + \frac{1}{2}\frac{1}{(\rho_2/\rho_1 - 1)^2} = \frac{h_1}{V_1^2} + \frac{1}{2}\frac{(\rho_2/\rho_1)^2}{(\rho_2/\rho_1 - 1)^2} \\
&h_2 = h_2 (P_2, T_2) \\
&\rho_2 = \rho_2 (P_2, T_2) \\
&\frac{D_2}{V_1} = \frac{1}{(\rho_2/\rho_1 - 1)}
\end{aligned}
\tag{2'}
$$

Equations (1) and (2') can be written in the universal form with a certain parameter i:

$$
\begin{aligned}
&\frac{p_{i+1}}{\rho_i V_i^2} + \frac{\rho_{i+1}/\rho_i}{(\rho_{i+1}/\rho_i - 1)^2} = \frac{p_i}{\rho_i V_i^2} + \frac{(\rho_{i+1}/\rho_i)^2}{(\rho_{i+1}/\rho_i - 1)^2} \\
&\frac{h_{i+1}}{V_i^2} + \frac{1}{2}\frac{1}{(\rho_{i+1}/\rho_i - 1)^2} = \frac{h_i}{V_i^2} + \frac{1}{2}\frac{(\rho_{i+1}/\rho_i)^2}{(\rho_{i+1}/\rho_i - 1)^2} \\
&h_{i+1} = h_{i+1} (P_{i+1}, T_{i+1}) \\
&\rho_{i+1} = \rho_{i+1} (P_{i+1}, T_{i+1}) \\
&\frac{D_{i+1}}{V_i} = \frac{1}{\rho_{i+1}/\rho_i - 1}
\end{aligned}
\tag{3}
$$

When i = 0, we obtain equations of the incident shock wave (1), when i = 1--reflected wave (2').

For a perfect gas $\gamma = const$ from (2') or (3) when i = 1, one can obtain a gas state behind the reflected shock wave if the pressure ratio P_1/P_0 on the front of the incident wave is known. This can be determined from the system of equations (1), using the measured value of the Mach number M_0 in the form (1):

$$\frac{P_1}{P_0} = \left\{\frac{2\gamma M_0^2 - (\gamma - 1)}{\gamma + 1}\right\} \cdot \left\{\frac{(3\gamma - 1)M_0^2 - 2(\gamma - 1)}{(\gamma - 1)M_0^2 + 2}\right\} \tag{4}$$

$$\frac{T_1}{T_0} = \frac{\{2(\gamma - 1)M_0^2 + (3\gamma - 1)\} \cdot \{(3\gamma - 1)M_0^2 - 2(\gamma - 1)\}}{(\gamma + 1)^2 M_0^2} \tag{5}$$

The ratio of the velocity of the reflected wave front to the velocity of the free-stream flow can be determined in the form [1]

$$\frac{D_2}{U_0} = \frac{2 + \frac{2}{\gamma - 1}\frac{P_1}{P_0}}{\frac{U_1^2}{\gamma P_1} + \frac{P_1}{P_0}}$$

or by replacing P_1/P_0 with its value via M_0 and γ, we obtain:

$$\frac{D_2}{U_0} = \frac{2(\gamma - 1)\{2\gamma M_0^2 - (\gamma - 1)\} + 2(\gamma - 1)}{(\gamma + 1)\{2\gamma M_0^2 - (\gamma - 1)\} + (\gamma - 1)} \tag{6}$$

CALCULATION OF THE EQUILIBRIUM GAS PARAMETERS

A program of calculating chemical equilibrium of an arbitrary, multicomponent gas system was used to find h and ρ in the system (3). In order to calculate the integral and differential thermodynamic characteristics $\mu, h, u, s, c_p, c_v, \gamma, a, \rho$, it is necessary to know the equilibrium gas composition. Finding the equilibrium composition of a chemically reacting gas at assigned temperature and pressure pertains to solving a system of nonlinear, algebraic equations in which the following are mathematically written: The law of conservation of matter, Dalton's law and the law of moving masses. An equation of neutrality of the gas mixture is inserted into the general system, if ionized components are considered in the reaction products. The ionized reaction products are included in the material balance

equation, the Dalton equation, and increase the number of equations of the law of acting masses. The nonlinear, algebraic equation system is solved by the Newton method. The linear equation system obtained in this case for the logarithmic correction is solved by the Gaussian method with selection of the main component.

Practical work with the program includes the following stages. The number K is determined on the basis of the initial chemical composition of the gas system. One then determines the number i, where K is the number of elements, including the electrons, while i is the number of components. A strict order of gas system components is preliminarily established, and then all atomic components and electrons are arranged at the beginning of the list. A matrix of stoichiometric coefficients $\|A_{ik}\|$ is constructed according to the selected i and K numbers. Coefficients of polynomials φ_i^* for the thermodynamic potentials, the level of determining enthalpy ΔH_i, the material constants $c_k = \sum_i A_{ik} N_i$, and the initial approximation $\ln N_0^*$, $\ln N_1^*, \ldots, \ln N_i^*$ are written in the point from which the calculation begins. $N_0^* = \sum$ --total number of moles, while $N_1^*, \ldots N_i^*$ --number of moles of the base components.

The program provides for orientation to any set of the K base components of all sets i. The transition in the calculation process to orientation according to the predominant components provides a gain during calculations and expands the region of convergence of the Newton method.

When making the series of calculations in a certain range of temperature, it is more convenient to begin the calculation with the higher temperatures, inasmuch as one can take the composition of the fully dissociated mixture as the initial approximation in this case.

The final results subject to print out are arranged, beginning with a cell $\alpha \ldots (N+13)+5K+9$, where $\alpha = (1000)_8$. The following values are printed out $T, P, N_0, N_1, \ldots, N_i$.

$S, h, a, c_p, c_v, \gamma, \sigma, \mu, \gamma$.

where T and P are temperature and pressure at which the thermodynamic values and the mixture's composition are calculated, N_o--total number of moles, N_i--number of moles of the components i, s--entropy of mixture, h--enthalpy, u--internal energy, C_p and C_v--heat capacities at constant pressure and volume, respectively, $\gamma = C_p/C_v$ -- adiabatic exponent, μ--molecular weight of mixture, ρ--density. The last occupied MOZU cell (ρ) has the address $\alpha + (K+4) + 5K + 6$

This program can be used as a subprogram, for example, for solving the gas dynamic problem.

The maximum possible values of i and K can be determined from the approximate relationship:

$$512 + 2(K+14) + 5K + 16 = 3071$$

or

$$2K + 14i + 5K = 2543$$

Assuming that K = 10, we obtain $i = 104$, etc.

One can familiarize one's self in detail with the mathematical process and the method of solution [2].

Calculation time on the triple address computer with an operational memory volume of $(4096)_{10}$ cells of 1 point (T, P) ranges from a few seconds to 1-1/2 minutes, depending on K and i, as well as on the method of assigning the initial approximations during transition from one point to another. The simplest method was chosen in the given version: The solution in the preceding point is taken as the initial approximation in the next point.

THE NUMERICAL SOLUTION

Numerical calculations of the thermodynamic and gas dynamic parameters behind the plane incident and reflected shock waves in a

mixture of gases consisting of Ar and H_2O were made as an example. The system of equations (3) was solved by the Newton method with the following initial conditions: P_o = 0.0065 atm, T_o = 293.15°K; a range of the velocities of the incident wave from 1500 m/sec to 5000 m/sec with a step ΔU_o = 250 m/sec was examined. The program took into account the following components: $H, O, Ar, H_2, O_2, H_2O, OH$. Calculations were made with various initial molar concentrations of water in the mixture: $\chi(H_2O) = 10^{-9}$; 0,001 ; 0,01 ; 0,05 ; 0,1 ; 0,2 ; 0,3 ; 0,5.

Figures 1-8 give the results of calculating the gas dynamic parameters behind the incident and reflected shock wave depending on the velocity of free-stream flow and the molar concentrations of the gas in the cold state. The dash curve in all the graphs is a calculation of the mixture of gases consisting of $\chi(H_2O) = 10^{-9}$ and $\chi(Ar) = 1 - 10^{-9}$ in the cold state, i.e., an "almost" perfect gas. It follows from an examination of the thermodynamic potential of argon

$$\Phi_T^\circ(Ar) = 49,4668 + 4,9682 \ln T$$

that the enthalpy of argon acquires the form:

$$h(Ar) = \Phi_T^{\circ\prime}(Ar)T^2 + \Delta H(Ar) = 4,9682T + \Delta H(Ar) = C_pT + \Delta H(Ar),$$

where C_p = 4.9682. It follows from the relationship $c_p - c_v = R$ that γ = 1.66.

According to the theory of the reflected wave, gas pressure and temperature increase approximately as the square of velocity, while density tends toward a finite value in a perfect gas, with the increase in shock wave velocities (formulas (4) and (5)).

The velocity of the reflected shock wave was calculated according to formula (6) for certain values of velocity of the free-stream flow and a comparison was made with the numerical results. The deviation does not exceed 4 m/sec.

Figures 1 and 2 give the relationship between the velocity of gas behind the incident and reflected shock waves in the laboratory coordinate system and the velocity of the free-stream flow.

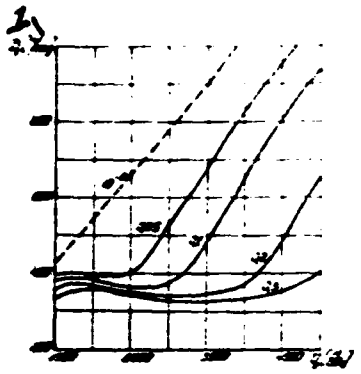

Figure 1
Key: (1) 1 M/sec

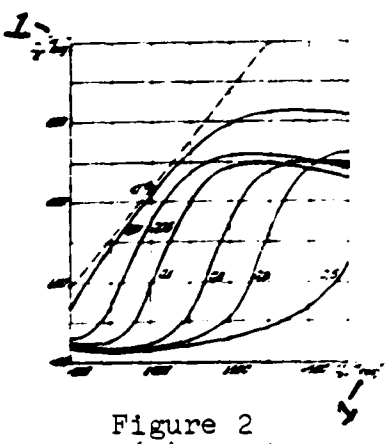

Figure 2
Key: (1) 1 M/sec

On each curve, the molar concentration of water in the cold state which corresponds to this version is indicated. The great difference between the dash curve and the solid lines is due to the transport of part of the kinetic energy of the gas to vibratory energy of the molecules in the real gas, by energy expenditures on the dissociation of molecules into atoms and electron excitation of atoms. The given calculation did not take into account the ionization of atoms and molecules, but this effect does not introduce additional difficulties into the function of the program and can easily be taken into account if desired.

Velocity behind the incident and reflected shock waves begins to diminish with the increase in the velocity of the free-stream flow V_0 from a value V_0 = 1500 M/sec. This decrease is associated with excitation of the internal degrees of freedom of the molecules and dissociation of molecules into atoms. It is interesting to note one characteristic of this problem. In those points in which velocity behind the incident and the reflected shock waves acquires its least value, the concentrations of H_2, O_2 and OH reach their maximum value. With the subsequent increase in velocity of the free-stream flow these components begin to dissociate. This is because the equilibrium constants of H_2, O_2 and OH are very similar at these temperatures. Dissociation practically terminates with the increase in velocity of incident wave, and the gas behaves as a perfect gas. At high velocities of the free-stream flow, the electron excitation of atoms entails a loss of kinetic energy of the gas, and as a

consequence, a decrease in the growth of gas velocity behind the incident wave, and even a slight drop in velocity of the reflected shock wave.

Figures 3 and 4 give the distribution graphs of density behind the incident and reflected waves depending on the velocity of the free-stream flow. As should have been expected, the ρ/ρ_0 ratio for the "nearly" perfect gas tends toward 4 with the increase in velocity of the free-stream flow, inasmuch as, according to the formula $\rho/\rho_0 = \frac{(\gamma+1)M_0^2}{(\gamma-1)M_0^2+2}$ when $M_0 \to \infty$ and $\rho/\rho_0 \to \frac{\gamma+1}{\gamma-1}$.

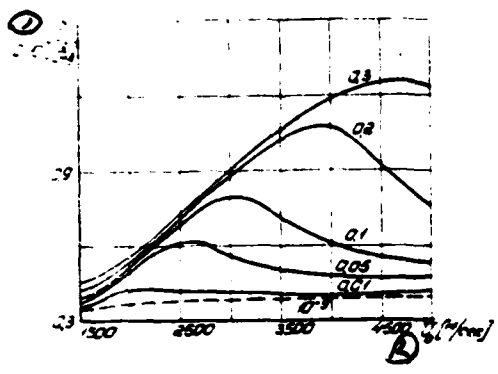

Figure 3
Key: (1) 1 m/sec^2 $\frac{G}{CM^3}$
(2) (M)sec

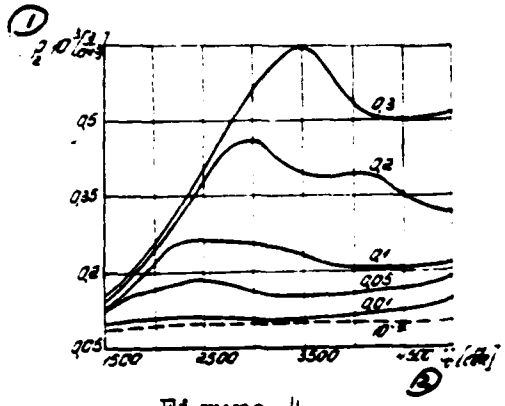

Figure 4
Key: (1) 1 m/sec^2 $\frac{G}{CM^3}$
(2) $\frac{M}{sec}$

Figures 5 and 6 show the relationship between temperature and the velocity of the free-stream flow. At low velocities of the free-stream flow, only the advancing and rotational degrees of freedom of the gas molecules are excited. In this case, as in the case of the ideal gas, temperature is the subordinate to an approximately parabolic relationship with shock wave velocity. Heat capacity of the gas increases with the increase in the velocity of the incident wave as the result of the excitation of the vibratory degrees of the molecules. Therefore, its temperature decreases more slowly than the temperature of an ideal gas. This slowing becomes particularly noticeable when thermal energy is expended on dissociation.

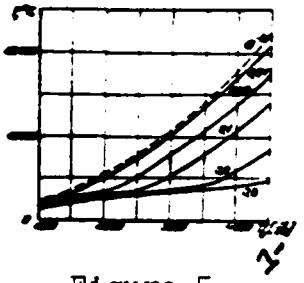

Figure 5
Key: 1 M/sec

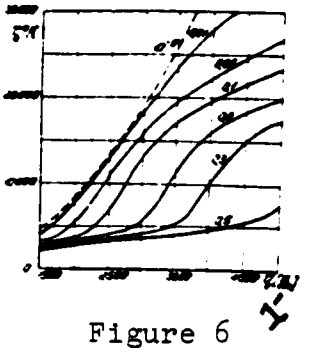

Figure 6
Key: 1 M/sec

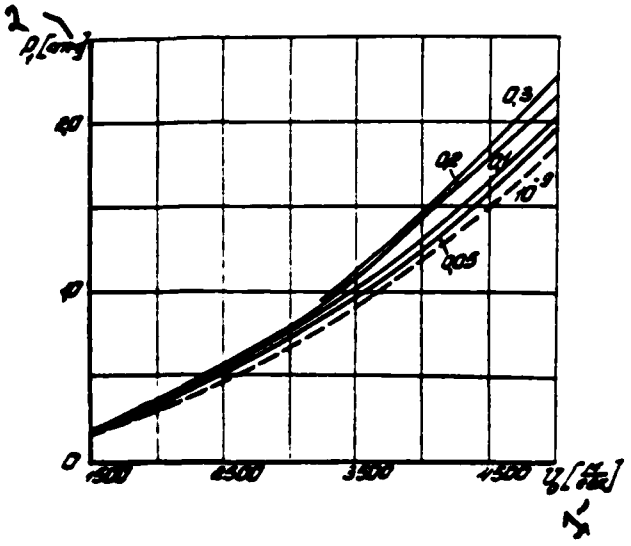

Figure 7
Key: 1 M/sec 2 atm

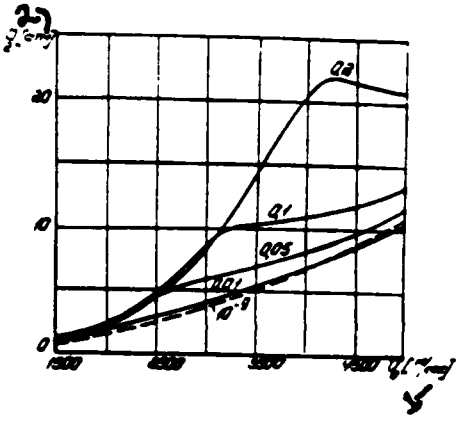

Figure 8
Key: 1 M/sec
2 atm

Figures 7 and 8 depict graphs of pressure behind the incident and reflected shock wave depending on velocity of the free-stream flow.

REFERENCES

1. Гейдон А.Г., Герл И.Р. Ударные трубы в химической физике высоких температур. М., "Мир", 1966.

2. Рождественский И.Б., Шевелев В.П., Овсянников К.К. Сб. Физическая газодинамика. М., "Наука", 1967.

INVESTIGATION OF A SPATIAL, SUPERSONIC FLOW AROUND THE LEADING PART OF BLUNT BODIES BY THE ESTABLISHMENT METHOD

by

Yu. M. Lipnitskiy, Yu. Ya. Mikhaylov and K. G. Savinov

In order to solve the problem of supersonic flow around blunt bodies, the establishment method was used. This method is based upon a difference device [1,2] in combination with the trigonometric approximation. The results of calculations of triaxial ellipsoids are given as an example. Primary attention was paid to investigating flows without a symmetry plane. The described algorithm is a modification of methods presented in works [3,5].

We shall take a system of gas dynamic equations in the spherical coordinate system r, θ, φ, which describes the unsteady three-dimensional flows, in the following characteristic form:

$$A\frac{\partial X}{\partial t} + \Lambda A \frac{\partial X}{\partial \xi} = f$$

$$X = \begin{bmatrix} v \\ c \\ V \\ W \\ \beta \end{bmatrix} \qquad A = \begin{bmatrix} \gamma/c & -1 & 0 & 0 & 0 \\ \gamma/c & 1 & 0 & 0 & 0 \\ 0 & 0 & 1 & 0 & 0 \\ 0 & 0 & 0 & 1 & 0 \\ 0 & 0 & 0 & 0 & 1 \end{bmatrix} \tag{1}$$

Here t' is time; $\xi = \xi(t, r, \theta, \varphi)$ --a function which satisfies conditions $\xi[t, G(t,\theta,\varphi), \theta, \varphi] = 0$, $\xi[t, F(t,\theta,\varphi), \theta, \varphi] = 1$, $r = \theta(t, \theta, \varphi)$ and $r = F(t, \theta, \varphi)$ equations of the surfaces of the body and the shock wave, γ--relationship of specific heat capacities, c--speed of sound, $\beta = \xi_t + \gamma \xi_r, v = (u\xi_r + v\xi_\theta/r + w\xi_\varphi/r\sin\theta)/|\nabla|$ is the projection of velocity vector on the normal to the surface $\xi(t, r, \theta, \varphi) = \text{const}$ $(n:[\xi_r; \xi_\theta/r; \xi_\varphi/r\sin\theta])$, and V and W are projections on 2 linearly independent vectors of the orthogonals $n(V = (v\xi_\theta - u\xi_\theta/r)/|\nabla|$, $W = (w\xi_\theta - u\xi_\varphi/r\sin\theta)/|\nabla|$; u, v, w -components of the velocity vector along axes (r, θ, φ). Λ--diagonal matrix with elements of the type

$$\lambda(\eta) = \xi_t + (U + nC)|N| \quad . \tag{2}$$

namely, $\Lambda_{11} = \lambda(-1)$, $\Lambda_{22} = \lambda(1)$, $\Lambda_{33} = \Lambda_{44} = \Lambda_{55} = \lambda(0)$.
In addition to the sought functions and their derivatives according to Θ and ψ, $\xi_{t\theta}$ and $\xi_{t\psi}$ also enter into the composition of the vector of the right hand part of f.

The solution is sought in the region bounded by the surface of the body, the shock wave, and the conical surface $\theta = \theta_s$. This surface is selected such that the velocity component normal to it is greater than the speed of sound. One should impose the following boundary conditions for unity of solution to the examined problem. On the body $(\xi = 0)$ condition,

$$U = G_t/|N| \tag{3}$$

should be satisfied and $(\xi = 1)$ should be satisfied on the shock wave--conditions of conservation of flows of mass, energy, and momentum

$$\rho(U - D) = \rho_\infty(U_\infty - D) \tag{4}$$

$$p + \rho(U - D)^2 = p_\infty + \rho_\infty(U_\infty - D)^2 \tag{5}$$

$$(U - D)^2 + 2H = (U_\infty - D)^2 + 2H, \quad H = H(p, \rho) \tag{6}$$

$$V = V_\infty, \quad W = W_\infty. \tag{7}$$

Here the subscript ∞ designates parameters ahead of the shock wave while $D = -\xi_t/|N|$ designates the relative velocity of displacement of the shock wave in the normal direction.

It is assumed that t = 0 assigns the position of the shock wave and the distribution of all gas dynamic parameters in the region where the solution is sought at an initial moment of time. The steady-state solution is obtained as the unsteady limit, when $t \to \infty$ with boundary conditions of the problem that do not change in time (parameters of the free-stream flow and the conditions of non-flow on the surface of the body). It is subsequently considered that $G_t = 0$.

We take the following grid during construction of the numerical method $t_n = n\tau$,

$$\xi_m = m/M\ ,\ \theta_\ell = \ell\theta_0/L\ ,\ \psi_k = 2\pi k/K\ ;\ n = 0,1,\ldots;$$
$$m = 0,1,\ldots,M\ ;\ \ell = 0,1,\ldots,L\ ;\ k = 0,1,\ldots,K-1\ .$$

Following work [6], we used the trigonometric approximation according to ψ for smooth bodies, and for the nonsymmetrical bodies, in order to improve accuracy, we introduce the radius of the body into the approximation formulas. With an even K, such an approximation has the form:

$$X = G(\theta,\psi)\left[\sum_{i=0}^{K/2} a_i \cos i\psi + \sum_{i=1}^{\frac{K}{2}-1} b_i \sin i\psi\right].$$

The inclusion of the trigonometric approximation makes it possible to insure sufficient accuracy without a significant increase in the grid nodes.

Equations of the system which is obtained following the trigonometric approximation are replaced by difference equations in the following way: All equations which correspond to the first two equations in system (1) are approximated in the nodes $(n+\frac{1}{2},\ m+\frac{1}{2},\ \ell,\ k)$.

$$\left.\begin{aligned}
&\frac{\partial X}{\partial t} = \frac{1}{2\tau}\left(X^{n+\frac{1}{2}}_{m,\ell,k} + X^{n+\frac{1}{2}}_{m+1,\ell,k} - X^{n}_{m,\ell,k} - X^{n}_{m+1,\ell,k}\right) - \\
&-\frac{\mu_1 m_2}{2\tau}\left(X^{n}_{m,\ell+1,k} - 2X^{n}_{m,\ell,k} + X^{n}_{m,\ell-1,k} - X^{n}_{m+1,\ell+1,k} - 2X^{n}_{m+1,\ell,k} + \right. \\
&\left. + X^{n}_{m+1,\ell-1,k}\right) - \frac{\mu_2}{2\tau}\left[\left(\frac{\partial^2 X}{\partial \psi^2}\right)^{n}_{m,\ell,k} + \left(\frac{\partial^2 X}{\partial \psi^2}\right)^{n}_{m,\ell,k}\right]
\end{aligned}\right| \qquad (8)$$

$$\left.\begin{aligned}
&\frac{\partial X}{\partial \xi} = \frac{m_2}{\tau}\left[\alpha\left(X^{n-\frac{1}{2}}_{m-1,\ell,k} - X^{n-\frac{1}{2}}_{m,\ell,k}\right) + \beta\left(X^{\circ}_{m-1,\ell,k} - X^{\circ}_{m,\ell,k}\right)\right. \\
&\frac{\partial X}{\partial \theta} = \frac{m_2}{4\tau}\left[\alpha\left(X^{n-\frac{1}{2}}_{m,\ell,k} + X^{n-\frac{1}{2}}_{m-1,\ell-1,k} - X^{n-\frac{1}{2}}_{m,\ell-1,k} - X^{n-\frac{1}{2}}_{m,\ell-1,k}\right) + \right. \\
&\left. + \beta\left(X^{\circ}_{m,\ell-1,k} + X^{\circ}_{m-1,\ell-1,k} - X^{\circ}_{m,\ell-1,k} - X^{\circ}_{m,\ell-1,k}\right)\right. \\
&\left. X = \frac{1}{4}\left(X^{n-\frac{1}{2}}_{m,\ell,k} + X^{n-\frac{1}{2}}_{m-1,\ell,k} + X^{\circ}_{m,\ell,k} + X^{\circ}_{m-1,\ell,k}\right)\right]
\end{aligned}\right\}$$

The remaining equations are approximated in the nodes $\{n+\frac{1}{2}, m, l, k\}$

$$\left.\begin{aligned}
&\frac{\partial X}{\partial t} = \frac{1}{\tau}\left(X^{n+\frac{1}{2}}_{m,l,k} - X^{*}_{m,l,k}\right) - \frac{\mu_1 m_1}{\tau}\left(X^{*}_{m,l-1,k} - 2X^{*}_{m,l,k} + X^{*}_{m,l+1,k}\right) - \\
&\quad - \frac{\mu_2}{\tau}\left(\frac{\partial^2 X}{\partial \varphi^2}\right)^{n+\frac{1}{2}}_{m,l,k} \\
&\frac{\partial X}{\partial \xi} = \frac{m_1}{2\tau}\left[A\left(X^{n+\frac{1}{2}}_{m,l,k} - X^{n+\frac{1}{2}}_{m-1,l,k}\right) + A\left(X^{*}_{m,l,k} - X^{*}_{m-1,l,k}\right)\right] \\
&\frac{\partial X}{\partial \theta} = \frac{m_2}{2\tau}\left[A\left(X^{n+\frac{1}{2}}_{m,l+1,k} - X^{n+\frac{1}{2}}_{m,l-1,k}\right) + A\left(X^{*}_{m,l+1,k} - X^{*}_{m,l-1,k}\right)\right] \\
&X = \frac{1}{2}\left(X^{*}_{m,l,k} + X^{n+\frac{q-1}{2}}_{m,l,k}\right)
\end{aligned}\right\} \qquad (9)$$

In formulas (8) and (9) $m_1 = \tau/h_1$, $m_2 = \tau/h_2$ $\left(h_1 = \frac{1}{M}, h_2 = \frac{\theta_0}{L}\right)$, $\alpha + \beta = 1$, $\alpha\beta > 0$, $q = 1, 2$.
And when $q = 1$ $\mu_1 > 0$, $\mu_2 > 0$ and when $q = 2$ $\mu_1 = \mu = 0$.
Such an approximation insures the second order of accuracy for the for the steady-state solution.

Boundary equations are written in the following way in the difference form:

on the body

$$v^{n+\frac{q}{2}}_{m,k,l} = 0 \qquad (10)$$

on the shock wave

$$\rho^{n+\frac{q}{2}}_{m}\left(v_m - D\right) = \rho_\infty\left(v^{n+\frac{q-1}{2}}_{\infty} - D\right) \qquad (11)$$

$$p^{n+\frac{q}{2}}_{m} + \rho^{n+\frac{q}{2}}_{m}\left(U_m - D\right) = p_\infty + \rho_\infty\left(v^{n+\frac{q-1}{2}}_{\infty} - D\right) \qquad (12)$$

$$\left(U_m - D\right)^2 + 2H^{n+\frac{q}{2}}_{m} = \left(v^{n+\frac{q-1}{2}}_{\infty} - D\right)^2 + 2H^{n+\frac{q}{2}}_{\infty} \qquad (13)$$

$$V_m = V^{n+\frac{q-1}{2}}_{\infty}, \quad W_m = W^{n+\frac{q-1}{2}}_{\infty} \qquad (14)$$

$$U_m = \left[u^{n+\frac{q}{2}}_{m} - \left(\frac{r_\varphi}{r}\right)^{n+\frac{q-1}{2}} v^{n+\frac{q}{2}}_{m} - \frac{1}{\sin\theta}\left(\frac{r_\varphi}{r}\right)^{n+\frac{q-1}{2}} w^{n+\frac{q}{2}}_{m}\right] \Big/ |N|^{n+\frac{q-1}{2}}_{m}$$

$$V_m = \left[v^{n+\frac{q}{2}}_{m} + \left(\frac{r_\varphi}{r}\right)^{n+\frac{q-1}{2}} u^{n+\frac{q}{2}}_{m}\right] \Big/ |N|^{n+\frac{q-1}{2}}_{m}$$

$$W_m = \left[w^{n+\frac{q}{2}}_{m} + \frac{1}{\sin\theta}\left(\frac{r_\varphi}{r}\right)^{n+\frac{q-1}{2}} u^{n+\frac{q}{2}}_{m}\right] \Big/ |N|^{n+\frac{q-1}{2}}_{m}$$

$$D = F_c^{n+\frac{q}{2}} \Big/ |N|^{n+\frac{q-1}{2}}_{m}$$

Here the coordinates of the shock waves and their derivitives according to Θ and ψ are taken from the previous iteration.

Unilateral differences are used on the boundary of the region situated in the supersonic part of the flow (i.e., when $l = L$) in place of the symmetrical differences for approximating the derivations according to Θ. Another deviation from the presented approximation is the $\Theta = 0$ line, where the existing characteristics are preliminarily revealed according to the L'Hopital rule. Here, too, the unilateral differences are used for approximating all expressions which contain differentiation according to Θ.

After replacing the differential equations with differences, the determination of all sought values of $x^{\cdots}_{m,l,k}$ breaks down into a series of independent boundary problems. For $v^{\cdots}_{m,l,k}$ and $\varepsilon^{\cdots}_{m,l,k}$ with identical k, l indices, this is a system of the type

$$\begin{bmatrix} \omega^{(1)}_{m-\frac{1}{2}} & 0 \\ 0 & 1 \end{bmatrix} \begin{bmatrix} \gamma/c & 1 \\ \gamma/c & -1 \end{bmatrix} \begin{bmatrix} v \\ \varepsilon \end{bmatrix}_{m-1} + \begin{bmatrix} 1 & 0 \\ 0 & \omega^{(2)}_{m-\frac{1}{2}} \end{bmatrix} \begin{bmatrix} \gamma/c & 1 \\ \gamma/c & -1 \end{bmatrix} \begin{bmatrix} v \\ \varepsilon \end{bmatrix}_{m} = \bar{f}_{m-\frac{1}{2}} \qquad (15)$$

$$m = 0, 1, \ldots, M$$

jointly with the boundary conditions (10)-(13). The following systems are obtained for the other values

(16)

$$\omega^{(3)}_m y_{m+1} + y_m - \omega^{(3)}_m y_{m-1} = h \quad ; \quad m = 0, 1, \ldots, M-1$$

$$y = V, \text{ or } W, \text{ or } \delta$$

$$\omega^{(1)} = \frac{1 - 2\alpha\, m, \lambda(+1)}{1 + 2\alpha\, m, \lambda(+1)}, \quad \omega^{(2)} = \frac{1 + 2\alpha\, m, \lambda(-1)}{1 - 2\alpha\, m, \lambda(-1)}, \quad \omega^{(3)} = \frac{\alpha}{2}\, m, \lambda(0)$$

The indices $\cdots_{\frac{1}{2}}$, k and l are omitted in systems (15) and (16).

Such separation of the difference equations is achieved thanks to the transition from variables u, v, w to variables v, V, W. Otherwise, one must jointly solve the double flow difference equations as, for example, in a work [1].

The system (15) is solved by the trial and error method, when the direct course consists in the successive construction of

relationships

$$v_m = \alpha\varepsilon_m + \beta_m \qquad m = 0, 1, \ldots, M \qquad (17)$$

When m = 0, the boundary condition (10) is taken as (17). All subsequent trial and error relationships are obtained by excluding v_m, ε_m from the second equation (15) with the aid of the preceding trial and error relationship and the first equation (15). Relationship (17) when m = M, jointly with the boundary conditions on the shock wave (11)-(13) make it possible to determine all sought functions on the shock wave. The determination of v_m, ε_m in the other nodes takes place on the basis of the first equations of the system (15) and relationships (17).

Inasmuch as $\omega_-^{(0)}$ is proportional to $\lambda_m(0)$, then because of the boundary condition (10) we have $\omega_-^{(0)} = 0$. Thus, the difference equation (16) when m = 0 can be interpreted as a boundary condition. Consequently, finding V, W, and δ after solving the problem (15) pertains to solving boundary value problems for three-point scalar equations, whose solution methods are widely known.

The satisfaction of conditions of uniform correctness of the boundary value problems is necessary and sufficient for stability of the trial and error method. According to a work [7], this is equivalent to satisfying the inequalities

$$\lambda(-1) < 0 \qquad (18)$$

$$\lambda(+1) > 0 \qquad (19)$$

we note that in the case of using the approximation formulas (8) for all five equations (1), the conditions of uniform correctness are

$$\lambda(0) < 0 \qquad (20)$$

$$\lambda(+1) > 0 \qquad (21)$$

Conditions (18) significantly expand the region of stability of the trial and error method in comparison with (20) which makes it possible to select the transformation $\xi = \xi(t, x, \delta, \nu)$ proceeding from the condition of the best approximation of these sought functions.

The choice of the coefficient μ_1 is made taking into account the inequality

$$(|v|+c)^2 \frac{\tau}{2h_1} \leq \mu_1 . \qquad (22)$$

This condition is a sufficient condition of stability of the employed difference method for the scalar equation. When $\alpha \neq \beta$ conditions (22) are also necessary.

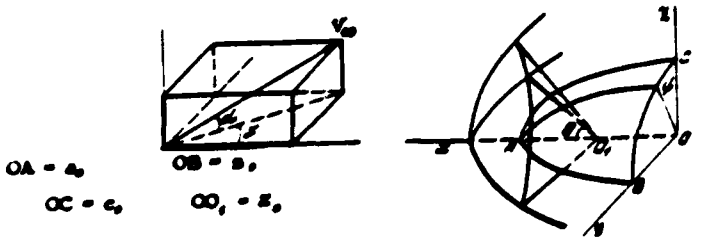

Figure 1

Calculations were made in the spherical coordinate system r, θ, ψ, whose center is situated on the axis x of the streamlined ellipsoid (Figure 1). The distance from the center of the coordinate system to the center of the ellipsoid is symbolized by x_0. The selected difference grid is characterized by the following parameters: M = 10, L = 20, K = 6. The transformation of $\xi = \xi(t, r, \theta, \psi)$ was taken in the form

$$\xi = [r - G(\theta, \psi)] / [F(t, \theta, \psi) - G(\theta, \psi)] .$$

The velocity components u, v, w relate to the maximum velocity V_{max}, pressure $p = k \rho_\infty V^2_{max}$, density $\rho = k \rho_\infty$. The linear dimensions pertain to the value of the semi-axis of the ellipsoid in the direction of the axis x, and the ellipsoid was characterized by the values $b_1 = \frac{a}{c}$, $b_2 = \frac{b}{c}$ (a, b, c)--dimensions of the ellipsoid semi-axis in the direction of axes x, y, z). The Mach number of the free-stream flow $M_\infty = 3$ for all calculations, and the adiabatic exponent $\gamma = 1.4$.

With the goal of making a comparison with the results obtained by other methods, calculation of flow around an ellipsoid with $b_1 = 2, b_2 = 1$ at an angle of attack $\alpha = 5^\circ$ ($M_\infty = 3$, $\gamma = 1.4$). was made. Figure 2 shows the picture of intersection of the shock

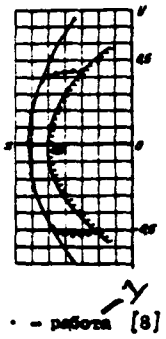

Figure 2
Key 1: work [8]

wave and the sonic surface by the plane $\varphi = 0.7$. In this same figure, the circles plot the values for the corresponding calculation obtained by the G. F. Telenin method [8]. As is evident, the coincidence of the geometrical pictures is very good. The comparison of the gas dynamic values in the shock layer that was made showed that the maximum difference that exists on the edge rays does not exceed 4%.

In order to investigate the effect of the non-axisymmetric nature of the body on the character of flow, flow was examined at a zero angle of attack on ellipsoids with fixed $\delta_1 = 2$ and $\delta_2 = 1$; $\delta_2 = 1.25$; $\delta = 1.5$ (in these calculations, $\Theta_R = 1.125$; $x_0 = 1.5$). It is interesting to trace how the change in flow occurs in the cross section $\psi = 0$, inasmuch as the contour of the body here is identical for all three ellipsoids. The position of the shock waves and the sonic lines for this cross section is shown in Figure 3. Pressure along the body according to the coordinate $\theta = \theta/\theta_*$ is shown in Figure 4. Figure 5 and Figure 6 give an idea of flow in the plane $\varphi = \frac{\pi}{2}$. The distributions of velocity, pressure and density on the axes plotted according to the coordinate ξ are identical for all three cases (figures 7 and 8). Consequently, the conclusion of a work(9) that flow on the axis is solely determined by parameters of the free-stream flow, which conclusion was drawn for axisymmetric bodies, can be generalized to a broader class of bodies.

The study of properties of spatial flow with the absence of a plane of symmetry in the shock layer is of particular interest. Such an investigation was made for an ellipsoid with parameters $\delta_1 = 3$ and $\delta_2 = 2$. With a fixed angle of attack $\alpha = 15°$, the slip angle changed from 0° to 15°. Figures 9-11 give the geometrical pictures of flow in the plane $\varphi = 0, \frac{\pi}{6}, \frac{\pi}{3}, \frac{\pi}{2}$ for angles of 0°, 5°, 10° and 15° (respectively, curves 1, 2, 3, 4). The distribution of pressure along the body according to the coordinate $\theta = \theta(x_* = 1.5)$ in the indicated planes is shown in Figures 12-14. When the slip angle increases from 0° to 15°, the greatest changes

in pressure distribution occur in the half- planes $\varphi = \frac{1}{3}\pi$ and $\varphi = \frac{4}{3}\pi$. For example, when $\theta = 38°$ in the half plane $\varphi = \frac{1}{3}\pi$ pressure increases by 27%, and pressure decreases by 26% in the half plane $\varphi = \frac{4}{3}\pi$.

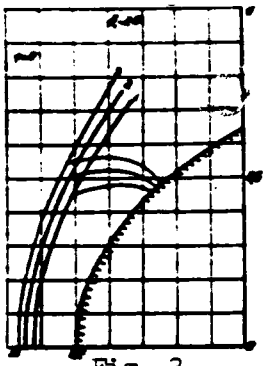

Fig. 3

1. – $\delta_2 = 1$; 2. – $\delta_2 = 1{,}25$; 3. – $\delta_2 = 1{,}5$

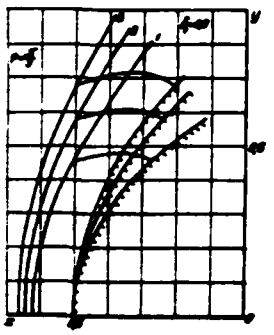

Рис. 5

1. – $\delta_2 = 1$; 2. – $\delta_2 = 1{,}25$; 3. – $\delta_2 = 1{,}5$

Figure 5

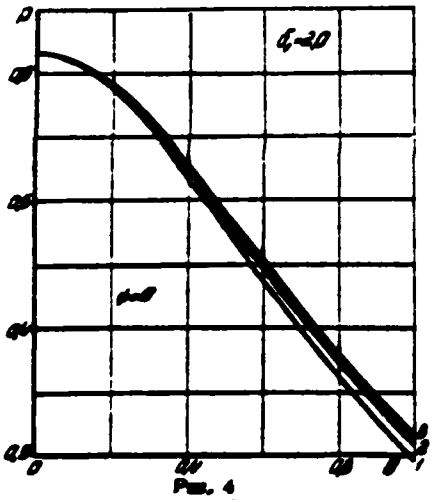

Рис. 4

1. – $\delta_2 = 1$; 2. – $\delta_2 = 1{,}25$; 3. – $\delta_2 = 1{,}5$

Figure 4

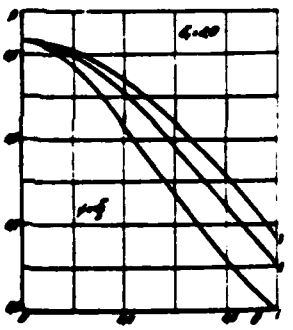

Рис. 6

1. – $\delta_2 = 1$; 2. – $\delta_2 = 1{,}25$; 3. – $\delta_2 = 1{,}5$

Figure 6

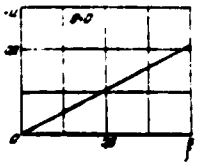

Figure 7

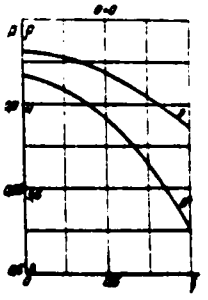

Figure 8

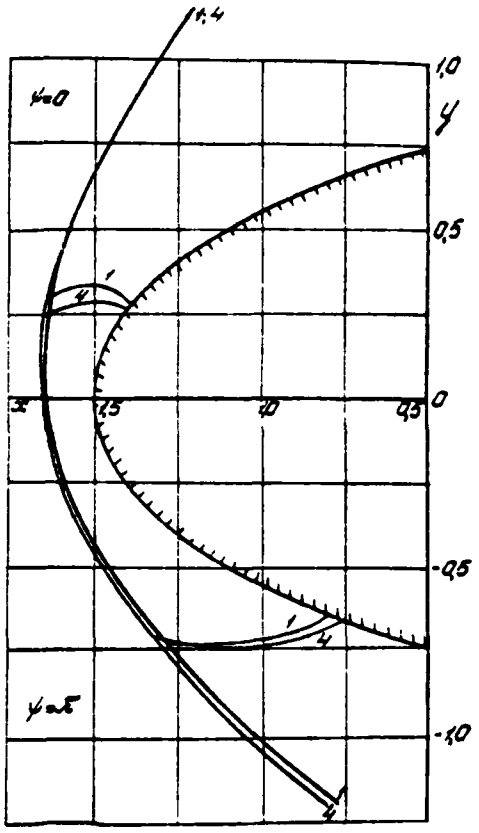

Figure 9

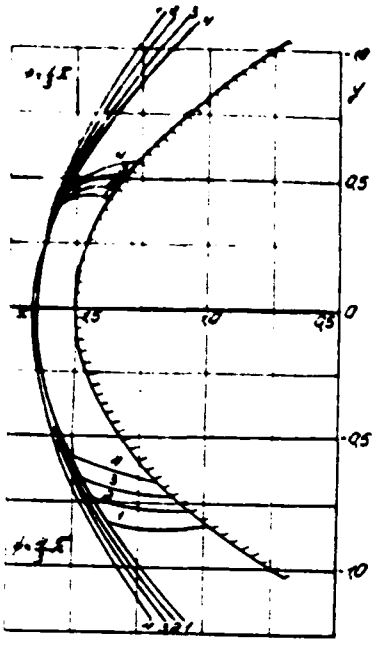

Figure 10

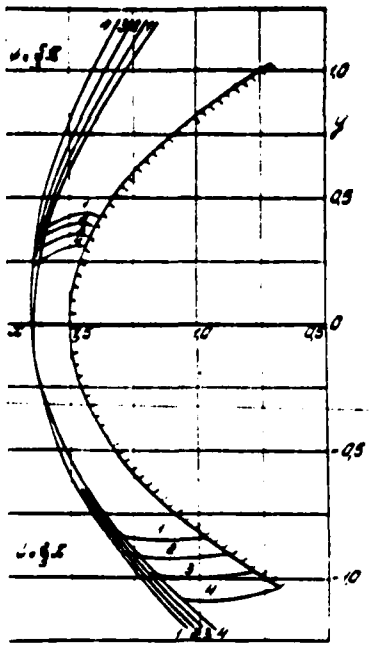

Figure 11

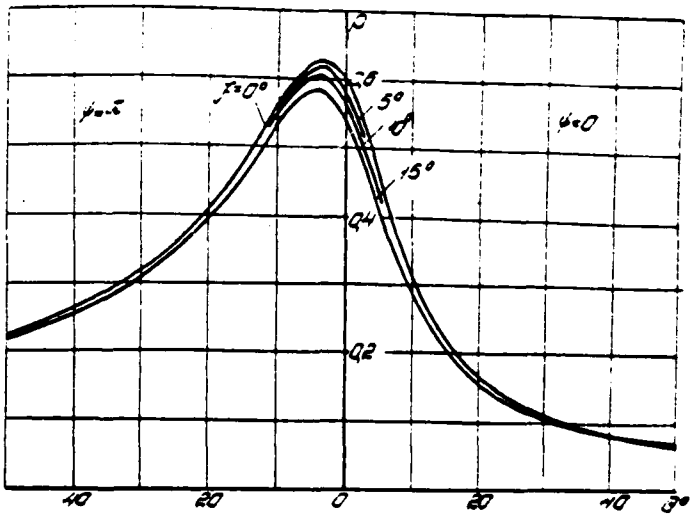

$\xi = 0, \quad \alpha = 15^{\circ}$

Figure 12

Figure 13.

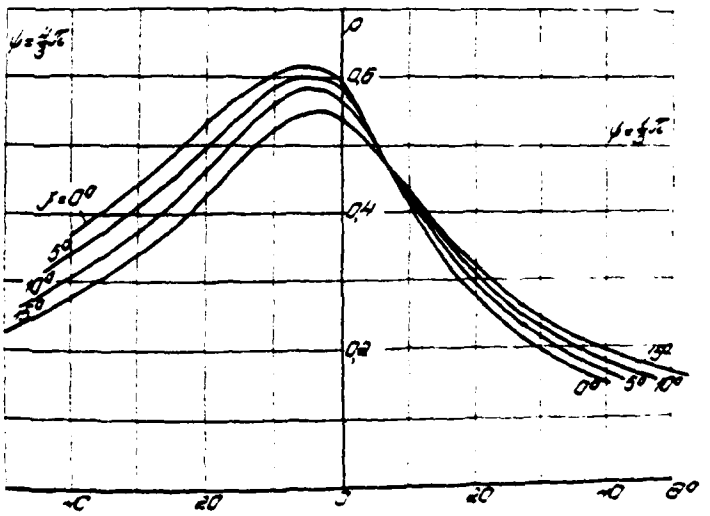

Figure 14.

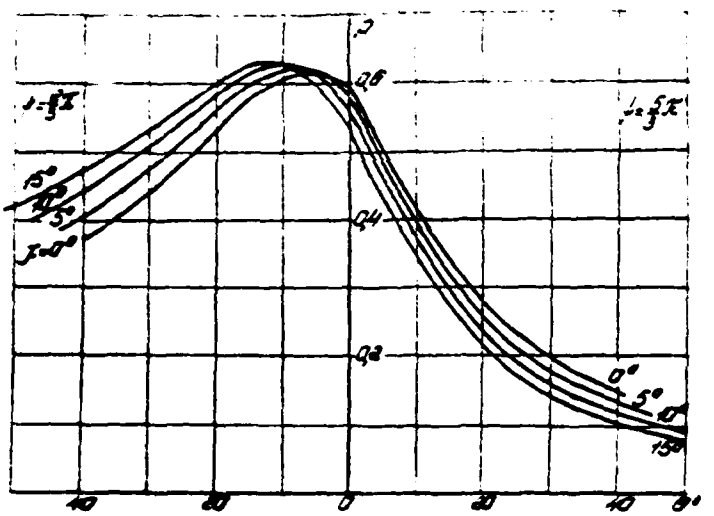

Figure 15.

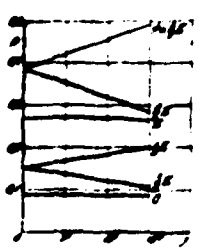

AD-A091 064 FOREIGN TECHNOLOGY DIV WRIGHT-PATTERSON AFB OH F/G 20/4
AERODYNAMICS OF HIGH VELOCITIES (COLLECTION OF ARTICLES).(U)
SEP 80
UNCLASSIFIED FTD-ID(RS)T-0590-80 NL

2 OF 2
AD A

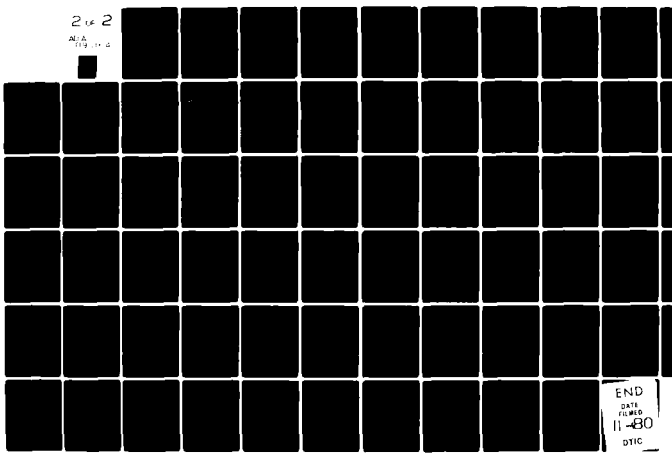

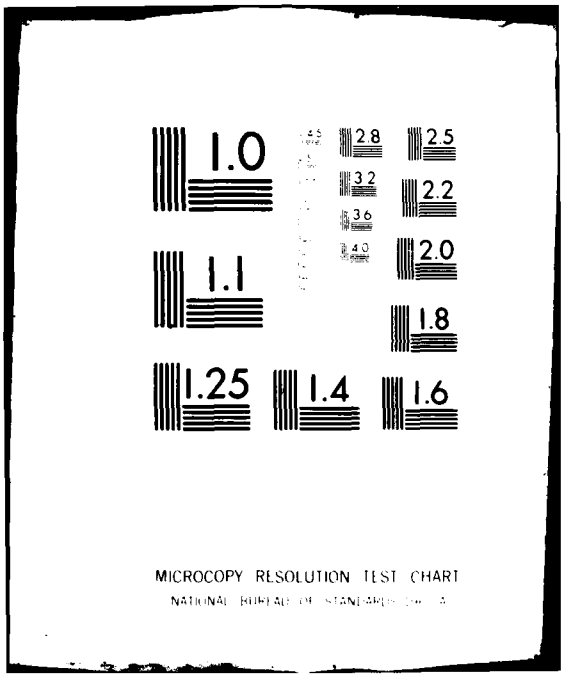
1.0
2.8
2.5
3.2
2.2
3.6
4.0
2.0
1.1
1.8
1.25
1.4
1.6
MICROCOPY RESOLUTION TEST CHART
NATIONAL BUREAU OF STANDARDS

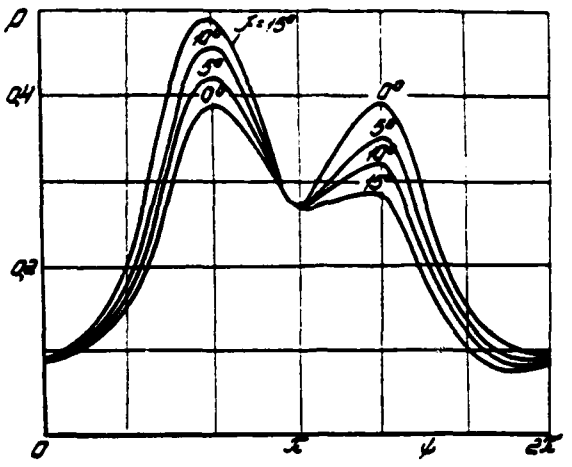

$\xi = 0$, $\theta = 38°$,
$\alpha = 18°$

Figure 16

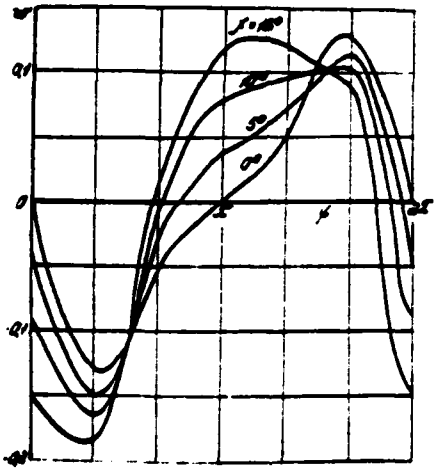

$\xi = 0$, $\theta = 38°$, $\alpha = 18°$

Figure 17

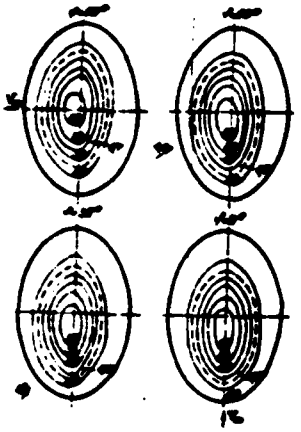

Figure 18

Analyzing the flow field in the shock layer, one can conclude that in the examined range of change in the angle χ with sufficiently large angles Θ, the relationship between the gas dynamic parameters with χ in the grid nodes ξ, Θ, ψ is nearly linear or is nearly linear. The linear relationship is particularly accurately satisfied in the planes $\psi = \frac{1}{3}\pi$ and $\psi = \frac{2}{3}\pi$. Figure 15 shows the change of pressure on the body when $\Theta = 38°$, as an example.

One can judge how significantly the character of flow changes in the shock layer with the presence of a slip angle according to Figures 16 and 17, which show distribution over the body when $\Theta = 38°$, pressure and the circular velocity component w according to the coordinate ψ.

Angle $\alpha = 0°, 30°, 60°, 90°$, in figure 18 for an ellipsoid with $\delta_1 = 1$, $\delta_2 = \frac{1}{2}$, when the vector of the free-stream flow forms an angle $\alpha' = 10°$ with the x axis and is parallel to the plane which passes through the axis x and stops with the axis z. In order to illustrate displacement of the critical point, isobaric projections on the $\Theta = 90°$ plane are given (the dash line corresponds to a sonic line, pressure relates to the double velocity head).

References

1. Кирова В.И., Лифшиц Ю.Б., Михайлов Ю.Я. О решении прямой задачи сопла Лаваля. Ученые записки ЦАГИ, т. 1, № 1, 1970.

2. Лапыгин Ю.М., Лифшиц Ю.Б. О расчете обтекания тел вращения трансзвуковым потоком. ПММ, т. 34, № 3, 1970.

3. Бабенко К.И., Русанов В.В. Разностные методы решения пространственных задач газовой динамики. Труды II Всесоюзного съезда по теоретической и прикладной механике (обзорные доклады; вып. 2), Наука, М., 1965.

4. Русанов В.В. Пространственное обтекание летящего тела сверхзвуковым потоком газа. Ж. вычисл. матем. и матем. физ., т. 5, № 3, 1965.

5. Бабенко К.И., Иванова В.И., Калиткин Н.Н., Кущенко М.А., Радиотис Ю.Б. Нестационарное обтекание головной части летящего тела идеальным газом. ИПМ АН СССР, 1965.

6. Теленин Г.Ф., Тишкин Г.И. Метод расчета пространственного обтекания тел с отошедшей ударной волной. ДАН СССР, № 5, 134, 1964.

7. Рябенький В.С. Необходимые и достаточные условия корректной обусловленности краевых задач для системы общепринятых разностных уравнений. Ж. вычисл. матем. и мат. физ., т. 4, № 2, 1964.

8. Павлов А.Ф., Тишкин Г.И. Расчет пространственного обтекания эллипсоидов вращения. Отчет № 364 Института механики МГУ, 1964.

9. Гильинский С.Н., Теленин Г.Ф. Сверхзвуковое обтекание тел различной формы с отошедшей ударной волной. Изв. АН СССР, Механика и машиностроение, № 5, 1964.

INVESTIGATION OF SPATIAL, NON-EQUILIBRIUM VOLUME AROUND SEGMENTAL BODIES

A. K. Burdel'nyy, V. B. Minostsev and V. P. Shkadova

Symbols: ∞V_∞, ∞V_∞, ∞V_∞ - velocity component VV_∞

V_∞ - maximum velocity;

$\rho\rho_\infty$ - density;

$\rho_\infty V_\infty^2$ - pressure;

$T\ T_\infty$ - temperature;

$\frac{MT_\infty}{m_\infty}$ - enthalpy of a mass unit;

α_j - ratio of frozen heat capacity;

$f_i/m_\infty \cdot m_i/\rho_\infty\rho$ - concentration of the small i-th component ;

n_i - number of moles of the i-th component per unit of volume;

$m\ m_\infty$ - molecular weight of mixture;

$\varepsilon_{v_i} RT_\infty$ - internal energy of vibratory degrees of freedom of the i-th component per 1 mole;

R - gas constant;

Φ - energy function of the effect of physico-chemical processes;

M - Mach number; 12a

R_0 - bluntness radius;

ξ, η, ψ - generalized curvilinear coordinate system;

$\theta, \varepsilon, \psi$ - sphereical coordinate system;

x, r, ψ - cylindrical coordinate system;

ξ, ε, ψ - generalized normed coordinate system;

$\varepsilon = \frac{\theta - \theta_\beta}{\theta_s - \theta_\beta}$ (or $\frac{r - r_\beta}{r_s - r_\beta}$)

H_1, H_2, H_3 - Lamé parameters

$$\zeta^* = -\frac{H_1(H_2^{-1} v \xi_\eta + H_3^{-1} w \xi_\psi)}{u}$$

$$\zeta^\pm = \frac{u^2\zeta^* \pm H_1 a\sqrt{(H_1^{-1} u \zeta^*)^2 + (u^2 - a^2)[(H_2^{-1}\xi_\eta)^2 + (H_3^{-1}\xi_\psi)^2]}}{u^2 - a^2}$$

$$\Psi^* = H_1^{-1} u \zeta^\pm + H_2^{-1} v \xi_\eta + H_3^{-1} w \xi_\psi$$

$$\lambda_1 = \xi_x - \zeta^-, \quad \lambda_2 = \xi_x - \zeta^+, \quad \lambda_3 = \xi_x - \zeta^*.$$

All geometrical values are related to R_0.

Indices: ∞ - parameters in the free-stream flow, s - on the shock wave, β - on the surface of the body.

The state of the dense high temperature layer which forms ahead of the blunt body flying at a high supersonic velocity in the atmosphere of the Earth depends on the physical transformations of air particles on the whole (dissociation, ionization), and upon the excitation of internal states of the molecules. The necessity of strictly taking these phenomena into account when determining the gas-dynamic characteristics of the flow significantly complicates the investigation of the problem of flow around blunt bodies.

The basic system of equations of the non-equilibrium flow consists of the gas dynamic and relaxation equations

$$\nabla\rho\vec{V} = 0$$
$$\vec{V}(\nabla p - a_f^2\nabla\rho) = \varkappa_f p\Phi \,,\ \vec{V}\nabla T_i = w_i \,,\ \vec{V}\nabla\ell_{v_i} = w_{v_i} \qquad (1)$$

The relaxation equations in system (1) which describe behavior of concentrations of the gas components and the oscillatory energies, are significantly nonlinear. A singularity arises in these with the approximation of relaxation processes to equilibrium. One should add the equation of state and the caloric equation to the system (1)

$$p = \frac{\rho T}{A_m} \,,\ h = \sum_{i=1}^{9} h_i(T)T_i \,. \qquad (2)$$

Processes of dissociation, associative ionization, exchange processes and the excitation of the oscillatory degrees of freedom of the O_2 and N_2 molecules are distinguished by the basic relaxation processes in air. Here one examines the components $O, N_2, NO, O, N, O_2^+, N_2^+, NO^+, \ell$ between which 13 chemical reactions take place, and the energy of the vibratory modes is ℓ_{v_1} and ℓ_{v_2}.

The boundary conditions of the problem are set on the shock wave and the surface of the body. In a nonviscous flow, the shock wave is a front of zero thickness on which the one kind-Rankine-Huboniot relationship is satisfied. The chemical components do not undergo a discontinuity, and the internal fluctuations of the degree of molecular freedom are not excited, i.e.,

$$T_{i_s} = T_{i_\infty} \,,\ \ell_{v_{i_s}} = 0 \,. \qquad (3)$$

The position of the shock wave in space is unknown and is determined in the solution process.

The condition of non- flow is satisfied on the surface of a body whose shape is assigned by the analytical expression, i.e., the normal velocity component vanishes.

As is known, the system of gas dynamic equations in the subsonic region of flow is a system of the elliptical type, that is hyperbolic in the supersonic region.

Therefore, in order to calculate flow in each of these regions, one needs a corresponding numerical schemes which will take into account the differing character of propagation of small perturbations in the flow. In this article, the solution to the problem of flow around the body of rotation by a supersonic air flow which is chemically active behind the shock wave was obtained with the use of two such methods.

The calculations were made for segmental bodies for whose spatial streamlining a number of results already exists. A work [1] contains a survey of investigations that have been conducted of the spatial flow of a perfect gas near segmented bodies. In work [2], an investigation was made of the problem of flow around the leading part of these bodies by a nonequilibrium gas at small angles of attack. The problem of non-equal flow around a segmented body in general was solved here. In this case, the data on the kinetics of the physico-chemical processes were taken from a work [3].

1. FLOW AROUND A BLUNT BODY

The solution to the problem of nonequilibrium flow in the subsonic-transonic region was obtained by the G. F. Telenin method. Generalization to the case of a nonequilibrium gas and a detailed presentation of the characteristics of employing this method relative to spatial flow is given in a work [2]. The very same work contains the result of flow around the leading part at angles of attack α from 0° to 10°. In this case, these results are expanded for an angle of attack from 10° to 25° according to nonequilibrium flow.

A segmented body which is circular in the middle region is examined. In the Cartesian coordinate system, the contour of the body in the region of rounding has the following analytical expression.

$$F=\left[(x-l_0)^2+(y-l_1)^2-z^2\right]^m+\left\{\frac{1}{\beta_0}\operatorname{arctg}\frac{\sqrt{(y-l_1)^2+z^2}}{x-l_0+\beta_0}\right\}^m=0, \qquad (4)$$

where l_0, l_1 - change in the origin of the coordinates with respect to the apex of the segment

$$\beta_0=\frac{\sin(\theta^\circ-\beta^\circ)}{\sin\theta^\circ}$$

Θ^* - half-angle of the segment, β^* - angle of the inverse cone. The position of the origin of the coordinates with different α is selected depending upon the size and position of the subsonic region of flow ahead of the body. For example, for an angle of attack $\alpha = 15°$ $\ell_1 = 0{,}0463$, $\ell_2 = -0{,}022$, , and for $\alpha = 25°$, $\ell_1 = 0{,}0427$, $\ell_2 = -0{,}0416$. In this case, $\Theta_H = 1.116$. In this case, the flow is supersonic on all outer rays and throughout all half planes.

The geometrical picture of flow of the leading surface in the symmetry plane when $\alpha = 15°$ and $\alpha = 25°$ is shown in Figure 1. The free-stream flow has the following parameters $M_\infty = 20$, $T_\infty = 250°K$, $P_\infty = 10^{-4}$ atm, the bottom radius, $R_0 = 1$ cm. With an increase in the angle of attack, the shock wave approaches the body from the windward side $\varphi = \pi$ and straightens in the region $\psi = 0$. The dimensions of the subsonic region significantly decrease. The body's critical point approaches the edge of the body. Figure 1 shows the position of stagnation points with different angles of attack, while the functional relationship (y stagnation) with α is given in Figure 2.

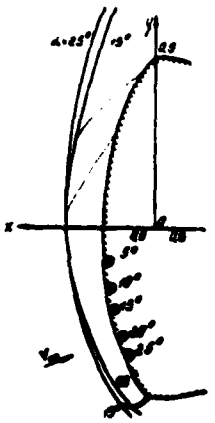

Figure 1

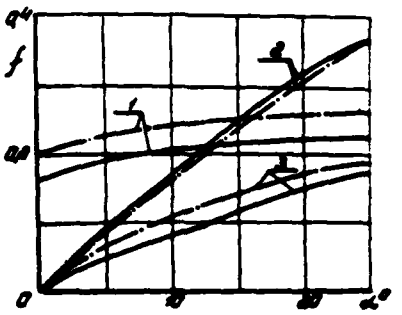

Figure 2

1. $f = \frac{\partial P}{\partial \theta}$; 2. $f = |\gamma_1|$; 3. $f = \frac{\partial W}{\partial \varphi}$

We shall examine the question of the effect of nonequilibrium processes in the flow on the flow gas dynamic characteristics in more detail. It was shown in work [2] that the spatial flow effects directly ahead of the body smooth as the result of a change in the chemical composition of the mixture. A sublayer of gas of increased

density which is homogeneous with respect to temperature and composition forms ahead of the body. The flow rate of the gas along the shock layer decreases in comparison with the case of flow of a perfect gas ($\varepsilon_1 = 1/4$).

Figure 2 gives the velocity gradients $\frac{\partial v}{\partial \theta}$ and $\frac{\partial w}{\partial \psi}$ in the stagnation point; the dot-dash line was obtained from a solution to the problem for a perfect gas.

Pressure in the entire shock layer at the leading surface of the body in the case of the nonequilibrium flow has a higher value than is the case for a perfect gas. A symmetry in its distribution along the surface is basically determined by the spatial character of flow (Figure 3).

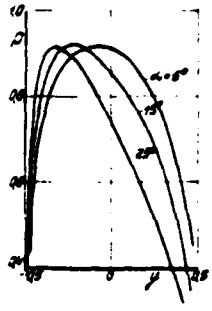

Figure 3

For angles of attack $\sim 10°$, spatial effects had practically no effect on the distribution of gas composition in space. The distribution of concentrations γ_i was nearly axesymmetrical throughout the entire flow region (for example, γ_i in figure 5 for $\alpha = 5°$).

At large angles of attack, one observes a noticeable effect of the three dimensionality of flow on the thermo-chemical structure of the gas in the shock layer. All functions which describe this state, ρ, T, γ_i at angles of attack $\alpha > 10°$ have clearly pronounced maxima (minima) in the vicinity of the stagnation point and change sharply along the body's surface.

In Figure 4, one can trace how gas temperature changes along the shock layer when $\alpha + 25°$. The solid lines $T(\theta)$ pertain to the plane $[0, \Pi)$, while the dash lines to the plane $(\frac{\pi}{2}, \frac{3\pi}{2})$. The asymmetry of temperature distribution decreases toward the body ($\xi = 0$) as the result of the contribution of energy of the nonequilibrium processes to the total flow energy, but temperature along the surface

already clearly is not constant for the case $\alpha = 5°$ [4] as well.

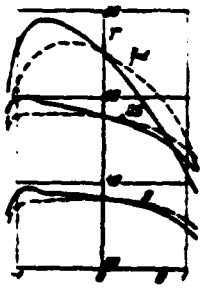

Figure 4

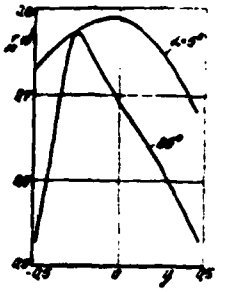

Figure 5

It is interesting to trace the character of the change in the electron concentration (Figure 5) along the body on the symmetry line. A sharp drop in γ_1 at the high angles of attack is a consequence of the more rapid expansion of flow from the leeward side and its sharper turn from the winward side.

2. FLOW AROUND THE LATERAL SURFACE OF A BODY

The previous section gave the results of calculating nonequilibrium flow in a shock layer near the leading surface of a segmented body. If the surface $\theta = \theta_H$ is a surface of the spatial type, i.e., if the normal flow velocity on it is greater than the local frozen velocity of sound a_f everywhere, then the data on the surface can be used as initial conditions for calculating the supersonic flow region.

For the case of near-equilibrium flow of the leading surface, a work [5] suggests an approximate method of calculating the effect of imperfection of the gas with hypersonic flow around segmented bodies which, as the conducted investigations showed, proved to be effective for investigating hypersonic flow around segmented bodies of short length with a large angle of inclination of the trailing cone generatrix and at comparatively small angles of attack. In this method, flow around the leading surface is considered to be completely equilibrium and is simulated by the flow of a perfect gas with an adiabatic exponent determined from the condition of equality

of the relationship of densities in the direct shock wave in the equilibrium and simulated flows. The adiabatic exponent is considered to be precisely the same for the entire supersonic flow region, except for points on the shock wave, and is, in fact, determined from the condition of freezing of the equilibrium gas composition in the region of the body's rounding. A work [6] gives calculations of flow around the lateral surface for conditions of developed non-equilibrium in the shock layer near the lateral surface of a segmented body under the condition of constancy of gas composition along the stream line in the supersonic flow region. The composition of the gas slows in each surface point $\Theta = \Theta_H$, and the frozen adiabatic exponent $\varkappa$, was determined according to the frozen composition. Precisely the same initial data were used as in this article. The calculation of flow in the supersonic flow region was made according to the method of a work [7]. In this case, the adiabatic exponent $\varkappa$, is determined on the layers by the Lagrange polynominal according to ξ and ψ. The numerical investigations of the spatial flow around bodies with inclusion of the chemical kinetics equations in the calculation requires a significant increase in calculation time and complication of the program, in the investigations that were made. Only one work has been published up to now [8] which is devoted to calculating the three-dimensional, nonequilibrium flow of a gas in the supersonic region of flow around bodies. This work investigates the effect of non-equilibrium dissociation on flow near blunt, inverse cones situated in the supersonic oxygen flow. The initial data for calculating the supersonic region was taken from the corresponding numerical solution for an oxygen flow in the shock layer near a sphere. There are presently no published works on calculating the spatial flow of non-equilibrium air in the supersonic region of flow.

As was already noted, the effect of the physico-chemical processes on the gas dynamic parameters in the supersonic flow region was estimated quite well with the aid of simulating non-equilibrium flow in the shock layer near the lateral surface of a body by a flow of gas with an adiabatic exponent $\varkappa$, . This property of the total effect of relaxation of the physico-chemical processes on the gas

dynamic flow parameters can be used when developing numerical schemes for calculating nonequilibrium flows in the supersonic flow region. The results of calculations cited in this section were obtained according to a method in which the gas dynamic parameters and rates of the physico-chemical processes differ sequentially according to the different schemes. In this case, the precise calculation of the rates of physico-chemical processes is only made in the symmetry plane of flow.

We shall examine the structure of a system of equations (1) which describe nonequilibrium gas flow. The first three relationships describe the behavior of gas dynamic parameters of flow. The next relationship describes the change in the chemical composition of gas and relaxation of the oscillatory degrees of freedom of the molecular components. In order to calculate flow in the supersonic flow region, the initial conditions are assigned on the surface of a spatial type $\Theta = \Theta_H$ from a solution to the problem of nonequilibrium flow of the leading surface of a body. The boundary conditions are precisely the same as for flow in the subsonic flow region.

As is evident from the system (1), the effect of a change in gas composition and the excitation of oscillations in the gas dynamic equations is only manifested cumulatively via the relationship between the frozen, specific heat capacities $\varkappa_f$ (or the frozen velocity of sound a_f) and the energy function of the effect of nonequibrial processes Φ.

In order to solve the gas dynamic equations in the supersonic region of flow with a known distribution of $\varkappa_f$ and Φ, one uses a scheme suggested by Yu. Ya. Mikhaylov for a perfect gas. According to this scheme, the gas dynamic equations are written in in the characteristic form

$$A_1\frac{\partial \vec{X}}{\partial \chi} + A_2\frac{\partial \vec{X}}{\partial \eta} + A_3\frac{\partial \vec{X}}{\partial \psi} + \vec{A}_4 = 0 \qquad (5)$$

where

$$A_1 = \frac{1}{H_1}\begin{bmatrix} \frac{\xi_t^\circ u}{H_1} & \frac{\xi_\eta u}{H_2} & \frac{\xi_\varphi u}{H_3} & \frac{\xi^\circ a_f^2}{x_f H_1} - \frac{\Psi^\circ u}{x_f} & 0 \\ \frac{\eta_t^\circ u}{H_1} & \frac{\eta_\eta u}{H_2} & \frac{\eta_\varphi u}{H_3} & \frac{\eta^\circ a_f^2}{x_f H_1} - \frac{\Psi^\circ u}{x_f} & 0 \\ 0 & 0 & 0 & -u & x_f u \\ u & -\frac{H_2 \xi^\circ}{H_1 \xi_\eta} u & 0 & \frac{a_f^2}{x_f} & 0 \\ 0 & -\frac{H_2 \xi_\varphi}{H_3 \xi_\eta} u & u & 0 & 0 \end{bmatrix}$$

$$A_2 = \Lambda A_1$$

$$A_3 = \frac{1}{H_3}\begin{bmatrix} \frac{\xi^\circ w}{H_1} & \frac{\xi_\eta w}{H_2} & \frac{\xi_\varphi w}{H_3} & -\Psi^\circ \frac{\xi_\varphi a_f^2}{x_f H_3} - \frac{\Psi^\circ w}{x_f} & 0 \\ \frac{\eta^\circ w}{H_1} & \frac{\eta_\eta w}{H_2} & \frac{\eta_\varphi w}{H_3} & -\Psi^\circ \frac{\eta_\varphi a_f^2}{x_f H_3} - \frac{\Psi^\circ w}{x_f} & 0 \\ 0 & 0 & 0 & -w & x_f w \\ w & -\frac{H_2 \zeta^\circ}{H_1 \xi_\eta} w & 0 & \frac{a^2 f}{x_f} & 0 \\ 0 & -\frac{H_2 \xi_\varphi}{H_3 \xi_\eta} w & w & 0 & 0 \end{bmatrix}$$

$$\bar{A}_0 = \frac{1}{H_1 H_2 H_3}\begin{Bmatrix} H_1^{-1} \xi g_1 + H_2^{-1} \xi_\eta g_2 + H_3^{-1} \xi_\varphi g_3 - \Psi^\circ g_4 \\ H_1^{-1} \eta^\circ g_1 + H_2^{-1} \eta_\eta g_2 + H_3^{-1} \eta_\varphi g_3 - \Psi^\circ g_4 \\ x_f \Phi \\ g_1 - H_2 \zeta^\circ (H_1 \xi_\eta)^{-1} g_2 \\ -H_2 \xi_\varphi (H_3 \xi_\eta)^{-1} g_2 + g_3 \end{Bmatrix},$$

where

$$g_1 = \Psi H_3 (u H_{1\eta} - v H_{2\xi}) + w H_2 (u H_{1\varphi} - w H_{3\xi})$$

$$g_2 = w H_1 (v H_{2\varphi} - w H_{3\eta}) + u H_3 (v H_{2\xi} - u H_{1\eta})$$

$$g_3 = u H_2 (w H_{3\eta} - u H_{1\varphi}) + v H_1 (w H_{3\eta} - v H_{2\varphi})$$

$$g_4 = u (H_2 H_3)_\xi + v (H_1 H_3)_\eta + w (H_1 H_2)_\varphi - \Phi$$

Λ - diagonal matrix

$$\Lambda = \begin{bmatrix} \lambda_1 & 0 & 0 & 0 & 0 \\ 0 & \lambda_2 & 0 & 0 & 0 \\ 0 & 0 & \lambda_3 & 0 & 0 \\ 0 & 0 & 0 & \lambda_4 & 0 \\ 0 & 0 & 0 & 0 & \lambda_5 \end{bmatrix}, \quad \bar{X} = \begin{Bmatrix} u \\ v \\ w \\ \Delta p \\ \Delta \rho \end{Bmatrix}$$

Equations (5) are written in the common, curvilinear coordinate system and are obtained from the system (1) by excluding the derivative of density and by proceeding to the logarithmic variables [illegible] and [illegible].

The first two equations of system (5) are the conditions of compatability on wave surfaces and the derivatives in these equations in the meridianal cross sections are written as in a work [9], according to a four point scheme. The last three equations are equations on the flow surfaces and their corresponding derivatives are written according to a six point scheme [10].

The obtained difference equations are solved in each meridional plane by the trial and error method. The change in derivatives according to the meridional angle ψ is taken into account in the interative fashion from layer to layer. The given scheme was used in a work [11] for calculating two dimensional flow around bodies by a perfect gas using the establishment method. Geometrical interpretation of the condition of the scheme stability is a requirement that in the meridional planes the grid line ξ = const proceeding from each point of the calculated region be located in a characteristic triangle, which is usually satisfied throughout the entire flow field.

We shall now assume that all flow parameters are known in layer nodes [illegible]. Calculation of the gas dynamic functions in the nodes of a layer n + 1 is made according to the method described above using the known values of [illegible] and Φ from a layer n.

We move elements of the stream line before the intersection with the surface [illegible] backward according to the found gas dynamic functions and the nodes of a layer n + 1 in the plane of symmetry. Values of the gas dynamic functions and chemical components in the points of interesection are found with the aid of quadratic interpolation according to known values in nodes of these n layer in the

flow symmetry plane.

The equations of the physico-chemical processes (the last relationships of system (1)) shall be solved according to the non-explicit Newton method (similarly to work [12]) using the equation of state (2).

Thus, in the plane of symmetry of flow, concentrations γ_i and oscillation energy ε_{vi} and then ε and Φ can be found in all nodes of the layer n + 1. The values ε and Φ in other meridional planes are determined according to the trigonometric approximation

$$\varepsilon_{\psi} = \frac{\varepsilon^{(n+1)}_{\psi=0} + \varepsilon^{(n)}_{\psi=0}}{2} + \frac{\varepsilon^{(n+1)}_{\psi=0} - \varepsilon^{(n+1)}_{\psi=\pi}}{2}\cos\psi \qquad (6)$$

$$\Phi_{\psi} = \frac{\Phi^{(n+1)}_{\psi=0} + \Phi^{(n)}_{\psi=0}}{2} + \frac{\Phi^{(n+1)}_{\psi=0} - \Phi^{(n+1)}_{\psi=\pi}}{2}\cos\psi$$

The obtained values of ε and Φ in all nodes of the n + 1 layer are the original ones for calculating the gas dynamic functions in nodes of the n + 2 layer, etc.

As was noted above, the effect of physico-chemical processes on gas dynamic parameters in the supersonic flow region can be quite well estimated according to the freezing principle. In the method of this work, only 1 assumption of the smoothness of change in ε and Φ according to the meridional angle, and the kinetic equations are completely calculated in the planes of symmetry. For the case of flow around segmental bodies, function Φ in the supersonic region decreases very rapidly and becomes practically equal to 0 and naturally has a very weak effect on the gas dynamic parameters. The relationship of the frozen heat capacities ε on the surface of the shock wave is equal to ε_{∞}, and on the surface of the body remains approximately the same in all points. The change in ε according to the meridional angle ψ with a fixed ξ is smooth, and, therefore, can be approximated according to formula (6) with sufficient accuracy. Because of the point weak effect of the change ε on the gas dynamic parameters of flow, one can hope that for quite short bodies (of the

segmental type) and with comparatively small angles of attack the developed method of calculation will give good results.

We shall examine the results of calculations of the supersonic region of nonequilibrium flow around a segmentally shaped body, made according to the given method, with angles of attack $\alpha = 15°$ (solid lines in figures 6-25), and 25° (dash lines). The calculations were made with the following parameters of the body and the free-stream flow:

$$\theta^* = 30°,\ \beta^* = 10°,\quad R_* = 1\ \text{cm},\ M_\infty = 20,\ T_\infty = 250°K,\ p_\infty = 10^{-4}\ \text{atm}$$

The initial data for calculating the supersonic region are assigned on a surface $\theta_* \theta_*$ (figure 6, the apex of the conical surface $\theta_* \theta_*$ is situated in a point with coordinates x = 0.3547 and y = -0.022 for $\alpha = 15°$ and x = 0.3573, y = -0.04165 for $\alpha = 25°$) from calculations of nonequilibrium flow in the shock layer near the frontal surface of the body (1). Calculation of rates of the physico-chemical processes and the thermodynamic functions in the supersonic regions was made according to precisely the same program as was used in the subsonic region of the shock layer.

Figure 6 shows the picture of flow in the symmetry plane calculated for an angle of attack $\alpha = 15°$. Here, as in the other figures as well, the dash-dot lines give the results of calculating flow around the given body by a perfect gas with an adiabatic exponent $\varkappa = 1.4$ when $\alpha = 15°$.

From the cited flow picture and distribution of stream lines between the surface of the body and the shock wave in the supersonic region, a different character of flow with the leeward ($\psi = 0$) and windward ($\psi = \Pi$) sides of flow is obvious.

The shock wave is situated very close to the surface of the body on the windward side of flow and the entire stream of gas in the shock layer near the point of rounding passes the region of the fan of the rarefaction wave, running from the contour rounding in the region of the middle. In this case, flow temperature sharply

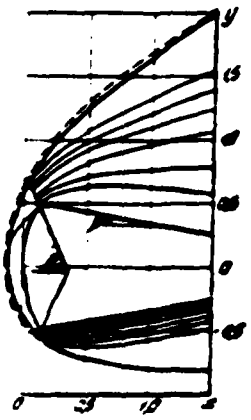

Figure 6

decreases (Figure 7), which leads to freezing of the physico-chemical processes and a decrease in their energy contribution to practically 0 (Figure 8). And although the values of T and Φ on the initial surface $\theta = \theta_*$ are significantly higher on the winward side (Figures 7, 8, and 9, 10) after a turn to $\theta = \frac{\pi}{2}$ (calculation is made in this region in the spherical coordinate system), they differ little from the corresponding values on the windward side of flow.

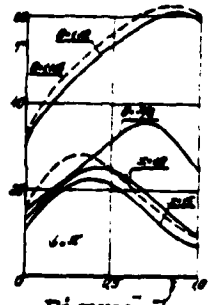

Figure 7

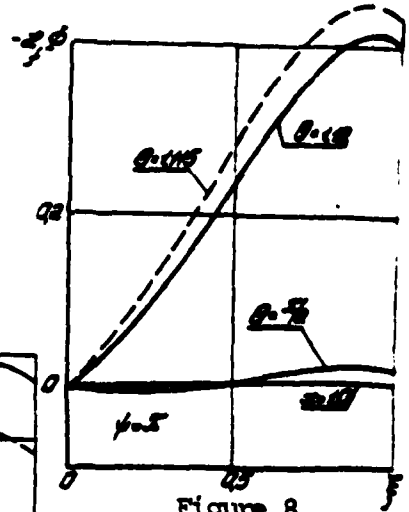

Figure 8

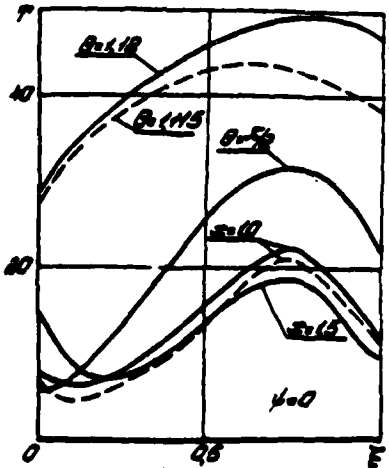

Figure 9

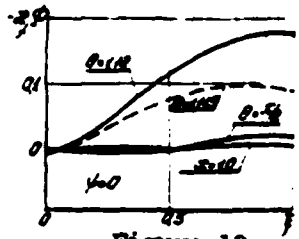

Figure 10

A significant drop in temperature along the shock wave leads to a situation such that the physico-chemical processes in the gas which has entered the shock layer in the supersonic region of flow are practically not excited. It is evident from Figure 6 that the stream line running from the subsonic flow region on the windward side completely transits the fan of rarefaction waves and proceeds in parallel to the surface of the body, proportional to the increase in the x coordinate (calculation after turn to [illegible] is made in the cylindrical coordinate system). The relative region occupied by these stream lines in the shock layer rapidly decreases and comprises approximately 40% for $\alpha = 15°$, when $x = 1.5$. The entire remaining shock region on the windward side of flow is occupied by a gas in which the physico-chemical transformations do not practically arise. On the leeward side of flow, the stream lines along which chemical reactions arise in the flow led to a noticeable change in composition on [illegible], occupy a significantly greater part of the shock layer. Although the gas composition remains constant along the stream lines, it proves to be variable with respect to ξ in the greater part of the shock layer even at the end of the calculated region.

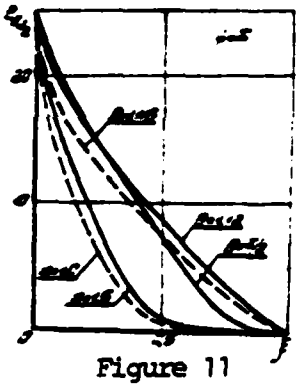

Figure 11

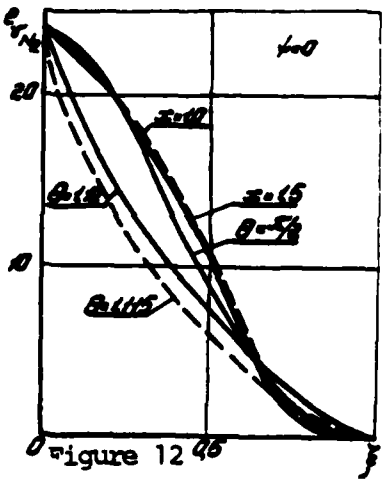

Figure 12

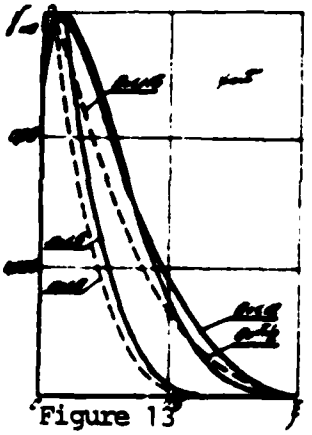

Figure 13

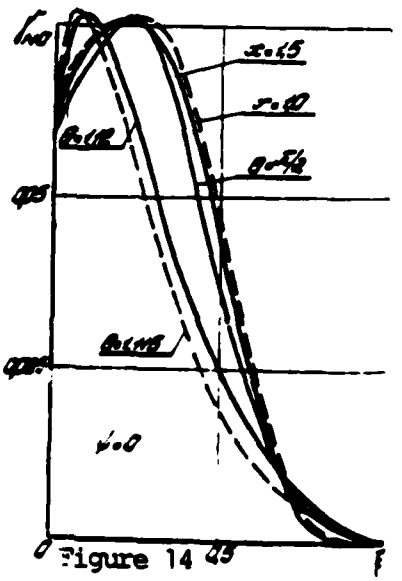

Figure 14

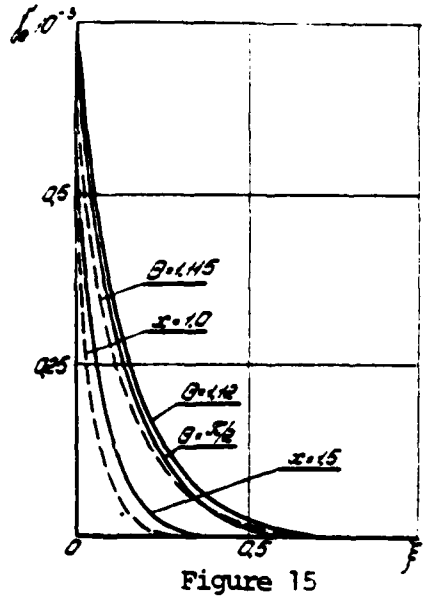

Figure 15

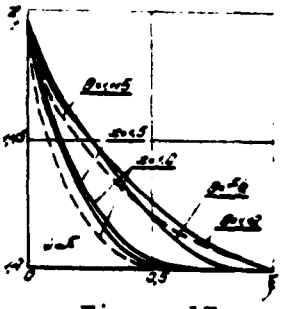

Figure 17

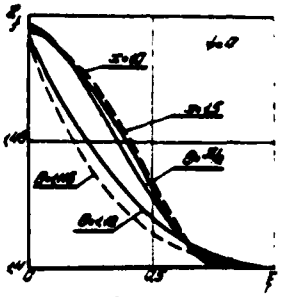

Figure 18

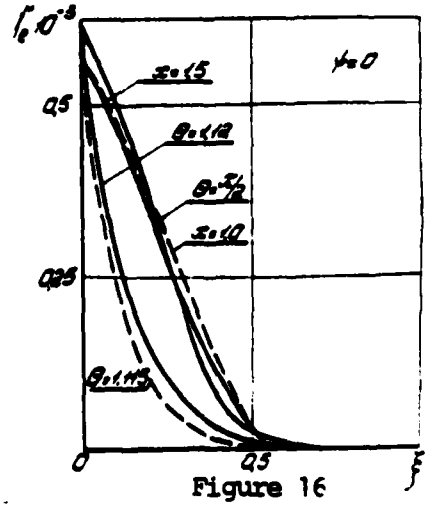

Figure 16

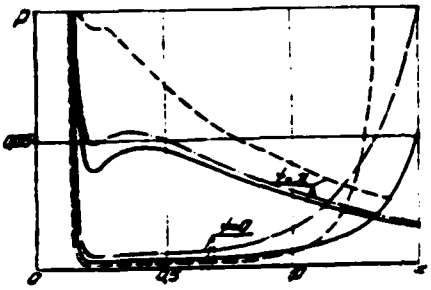

Figure 19

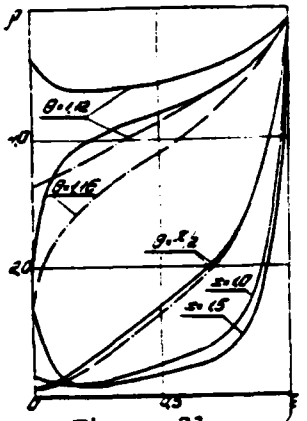

Figure 21

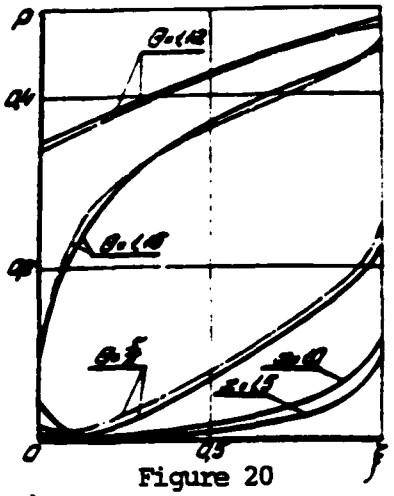

Figure 20

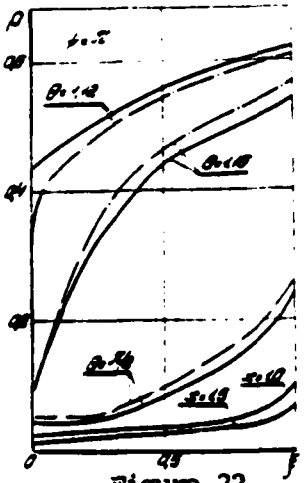

Figure 22

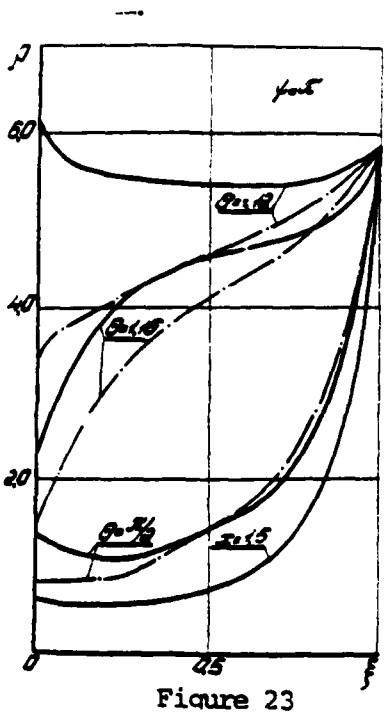

Figure 23

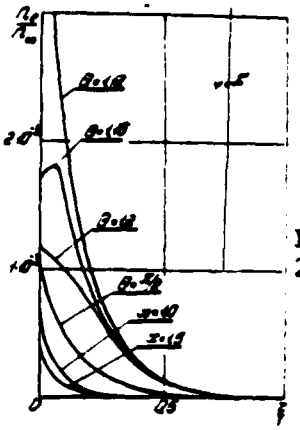

Figure 24

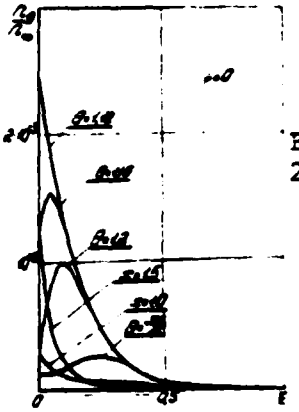

Figure 25

Figures 11-16 give the corresponding distribution of [illegible] as an illustration. Relationships of the frozen heat capacities [illegible], transverse to the shock layer (Figures 17 and 18) also practically remain constant along the stream lines everywhere in the region $x > 0.3$ and the character of its distribution according to ξ is actually determined by the flow picture.

The effect of increasing the angle of attack from a value $\alpha = 15°$ to $\alpha = 25°$ on the distribution of flow parameters is evident from the provided figures. Specifically, the increase in the angle of attack leads to a relative decrease in the region occupied by the reacted gas on the windward side, which is due to a large influx in the given cross section $x = \text{const}$ of the gas which passed through the wave region with lower intensity.

It was shown in work [1, 5] with the aid of an approximate method that the effect of physico-chemical processes on the distribution of pressure along the lateral surface is significant in the case of

near-equilibrium flow around the frontal surface of segmented bodies. In the examples of calculations cited in this article, flow around the frontal surface occurs under conditions far from equilibrium conditions. In this case, the effect of the physico-chemical processes on the distribution of gas dynamic parameters in the supersonic flow region should be significantly smaller.

Figure 19 shows the pressure distribution along the surface of the body in the symmetry plane of flow. The sharp increase in pressure on the leeward side of flow is due to overflow [1]. The distribution of pressure across the shock layer (Figures 20 and 22) also differs little from the case of a perfect gas. The distribution of density (Figures 21 and 23) on the initial surface ($\theta = 1.12$ for $\alpha = 15°$) before cases of flow by a nonequilibrium and perfect gas is significantly different. In the case of nonequilibrium flow near the surface of the body, there is a region of increased density due to the presense of physico-chemical processes. However, after the turn ($\theta = 1.16$), the character of density distribution already corresponds to density distribution in the perfect gas, and when [illegible], the corresponding density values are practically identical in those cases.

A sharp drop in density in the vicinity of the middle of the body leads to a characteristic change in the number of electrons per unit of volume [illegible] (Figures 24 and 25), where n_∞ - total number of particles per unit of volume of the free-stream flow. The increase in n_1 near the surface of the body on the leeward side at the end of the calculated region is due to flow stagnation.

When [illegible] for $\alpha = 15°$ and $x > 1.3$, for $\alpha = 25°$ the decrease in flow velocity on the leeward side of flow leads to a situation such that

Note: Pages missing in foreign text. FP 94 through 103.

CALCULATING VISCOUS FLOW AROUND A SPHERE BY A HYPERSONIC FLOW OF A GAS MIXTURE CONTAINING CARBON DIOXIDE GAS

by

V. G. Gromov

The work gives the method and certain results of calculating the viscous flow of a gas mixture of CO_2 - N_2 near the leading critical line of flow around a sphere. Calculation was made on the basis of a system of equations which is the first approximation of a complete system Navier -Stokes equations obtained by the method "truncated" series. A 9-component model of the gas mixture $(CO_2, CO, N_2, NO, O_2, CN, C, N, O)$ was used, taking into account 13 gas phase chemical reactions and with the assumption that the internal degrees of freedom of the mixture's components are equally excited.

By applying the method of "truncated" series [2] to the complete system of Navier -Stokes equations [1], and by limiting oneself to the first approximation, one obtains the following equation system which describes flow of ν-component of the reacting gas near the critical stream line of the sphere: The equation of continuity is

$$\frac{H}{\varepsilon}\frac{df}{d\xi} + 2(\bar{u}\rho + f) = 0 \quad . \tag{1}$$

the equation of motion

$$\frac{H}{\varepsilon}\frac{d}{d\xi}\left(p + \frac{f^2}{\rho} - \Pi_{\infty}\right) + 2f\left(\bar{u} + \frac{f}{\rho}\right) - 2(\Pi_{\infty} + \bar{\Pi}_{\infty} + \bar{\Pi}_{\infty}) = 0 \tag{2}$$

$$\frac{H}{\varepsilon}\left(f\frac{d\bar{u}}{d\xi} - \frac{d\bar{\Pi}_{\infty}}{d\xi}\right) + \bar{u}(\rho\bar{u} + f) + 2(p_2 - p) + 2\bar{\Pi}_{\infty} - 3\bar{\Pi}_{\infty} = 0 \quad , \tag{3}$$

the equations of continuity for mixture components

$$\frac{H}{\varepsilon}\left(f\frac{dc_i}{d\xi} + \frac{dk_i}{d\xi}\right) - m\Gamma_{\infty}\bar{\omega}_i + 2K_i = 0$$

$$i = 1, 2, \ldots, \nu - 1 \quad , \tag{4}$$

the equations of continuity for chemical elements

$$\frac{H}{\varepsilon}\left(f\frac{d\bar{c}_\ell}{d\xi} + \frac{d\bar{k}_\ell}{d\xi}\right) + 2\bar{K}_\ell = 0$$

$$\ell = 1, \ldots, \nu_1 - 1 \quad , \tag{5}$$

the energy equation

$$\frac{H}{\varepsilon}\left[\rho\frac{di_2}{d\xi} + \frac{d}{d\xi}\left(q + \rho\Pi_{\infty}\right)\right] + 2(q + \rho\Pi_{\infty}) = 0 \quad , \tag{6}$$

the equation of state

$$p = \rho T \sum_{i=1}^{k} \frac{C_i}{m_i} \quad (7)$$

$$\sum_{i=1}^{k} C_i = 1 \quad (8)$$

$$\frac{H}{\varepsilon}\frac{\partial \rho_i}{\partial \xi} = \dot{\omega}_i(\rho, u, \ldots) \quad (9)$$

Equations (2)-(6) can be rewritten in the vectorial form

$$\frac{H}{\varepsilon}\left(f\frac{\partial \vec{V}}{\partial \xi} + \frac{\partial \vec{R}}{\partial \xi}\right) + \vec{N} + \vec{S} = 0 \quad (10)$$

where

$$\vec{V} = \{u, v, c_i, \tilde{c}_l, I_0\}$$

$$\vec{R} = \{-\pi_{sn}, K_i, \tilde{K}_l, q - v\pi_{nn}\}$$

$$\vec{N} = \{\tilde{u}(\rho\tilde{u} + f) + 2(p_z - p); -H\Gamma_{ss}\dot{\omega}_i; 0; 0\}$$

$$\vec{S} = \{2\pi_{ss} - 3\pi_{sn}, 2K_i, 2\tilde{K}_l, 2(q - v\pi_{nn})\}$$

In these equations and below, s and n are coordinates which run along the surface of the body and along the normal to it, u and v are the corresponding velocity vector components, ρ is density, p is pressure, T is temperature, $I_0 = \sum c_i I_i + 0.5(u^2 + v^2)$ is total enthalpy, I_i is enthalpy of i-th component, C_i is the gravimetric concentration of the i-th component, $\tilde{c}_l$ is the gravimetric concentration of the l-th chemical element, $\dot{\omega}_i$ is the rate of formation of the i-th component in the chemical reactions, γ_i is the number of chemical elements that enter into the composition of the mixture components.

$$\tilde{u} = \left(\frac{\partial u}{\partial s}\right)_{s=0}, \quad p_z = 0.5\left(\frac{\partial^2 p}{\partial s^2}\right)_{s=0} + p$$

$$f = \rho v, \quad H = 1 + \varepsilon\xi, \quad \xi = n/\varepsilon$$

ε-norming factor;

$$R_\infty \pi_{ss} = 2\mu\frac{\tilde{u} + v}{H} + \mu_v \operatorname{div}\vec{V}$$

$$R_\infty \pi_{nn} = 2\mu\frac{1}{\varepsilon}\frac{\partial v}{\partial \xi} + \mu_v \operatorname{div}\vec{V}$$

$$R_\infty \pi_{ik} = \mu\left(-\frac{\vec{u}\cdot\vec{n}}{r} + \frac{1}{\xi}\frac{d\vec{u}}{d\xi}\right)$$

$$div\,\vec{V} = 2\frac{\vec{u}\cdot\vec{n}}{r} + \frac{1}{\xi}\frac{d\vec{w}}{d\xi}$$

$$R_\infty S_{c_\infty} \gamma_i = \frac{1}{\xi}\sum_k D_{ik}\frac{d\vec{z}_k}{d\xi}$$

$$\vec{z} = (z_1, \ldots, z_n)$$

$$\vec{\gamma}_i = \sum_{k=1}^{n} \alpha_{ik}\gamma_k$$

α_{ik} - gravimetric proportion of the l-th element in the i-th component;

$$R_\infty P_{r_\infty} \vec{q} = -\lambda\frac{1}{\xi}\frac{dT}{d\xi} + L_{r_\infty}\sum_{i=1}^{n} I_i \vec{\gamma}_i$$

Here μ, μ_∞ - coefficients of viscosity, λ - coefficient of heat conductivity, D_{ik} - generalized diffusion coefficients.

In the cited expressions and below, dimensionless variables are used and all lengths are related to the radius of the sphere L, velocity components to V_∞, density to ρ_∞, pressure to $\rho_\infty V_\infty^2$ enthalpy to V_∞^2, temperature to $V_\infty^2/(c_{p_\infty} R_\infty)$ / R_∞ - absolute gas constant, the transfer coefficients - respectively to $\mu_\infty, \lambda_\infty, D_\infty$. The index "infinity symbol" pertains to conditions in the unperturbed flow. The equations include dimensionless complexes

$$R_\infty = \frac{\rho_\infty V_\infty L}{\mu_\infty}, \quad P_{r_\infty} = \frac{\mu_\infty c_{p_\infty}}{\lambda_\infty}, \quad S_{c_\infty} = \frac{\mu_\infty}{\rho_\infty D_\infty}$$

$$L_{r_\infty} = \frac{\rho_\infty D_\infty c_{p_\infty}}{\lambda_\infty}, \quad \Gamma_\infty = \frac{L}{V_\infty \tau_{r_\infty}}$$

τ_{r_∞} characteristic reaction time.

It is assumed during statement of the problem that the surface of the sphere is impermeable, has an assigned temperature $(T_w < T_0)$ and has ideal catalytic properties. Moreover, the absence of slipping is postulated which is a good approximation in the case of a cold wall.

Boundary conditions on the surface of the body have the following form with such assumptions:

$$\bar{u} = 0 \ , \quad \rho = \rho_w \ ,$$

$$c_i = 0 \ , \quad i = CO \ , NO \ , CN \ , C \ , N \ , O \ ,$$

$$\bar{T}_e = \bar{C} \ , \quad e = C \ , N \ ,$$

$$\sum_{i=1}^{3} c_i = 1 \ , \tag{11}$$

$$T = T_w \ .$$

The flow parameters tend toward their values in the unperturbed flow proportional to distance from the body surface.

$$\bar{u} = 1 \ , \quad \bar{v} = 0 \ , \quad \bar{\rho} = 1 \ ,$$

$$c_i = c_{i\infty} \ , \quad \bar{T} = m_\infty / T_\infty M_\infty^2 (\gamma - 1) \ , \quad \bar{p} = 1 / \gamma M_\infty^2 \tag{12}$$

2. The system of equations (1)-(9), (11), (12) is solved by the method of finite differences. Equations (1)-(2), (10), (7)-(9) are approximated with the aid of a 3-point difference scheme of the following system of difference equations:

$$\frac{H_{m-0.5}}{\xi} \frac{f_m - f_{m-1}}{h} + 2(\bar{x}\beta + f)_{m-0.5} = 0 \tag{13}$$

$$\frac{H_m}{\xi h}\Big\{\Big[\sigma^{(a)}_{m+0.5}\Big(P + \frac{f^2}{\rho}\Big)_{m+1} + (1-\sigma^{(a)}_{m+0.5})\Big(P + \frac{f^2}{\rho}\Big)_m - (\bar{\pi}_{nn})_{m+0.5}\Big] -$$

$$\Big[\sigma^{(a)}_{m-0.5}\Big(P + \frac{f^2}{\rho}\Big)_m + (1-\sigma^{(a)}_{m-0.5})\Big(P + \frac{f^2}{\rho}\Big)_{m-1} - (\bar{\pi}_{nn})_{m-0.5}\Big] +$$

$$+ 2 f_m \Big(\bar{u} + \frac{f}{\rho}\Big)_m - \Big[(\bar{\pi}_{sn} + \bar{\pi}_{nn} + \bar{\pi}_{ss})_{m+0.5} + (\bar{\pi}_{sn} + \bar{\pi}_{nn} + \bar{\pi}_{ss})_{m-0.5}\Big] = 0 \tag{14}$$

$$\frac{H_m}{\xi}\Big\{f_m\Big(\sigma^{(a)}_m \frac{y^{(a)}_{m+1} - y^{(a)}_m}{h} + (1-\sigma^{(a)}_m)\frac{y^{(a)}_m - y^{(a)}_{m-1}}{h}\Big) +$$

$$+ \frac{1}{h}\Big(R^{(a)}_{m+0.5} - R^{(a)}_{m-0.5}\Big)\Big\} + N^{(a)}_m + 0.5\Big(S^{(a)}_{m+0.5} + S^{(a)}_{m-0.5}\Big) = 0 \tag{15}$$

$$K = 1 \ ; \ 2 \ , \ 4 \ ; \ 3 \ , \ 5 \ , \ 6$$

$$P_m = \rho_m T_m \sum_{i=1}^{3} \frac{c_{im}}{m_i} \tag{16}$$

$$\sum_{i=1}^{4} c_{i,m} = 1 \qquad (17)$$

$$\frac{H_{m+0.5}}{\tau}\frac{P_{i,m+1}-P_{i,m}}{h} = \sum_{k=1}^{4}\alpha_{ik}(K_k)_{m+0.5}$$

$$m = 1, \ldots, M-1 \qquad (18)$$

The system of equations (13)-(18) is closed by difference equations which approximate the boundary conditions

$$u_0 = 0 \;,\; v_0 = 0 \;,\; \rho_0 = \rho_w$$
$$c_{i,0} = 0 \;,\; i = CO,\ NO,\ CN,\ C,\ N \qquad (19)$$
$$(K_\ell)_{0+0.5} = 0 \;,\; \ell = C,\ N$$

$$T_0 = T_w \qquad (20)$$

$$u_\infty = 1 \;,\; v_\infty = -1 \;,\; \rho_\infty = 1 \;,$$
$$c_{i,\infty} = c_{i,\infty} \;,\; T_\infty = m_\infty / T_\infty M_\infty^2 \;(1^2/mmo)$$

$$P_{i,\infty} = 1/T_\infty M_\infty^2 \;. \qquad (21)$$

Here the following grid symbols are used:

$$\xi_m = mh \;,\; m = 0, 1, \ldots, M$$

$$f_m = f(\xi_m)$$

$$f_{m+0.5} = 0.5(f_m + f_{m+1})$$

$$R_\infty (\bar{T}_{ik})_{m+0.5} = 2\mu_{m+0.5}\frac{\bar{u}_{m+0.5} + \bar{v}_{m+0.5}}{H_{m+0.5}} +$$

$$+ \mu_{1,m+0.5}(\mathrm{div}\,\vec{V})_{m+0.5}$$

$$R_\infty (\bar{T}_{ik})_{m+0.5} = 2\mu_{m+0.5}\frac{1}{\xi}\frac{v_{m+1}-v_m}{h} + \mu_{1,m+0.5}(\mathrm{div}\,\vec{V})_{m+0.5}$$

$$R_\infty (\bar{T}_{ik})_{m+0.5} = \mu_{m+0.5}\left(-\frac{\bar{u}_{m+0.5}+v_{m+0.5}}{H_{m+0.5}} + \frac{1}{\xi}\frac{\bar{u}_{m+1}-\bar{u}_m}{h}\right)$$

$$(\mathrm{div}\,\vec{V})_{m+0.5} = 2\frac{\bar{u}_{m+0.5}+v_{m+0.5}}{H_{m+0.5}} + \frac{v_{m+1}-v_m}{\xi h}$$

$$R_\infty S_{c\infty}(K_i)_{m+0.5} = \frac{1}{\xi}\sum_k (\rho D_{ik})_{m+0.5}\frac{z_{i,m+1}-z_{i,m}}{h}$$

$$(\bar{K}_\ell)_{m+0.5} = \sum_{i=1}^{4}\alpha_{\ell i}(K_i)_{m+0.5}$$

$$R_\infty P_{r\infty}(q)_{m+0.5} = -\lambda_{m+0.5}\frac{1}{\xi}\frac{T_{m+1}-T_m}{h} +$$

$$+ \sum_{i=1}^{4} j_{i,m+0.5}(K_i)_{m+0.5}$$

$s^{(n)}$ - gravimetric functions whose specific selection will be stated below.

3. The system of difference equations shall be solved by the method of successsive approximations according to the following scheme. Initially, using the (n-1) approximation for the vector of the sought functions $\bar{x}^{(n-1)}=\{p^{(n-1)}, f^{(n-1)}, u^{(n-1)}, c^{(n-1)}\}$, from equations (18) and (21) we determine the n-th approximation for the function P_2. We then find the value $\bar{x}^{(n)}$ from equations (13)-(17), (19), (20). In order to calculate $\bar{x}^{(n)}$, we expand the left hand side of equations (13)-(17), (19) and (20) in a series in powers of $\delta\bar{x}=\bar{x}^{(n)}-\bar{x}^{(n-1)}$, $\delta\varepsilon=\varepsilon^{(n)}-\varepsilon^{(n-1)}$. Limiting ourselves to the linear terms, we obtain a system of linear equations relative to $\delta\bar{x}$, $\delta\varepsilon$

$$A_{0,0}\delta\bar{x}_0+A_{0,1}\delta\bar{x}_1+A_{0,\varepsilon}\delta\varepsilon+A_0+A_{0,w}\delta p_w=0 \tag{22}$$

$$\bar{A}_{m,m-1}\delta\bar{x}_{m-1}+\bar{A}_{m,m}\delta\bar{x}_m+\bar{A}_{m,m+1}\delta\bar{x}_{m+1}+ \tag{23}$$
$$+\bar{A}_{m,\varepsilon}\delta\varepsilon+\bar{A}_m=0$$
$$m=1,2,\ldots,M-1$$

$$A_{m,m}\delta\bar{x}_m+A_m=0 \tag{24}$$

We shall separately write the equation which corresponds to the difference approximation of the continuity equation in the point m + 0.5

$$a_{m,m+1}\delta\bar{x}_{m+1}+a_{m,m}\delta\bar{x}_m+a_{m,\varepsilon}\delta\varepsilon+a_m=0 \tag{25}$$

In order to reduce the volume of calculations during linearization of the difference equations, the transport coefficients can be viewed as values independent of $\bar{x}^{(n)}$, whose values are calculated according to the (n-1)-th approximation $\bar{x}^{(n-1)}$.

We shall employ the vector, trial and error method for solving the system of equations (22)-(24). With the direct trial and error method, we exclude δf_{m+1} from equation (23) with the aid of (25) and calculate the trial run coefficients

$$c_{m,m+1}\delta\bar{x}_{m+1}+\delta\bar{x}'_m+c_{m,\varepsilon}\delta\varepsilon+c_{m,w}\delta p_w+c_m=0 \tag{26}$$
$$m=0,1,\ldots,M-1$$

$$C_{0,1} = A_{0,0}^{-1} A_{0,1}, \quad C_{0,2} = A_{0,0}^{-1} A_{0,2}, \quad C_{0,m} = (-1, 0, \ldots, 0), \quad C_0 = A_{0,0}^{-1} A_0,$$

$$C_{m,m+1} = (A_{m,m} - A_{m,m-1} C_{m-1,m})^{-1} A_{m,m+1},$$

$$C_{m,\ell} = (A_{m,m} - A_{m,m-1} C_{m-1,m})^{-1} (A_{m,\ell} - A_{m,m-1} C_{m-1,\ell}), \tag{26}$$

$$C_{m,m} = (A_{m,m} - A_{m,m-1} C_{m-1,m})^{-1} (A_{m,m} - A_{m,m-1} C_{m-1,m}),$$

$$C_m = (A_{m,m} - A_{m,m-1} C_{m-1,m})^{-1} (A_m - A_{m,m-1} C_{m-1}).$$

Here $A_{m,m-1}, A_{m,m}, A_{m,m+1}, A_{m,\ell}$ are the corresponding matrix coefficients of equation (23) after excluding δf_{m-1}.

Using boundary conditions (24) and relationships (25) and (26) when $m = M-1$ we express δp_M through $\delta\varepsilon$

$$\delta p_M = k_\ell \delta\varepsilon + k \tag{27}$$

and carry out the first inverse trial run

$$\delta\bar{x}_m = z_{m,\ell} \delta\varepsilon + z_m = 0, \quad m = M, M-1, \ldots, 0$$

$$z_{m,\ell} = -C_{m,m+1} z_{m+1,\ell} + C_{m,M} k_\ell + C_{m,\ell} \tag{28}$$

$$z_m = -C_{m,m+1} z_{m+1} + C_{m,M} k + C_m$$

$$z_{M,\ell} = 0, \quad z_M = A_{M,M}^{-1} A_M.$$

From the supplementary condition

$$p_M = p^* \tag{29}$$

we determine the value of $\delta\varepsilon$, and during the second inverse trial run we find the values $\delta\bar{x}, \delta\varepsilon$ and $x^{(n)}, \varepsilon^{(n)}$

$$\bar{x}_m^{(n)} = \bar{x}_m^{(n-1)} + z_{m,\ell} \delta\varepsilon + z_m$$

$$m = 0, 1, \ldots, M-1 \tag{30}$$

$$\varepsilon^{(n)} = \varepsilon^{(n-1)} + \delta\varepsilon$$

4. The method examined above was employed for calculating flow of the CO_2-N_2 gas mixture. The model of a rigid rotor - a harmonic oscillator with the following values of the characteristic vibratory

temperature was used during the description of the thermodynamic mixture properties:

	CO_2	CO	N_2	NO	O_2	CN
T_*, °K	3900, 1950, 3380	3100	3573	2100	2250	2070

It was assumed that the atomic components only have sequential degrees of freedom. The heats of formation of components under steady-state conditions were taken from a work [3].

During calculation of the transport characteristics of the mixture, the following simplified assumptions were used:

1/ the viscosity coefficient does not depend on the composition of the mixture and is determined by the formula

2/

$$\mu = \mu(T_\infty)(T/T_\infty)^{0,75}$$

$$\mu_1 = -2/3\,\mu$$

3/ the binary diffusion model is used

$$K_i = -\rho \mathcal{D} \frac{dC_i}{dn} \quad , \quad S_c = \frac{\mu}{\rho \mathcal{D}} = 0,7$$

4/ the heat conductivity coefficient is determined from the condition

$$P_r = \frac{\mu \bar{C}_p}{\lambda} = 0,7 \quad .$$

13 gas phase reactions were taken into account in the calculations:

1. $CO_2 + M \rightleftharpoons CO + O + M$;
2. $CO + M \rightleftharpoons C + O + M$;
3. $N_2 + M \rightleftharpoons N + N + M$;
4. $NO + M \rightleftharpoons N + O + M$;
5. $O_2 + M \rightleftharpoons O + O + M$;
6. $CN + M \rightleftharpoons C + N + M$;
7. $N_2 + C \rightleftharpoons CN + N$;
8. $N_2 + O \rightleftharpoons NO + N$;
9. $CO + N \rightleftharpoons CN + O$;
10. $CN + O \rightleftharpoons C + NO$;
11. $O + NO \rightleftharpoons O_2 + N$;
12. $CO + N \rightleftharpoons NO + C$;
13. $CO_2 + O \rightleftharpoons CO + O_2$.

The rate constants of these reactions, given in Table 1, were calculated on the basis of recommendations made in the works of a number of authors who studied chemical processes in CO_2-N_2 mixtures.

Calculations were made on a uniform grid with M = 80. Values of the gravimetric functions were determined as follows:

$$\sigma^{(0)} = 0 \text{ when } \rho > \rho^*$$
$$\sigma^{(0)} = 1 \text{ when } \rho < \rho^*$$
$$\sigma^{(k)} = 1, \quad k = 1; 2, 4; 3, 5; 4$$

Such a choice of $\sigma^{(k)}$ insures stability of the trial and run method, good stability properties of the scheme, and an error of approximation on the order of h throughout the entire examined range of values of the R_∞ number. Calculations were made when $\rho^* = 2$.

Convergence of the iteration process employed for solving the difference equations depends significantly on the choice of the initial approximation. In the cited calculations, the initial distribution of the sought functions was determined in the process of motion according to the value of the R_∞ number. The calculation started with finding a solution when $R_\infty = 10^{4.5}$. Quite arbitrary profiles of these sought functions were used in this case as the zero approximation, but when making the first two iterations, for $\delta\bar{x}$ damper $\delta = 0.5$ was used.

$$\bar{x}^{(n)} = \bar{x}^{(n-1)} + 0.5\delta\bar{x}$$

The motion step according to $R_\infty = R_{\infty,n}/R_{\infty,1}$ was chosen experimentally and changed within limits of from $10^{0.25}$ to 10.

Figures 1-13 give certain calculated characteristics of flow obtained with the following values of exterior parameters:

$$T_\infty = 150^\circ K, \quad V_\infty = 5500 \text{ m/sec} \; (V_\infty' = 1 \text{ m/sec}, R_\infty' = 3300^\circ K)$$
$$(C_{CO_2})_\infty = 0{,}88, \quad (C_{N_2})_\infty = 0{,}06, \quad T_w = 1000^\circ K,$$
$$\mu(T_\infty) = 770 \cdot 10^{-7} \text{ g/cm} \cdot \text{sec}$$
$$R_\infty = 10^{4.5} - 10^{5.5}, \quad P_\infty = 10^{-6} \text{ atm}$$

The number 1 in the figure corresponds to $R_\infty = 10^{4.8}$, 2 - $10^{4.6}$ 3 - $10^{4.5}$, 4 - $10^{4.3}$.

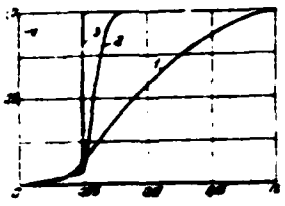

Figure 1

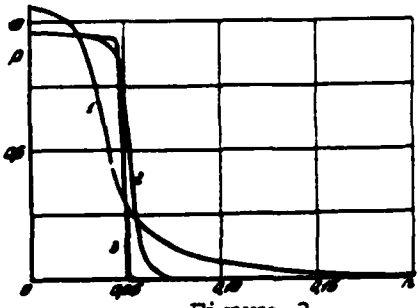

Figure 3

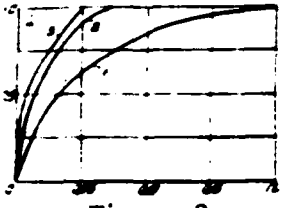

Figure 2

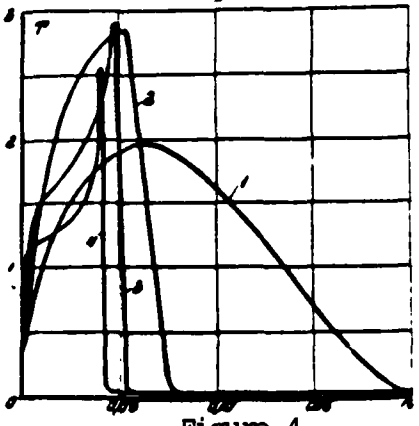

Figure 4

Figures 1-4 show the change in distribution along the critical stream line of the basic hydrodynamic functions v, ε, ρ, T with a sequential increase in the R_∞ number.

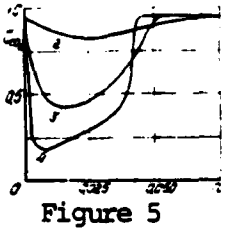

Figure 5

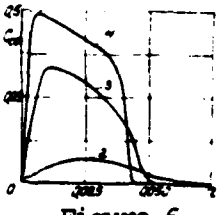

Figure 6

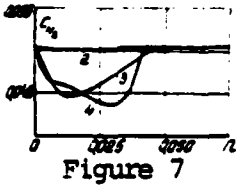

Figure 7

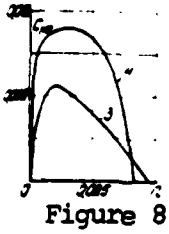

Figure 8

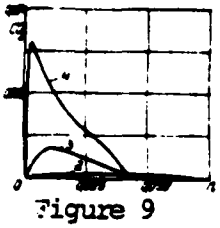

Figure 9

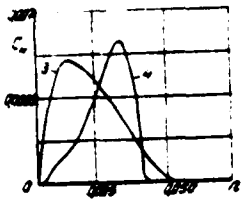

Figure 10

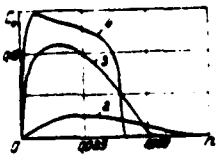

Figure 11

Figures 5-11 show the distribution of concentrations of components of the $CO_2, CO, N_2, NO, O_2, N, O$ mixture. The concentration of atomic carbon and cyanogen does not exceed $0.5 \cdot 10^{-5}$ throughout the entire examined range of parameters.

It is evident from the cited graphs, under the given conditions intensive processes began in the gas already following the establishment of the dynamic flow structure characteristic for high Reynolds numbers--the "shock wave-nonviscous gas layer--boundary layer". In this case, one should note that the equilibrium gas composition does not established before $R_\infty \cdot 10^{4.5}$ on the "outer boundary" of the boundary layer.

Figure 12 illustrates the change in "regression" of the shock wave ε with the change of R_∞. The value of ε decreases monotonically with the increase in R_∞ and up to $R_\infty \sim 10^4$, the decrease in ε is basically associated with the change in the dynamic structure of flow, but with large R_∞ values, the decrease ε is due to an increase in density in the shock layer because of gas dissociation.

Figure 12

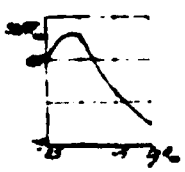

Figure 13

Figure 13 shows the calculation relationship between the heat exchange parameter $st\sqrt{R_\infty} \cdot \dots$ and the value of R_∞. The cited data on heat exchange which correspond to high R_∞ ($\sim 10^5$) evidently need refining inasmuch as the values were obtained with comparatively small number of points in the region of the boundary layer ($\sim$5-10).

TABLE 1

REACTION RATE CONSTANTS TABLE

$k_f = A\,T^{n}\exp\left(-\frac{E}{RT}\right)$ cm^3 mole sec^{-1} °K^{-n}

No.	REACTION	M	A	E	R
1	2	3	4	5	6
1.	$CO_2 + M \rightleftarrows CO + O + M$	CO_2, N_2, NO, CN, C, N, O, CO, O_2	10^{15}	6.34	−3.21
			$0.2 \cdot 10^{15}$	6.34	−3.21
2.	$CO + M \rightleftarrows C + O + M$	CO_2, CO, N_2, NO	$0.36 \cdot 10^{15}$	12.9	−0.5
		O_2, CN, C, O	$0.48 \cdot 10^{15}$	12.9	−0.5
		N	$0.43 \cdot 10^{17}$	12.9	−1.5
3.	$N_2 + M \rightleftarrows 2N + M$	CO_2, CO, N_2, NO	$0.36 \cdot 10^{15}$	11.32	−0.5
		O_2, CN, C, O	$0.48 \cdot 10^{15}$	11.32	−0.5
		N	$0.43 \cdot 10^{17}$	11.32	−1.5
4.	$NO + M \rightleftarrows N + O + M$	CO_2	$1.23 \cdot 10^{15}$	7.56	−1.5
		CO, N_2, O_2	$0.41 \cdot 10^{15}$	7.56	−1.5
		NO, CN, C, N, O	$0.82 \cdot 10^{15}$	7.56	−1.5
5.	$O_2 + M \rightleftarrows 2O + M$	CO_2	$0.77 \cdot 10^{15}$	5.94	−0.5
		CO, N_2	$0.38 \cdot 10^{15}$	5.94	−0.5
		NO, O_2, CN, C	$1.1 \cdot 10^{15}$	5.94	−2.5
		C, O	$0.22 \cdot 10^{16}$	5.94	−1.0
6.	$CN + M \rightleftarrows C + N + M$	CO_2	$1.23 \cdot 10^{15}$	9.76	−1.5
		CO, N_2, O_2	$0.54 \cdot 10^{15}$	9.76	−1.5
		NO, CN, C, N, O	$1.1 \cdot 10^{16}$	9.76	−1.5
7.	$N_2 + C \rightleftarrows CN + N$	-	$0.05 \cdot 10^{12}$	3.72	0

1	2	3	4	5	6
8.	$N_2 + O \rightleftarrows NO + N$	-	$0.71 \cdot 10^{9}$	3.80	0
9.	$CO + N \rightleftarrows CN + O$	-	$0.44 \cdot 10^{13}$	4.13	0
10.	$CN + O \rightleftarrows C + NO$	-	$0.32 \cdot 10^{13}$	1.75	0
11.	$NO + O \rightleftarrows O_2 + N$	-	$0.32 \cdot 10^{10}$	1.97	1.0
12.	$CO + N \rightleftarrows NO + C$	-	$0.44 \cdot 10^{13}$	3.37	0
13.	$CO_2 + O \rightleftarrows CO + O_2$	-	$0.81 \cdot 10^{12}$	1.78	0

REFERENCES

1. Гирифельдер Дж., Кертисс Ч., Берд Р. Молекулярная теория газов и жидкостей. [illegible], 1961.

2. Као Х. Гиперзвуковое малое течение вблизи критической линии тела затупленного типа. AIAA, № 11, 1964.

3. Термодинамические свойства индивидуальных веществ. Под ред. акад. В.П. Глушко, изд-во АН СССР, 1962.

III. LOSS OF STABILITY AND SELF EXCITED VIBRATIONS IN THE FLOW

The Interaction of Plane and Cylindrical Supersonic Streams with Acoustical Fields

by

M. G. Lebedev and G. F. Telenin

The flow of gas streams into the external medium is accompanied by the emission of noise from the stream surface. When supersonic stream flow, the spectrum of their noise contains discrete components of significant intensity under certain conditions. In this case, the stream pulsates at a certain frequency which is equal to the frequency of the discrete component, and emits acoustical waves into the ambient medium which are similar in shape to spherical waves and are in counter phase on the opposite sides of the stream. The emission of these waves chiefly occurs from the region of stream disintegration.

Analysis of the experimental data makes it possible to conclude that the stream emitting sound at a discrete frequency is a self-vibratory system in which the inverse relationship is accomplished by acoustical waves propagating through the ambient medium, and, in their turn, acting upon the stream. A. Powell [10], who first observed the examined phenomenon [1953], supports this idea.

In works [1,2] the authors suggested a possible physical scheme which explains the appearance and maintenance of pulsations of supersonic jets at a discrete frequency, based upon the idea mentioned above and analysis of the available experimental data. According to this scheme, the supersonic stream can play the role of a resonator because of its periodic (cellular) structure. Actually, if a periodic wave runs along the surface of such a stream, then the perturbations in the stream caused by this wave will also be quasiperiodic in the direction along the stream. Then, having chosen frequency ω_* of the exterior acoustical wave in a certain fashion, one can so synchronize this wave with the propagation of perturbations in the stream that perturbations increase, with respect to absolute value, along the stream to the region of its disintegration, exceeding surface perturbations. Thus, the stream will intensify the perturbations coming in from without at a certain frequency (or frequencies) ω_*; this critical frequency ω_* is comparable with the natural resonator frequency.

It is natural to assume the presence of a relationship between the intensity of pulsations in the stream and the intensity of acoustical waves emitted from the region of its disintegration. Then the system which includes this region, which is the source of the acoustical omission, and the acoustical waves themselves which propagate through the ambient medium and the perturbed stream will be a free vibratory one.

[1,2] examine the problem of interaction of a plane supersonic stream flowing into a flooded space with plane acoustical waves of assigned frequency propagating through a circular stream in space in the direction of the nozzle, corresponding to the suggested diagram of the phenomenon. In solving this problem (for the calculated stream in the linear approximation), critical values of frequencies of the exterior acoustical waves were detected. At these frequencies, the amplitude of perturbations within the stream caused by the periodic wave on its surface increases infinitely with distance from the nozzle, while at the same time the relationship between perturbations and the coordinates x at all other frequencies along the stream will have

a periodic character. The intensification of perturbations within stream in comparison with the assigned perturbations on its boundaries at the critical frequency is maximum; in this case, a sharp increase in perturbations in the stream in the vicinity of this frequency takes place in a narrow range of frequencies, outside which the perturbations have precisely the same order as in the exterior acoustical wave. The obtained results thus confirm the suggested physical scheme of the phenomenon of pulsations of supersonic streams with a discrete frequency.

We note that the problem of interaction of the stream with the external acoustical waves was solved in [1,2] in a simplified presentation, when the removal of acoustical energy from the surface of the pulsating stream into the surrounding space was ignored. This made it possible to obtain the solution to the problem in the analytical form, and specifically, to derive formulas for the critical frequencies of external acoustical waves. Precisely the same problem is solved in this work without the simplifying approximations. In this case, we shall examine cases for both the plane and the cylindrical supersonic jet with the symmetrical and antisymmetrical character of perturbations in the exterior acoustical field.

1. Statement of the problem and method of solution. Let a supersonic cylindrical or plane jet with a Mach number M flow from a rigid cylinder $2R$ in diameter or a flat slot with the width $2R$ into a flooded space; pressure in the jet and the ambient medium is p. Flow in the underperturbed jet is uniform; the problem of interaction of such a jet with the exterior acoustical field will be solved in the linear approximation, whose bases are given in [1,2].

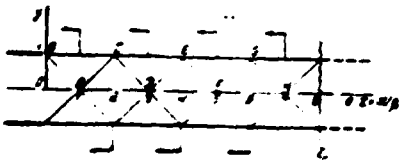

Figure 1

In accordance with the physical phenomenon of emission of sound at a discrete frequency by a jet simulated by us, we shall consider that the jet disintegrates at a distance x_0 from the nozzle's cross-section and that the region of disintegration of the jet is a source of emission of acoustical waves with a cyclic frequency ω. We shall term this emission basic emission; let it be described by the potential ψ_0:

$$\psi_0(x,y,\theta,t) = Re\left[\Psi_0(x,y)\exp(-i\omega t)\right]\cos j\theta \,. \qquad (1)$$

where

$$\Psi_0 = \Psi_{0m} + i\Psi_{0a} \,.$$

In (1), x, y are cylindrical coordinates (Figure 1), Θ - meridional angle, j = 0 or 1 in the case of symmetrical or antisymmetrical perturbations. We shall give the entire presentation for the cylindrical case (m = 1), and slight changes which should be inserted into the initial equations and calculation formulas for the plane case (m = 0) will be indicated at the end of the section.

Propagating through the space which surrounds the jet, the acoustical waves (1) act on the jet and bring it into the perturbed state. Let perturbed flow in the jet be described by a potential φ

$$\varphi(x,y,\theta,t) = Re\left[\Phi(x,y)\exp(-i\omega t)\right]\cos j\theta \,. \qquad (2)$$

Oscillations of the perturbed jet lead to the emission of acoustical waves from the surface of the jet into the exterior medium. We shall term this emission secondary emission; let it be described by the potential ψ:

$$\psi(x,y,\theta,t) = Re\left[\Psi(x,y)\exp(-i\omega t)\right]\cos j\theta \qquad (3)$$

Potential φ of the perturbed flow in the jet and potential ψ of secondary emission satisfy the following wave equations:

$$\beta^2\frac{\partial^2\varphi}{\partial x^2} + \frac{\partial^2\varphi}{\partial y^2} + \frac{1}{y}\frac{\partial\varphi}{\partial y} + \frac{1}{y^2}\frac{\partial^2\varphi}{\partial\theta^2} + 2M\frac{\partial^2\varphi}{\partial x\,\partial\tau} + \frac{\partial^2\varphi}{\partial\tau^2} = 0 \,. \qquad (4)$$

$$\frac{\partial^2\psi}{\partial x^2} + \frac{\partial^2\psi}{\partial y^2} + \frac{1}{y}\frac{\partial\psi}{\partial y} + \frac{1}{y^2}\frac{\partial^2\psi}{\partial\theta^2} - \frac{\partial^2\psi}{\partial\tau_0^2} = 0 \,. \qquad (5)$$

In these equations and everywhere subsequently, coordinates x, y relate to the radius of the jet R; moreover, dimensionless time values

are inserted $\tau = a R^{-1} t$, $\tau_e = a_e R^{-1} t$, where α and α_e are the velocities of sound in the jet and in the exterior medium. We shall also use dimensionless values of the cyclic frequency $\vartheta = a^{-1} R \omega$ and $\vartheta_e = a_e^{-1} R \omega$ such that $\pi = \vartheta_e \tau_e = \omega t$ and $a\vartheta = a_e \vartheta_e$. Finally, in equation (4) $s = \sqrt{M^2 - 1}$.

Velocity perturbations $\overline{V}'$ and $\overline{V}_e'$ and pressure perturbations p' and p_e' in the jet and in the exterior medium (from the secondary emission) are expressed through the potentials φ and ψ in the following way:

$$\overline{V}' = a \operatorname{grad} \varphi \quad , \quad \overline{V}_e' = a_e \operatorname{grad} \psi \tag{6}$$

$$\begin{cases} p' = -\gamma p \frac{R}{a} \frac{d\varphi}{dt} = -\gamma p \left(\frac{\partial \varphi}{\partial \tau} + M \frac{\partial \varphi}{\partial x} \right) \\ p_e' = -\gamma_e \rho \frac{R}{a_e} \frac{d\psi}{dt} = -\gamma_e \rho \frac{\partial \psi}{\partial \tau_e} \end{cases} \tag{7}$$

where p is unperturbed pressure, identical in the jet and in the exterior medium, γ, γ_e - adiabatic exponents.

The potential of basic emission ψ_0 and the potential of total emission $\varphi_2 = \varphi_0 + \varphi$ together with ψ satisfy the wave equation (5). The corresponding velocity and pressure perturbations can be determined according to formulas similar to (6) and (7).

The basic purpose of this work is to study the amplitude-frequency characteristic of the supersonic jet interacting with the exterior acoustical field. During the presentation of this problem we shall pose, as it were, the inverse relationship in the "jet-exterior acoustical waves" self-oscillatory system and shall hypothesize the presence of a generator of basic acoustic emission ψ_0 independent of of the jet. Thus, we shall investigate a perturbed flow in the jet and secondary emission from the jet under the effect of assigned acoustical waves which have a potential ψ_0.

The basic acoustical field ψ_0, whose source lies in the region of jet disintegration, has not been sufficiently studied experimentally at present. Therefore, we shall make assumptions relative to its

character which simplify the calculations and at the same time do not contradict known experimental facts. We shall consider that derivative $\partial\varphi_0/\partial y = 0$, on the surface of the jet (y = 1), i.e., the effect of the basic emission on the jet occurs only via pressure, while the pressure perturbation itself is a pressure wave running in the direction of the nozzle when y = 1;

$$p'(x, \theta, t) = P\cos(\vartheta_z \tau_z + \vartheta_z x)\cos j\theta \quad (8)$$

One can assume that a number of solutions to the wave equation exists which precisely or approximately satisfy the indicated condition and the condition of limitation at infinity. In the symmetrical case, for example, a plane wave propagating from $x = -\infty$ to a nozzle is such a solution:

$$\varphi_0(x, t) = -(\gamma_z \vartheta_z)^{-1} P\sin(\vartheta_z \tau_z + \vartheta_z x) . \quad (9)$$

In the antisymmetrical case, the following can serve as an example of such a solution:

$$\varphi_0(x, y, \theta, t) = -(\gamma_z \vartheta_z)^{-1} k\left[N_1'(k) J_1(ky) - J_1'(k) N_1(ky)\right] P\sin(\vartheta_z \tau_z + \sqrt{\vartheta_z^2 - k^2}\, x)\cos\theta . \quad (10)$$

Here, k > 0 - a small constant value, T_1 and N_1 - Bessel functions and Neumann functions of the first order. We note that the distribution $\varphi_0(y)$ qualitatively corresponds to distribution from a dipole whose axis is normal to the axis of the jet; when $y \to \infty$ $\varphi_0(y) \to 0$. When $k \to 0$, the wave equation corresponding to the potential (10) can be made as close to (8) as one wants. (However, when $k = 0$ $\varphi_0 \to \infty$ when $y \to \infty$). Subsequently, we shall need an expression for pressure corresponding to the basic emission only on the surface of the jet, and we shall use formula (8) in both the symmetrical and the antisymmetrical cases; moreover, it will everywhere be assumed that $(\partial\varphi_0/\partial y)_{y=1} = 0$.

The boundary conditions which uniquely determine the perturbed flow in the jet and the external acoustical field should be specified applicable to the physical character of the examined problem [1,2]. When the jet is producing sound at a discrete frequency, effective interaction between the jet and the exterior medium only exists in the region from the cross-section of the nozzle to the region of jet disintegration $(0 \leq x \leq x_*)$. Therefore, the conditions of equality of

pressures and displacements on the boundary between the jet and the exterior acoustical field should only be imposed when $0 \leq x \leq x_*$ and $x > x_*$. One can select the condition of rapid damping of vibrations of the boundary of the jet and the exterior acoustical field with the growth of X (c[1,2]). When $x < 0$ on the surface of a rigid cylinder, the ordinary condition of non -flow is imposed.

Let

$$y(x,\theta,t) = \mathrm{Re}[Y(x)\exp(-i\omega t)]\cos j\theta , \tag{11}$$

be perturbation of the boundary surface, calculated according to the parameters of perturbed flow in the jet, and

$$y_e(x,\theta,t) = \mathrm{Re}[Y(x)\exp(-i\omega t)]\cos j\theta \tag{12}$$

be precisely the same value, but one calculated according to parameters of the perturbed state at the exterior medium. The boundary conditions when y = 1, which impose limitations on mixing of the jet and the exteror medium, can be written in the following form:

$$y_e(x,\theta,t) = \begin{cases} c & \text{when } -\infty < x < 0 \\ y(x,\theta,t) & \text{when } 0 < x < x_* \\ \xi(x,\theta,t) & \text{when } x_* < x < \infty \end{cases} \tag{13}$$

where ξ is a function which rapidly vanishes with the increase in x.

Values Y_e and Y are determined according to the potentials φ and ψ with the aid of differential equations:

$$\frac{\partial y_e}{\partial \tau_e} = \left(\frac{\partial \psi}{\partial y}\right)_{y=1} , \tag{14}$$

$$\frac{\partial y}{\partial \tau} + M\frac{\partial y}{\partial x} = \left(\frac{\partial \varphi}{\partial y}\right)_{y=1} \tag{15}$$

The condition of equality of pressure perturbations on the boundary surface when $0 \leq x \leq x_*$ can be written in the form:

$$p'(x,\theta,t) = p'_e(x,\theta,t) + P\cos(\nu_e \tau_e + \nu_x x)\cos j\theta \tag{16}$$

In order that the solution be completely determined, it is necessary to add the condition of emission for the exterior acoustical field Ψ at infinity to the described condition, and for the perturbations in the jet, a condition on the axis, $\varphi = 0$ when $j = 1$ or $\partial\varphi/\partial y = 0$ when $j = 0$, and a condition on the nozzle cross-section $\varphi = y\alpha\bar{d}\,\varphi = 0$ when $x = 0,\ 0 \leq y \leq 1,\ 0 \leq \theta \leq 2\pi$

Thus, the problem consists in solving the wave equations (4) and (5) with boundary conditions (13)-(16), as well as on the nozzle's cross-section, on the axis, and at infinity. We shall make one remark here. We shall note equation (5) which describes the perturbed state of the exterior medium, with equation

$$\frac{\partial^2\psi}{\partial x^2} + \frac{\partial^2\psi}{\partial y^2} + \frac{1}{y^2}\frac{\partial^2\psi}{\partial\theta^2} - \frac{\partial^2\psi}{\partial\tau_\varepsilon^2} - \varepsilon\frac{\partial\psi}{\partial\tau_\varepsilon} = 0 \tag{17}$$

in which the term $\varepsilon(\partial\psi/\partial\tau_\varepsilon)\ (\varepsilon > 0)$, , which describes the dispersion of energy is present. Such a substitution provides certain advantages during the solution of the wave equation by means of the Fourier transformation. It is ordinary, for example, when using the Wiener-Hopf method [4], where we pass to the limit $\varepsilon = 0$ in the final solution. In this work, during the numerical solution of our problem, we shall assume that ε is small, but differs from 0, considering that the solution to equation (17) with ε is similar to the solution to equation (5). The investigation of the relationship between the solution and the parameter ε confirms this conclusion.

Having substituted expressions (2), (3), (11) and (12) in equation (4), (17), (14), and (15) and having used the relation (7) between perturbations of pressure and the potentials, we obtain the equations and boundary conditions for the complex potentials Θ and Ψ: when $0 \leq y \leq 1,\ 0 \leq x < \infty$

$$\beta^2\frac{\partial^2\Phi}{\partial x^2} + \frac{\partial^2\Phi}{\partial y^2} + \frac{1}{y}\frac{\partial\Phi}{\partial y} + 2iM\delta\frac{\partial\Phi}{\partial x} + \left(\frac{l^2}{y^2} + \delta^2\right)\Phi = 0 \tag{18}$$

when $y \geq 1,\ -\infty < x < \infty$

$$\frac{\partial^2\Psi}{\partial x^2} + \frac{\partial^2\Psi}{\partial y^2} + \frac{1}{y}\frac{\partial\Psi}{\partial y} + \left(\frac{l^2}{y^2} - k^2\right)\Psi = 0 \tag{19}$$

where

when

$$\begin{cases} \Phi = 0 & \text{when} \quad j = 1 \\ \partial\Phi/\partial y = 0 & \text{when} \quad j = 0 \end{cases} \tag{20}$$

when

$$\Phi = \text{grad}\,\Phi = 0 \tag{21}$$

when

$$\text{grad}\,\Phi - M\,\partial\Phi/\partial x) = \Pi(x) = P\exp(-i\vartheta_0 x) \tag{22}$$

where $\Pi(x) = \Gamma_0 i\vartheta_0 \Psi$.

when y = 1

$$\frac{\partial\Psi}{\partial y} = \Theta(x) = \begin{cases} 0 & , \quad x < 0 \\ \frac{\sigma}{\sigma_0}\left(\frac{\partial\Phi}{\partial y} - M\frac{d\Psi}{dx}\right) & , \quad 0 < x < x_0 \\ \Theta(x) = 0 & , \quad x_0 < x \end{cases} \tag{23}$$

when

$$\sqrt{x^2 + y^2} \to \infty \quad , \quad |\Psi| < \infty \quad . \tag{24}$$

We shall determine the solution to equation (18) with boundary conditon (20), (22) and equation (19) with boundary condition (23), (24), considering that functions $\Pi(x), \Theta(x)$. that enter into (22), (23), are known. We seek the solution to equation (18) in the form

$$\Phi(x,y) = F(x,y)\exp(i\sigma x) \, . \tag{25}$$

where

$$F = F_1 + iF_2 \, , \quad \sigma = M\vartheta/\beta^2 \, .$$

Then (18), (22) are transfcrmed to theform:

$$\beta^2\frac{\partial^2 F}{\partial x^2} + \frac{\partial^2 F}{\partial y^2} + \frac{1}{y}\frac{\partial F}{\partial y} + (\lambda^2 + \lambda^2)F = 0 \, , \quad (\lambda = 1/\beta) \tag{26}$$

$$\lim_{x\to\infty}\frac{\partial F}{\partial x} - i(\beta - \delta M)F = -P\exp[-i(\delta + \beta_0)x] - \Pi(x)\exp(-i\delta x) \qquad (27)$$

We apply the Laplace transformation to equation (26) and (27)

$$G(p,y) = \int_0^\infty F(x,y)e^{-px}\,dx \quad , \qquad (28)$$

where p is a complex value, $\mathrm{Re}\ p > C$. Taking (21) into account for determining G, we have the equation

$$\frac{d^2G}{dy^2} + \frac{1}{y}\frac{dG}{dy} - \left(\mu^2 + \frac{j^2}{y^2}\right)G = 0 \qquad (\mu^2 = p^2\beta^2 + \lambda^2) \qquad (29)$$

with a boundary condition with y = 1

$$G(p) = \frac{1}{\gamma}\frac{1}{pM - i(\beta - \delta M)}\left[\frac{1}{p + i(\delta + \beta_0)} + \bar{\Pi}(p)\right] \quad , \qquad (30)$$

where

$$\bar{\Pi}(p) = \int_0^\infty \Pi(x)e^{-i\delta x}e^{-px}\,dx \quad . \qquad (31)$$

The solution to equation (29) which satisfies the condition F = 0 on the axis for j = 1 or $\partial F/\partial y = 0$ for j = 0,

$$\theta(p,y) = A(p)I_j(\mu y) \quad . \qquad (32)$$

where I_j is the Bessel function of an imaginary argument of the order j. The constant A(p) is determined from condition (30). Having completely determined $\theta(p,y)$, we find F(x,y) with the aid of the inverse Laplace transformation

$$F(x,y) = \frac{1}{2\pi i}\int_{s-i\infty}^{s+i\infty} G(p,y)e^{px}\,dp \qquad (s > 0) \quad . \qquad (33)$$

In order to find the solution to equation (19), we apply a Fourier transformation to it

$$H(\alpha,y) = \int_{-\infty}^{+\infty} \Psi(x,y)e^{i\alpha x}\,dx \qquad (0 < \mathrm{Im}\,\alpha < k_2) \quad . \qquad (34)$$

Function $H(\alpha,y)$ satisfies the equation

$$\frac{d^2H}{dy^2} + \frac{1}{y}\frac{dH}{dy} - \left(\xi^2 + \frac{j^2}{y^2}\right)H = 0 \quad , \qquad (35)$$

where

$$\xi^2 = \alpha^2 - k^2 = \alpha^2 - \beta_0^2 - i\varepsilon\beta_0 \quad . \qquad (36)$$

The solution to equation (35), which satisfies the condition of limitation at infinity is

$$H(\alpha,y) = A(\alpha)\cdot K_j(\xi y) \quad . \qquad (37)$$

where K_j - a MacDonald function on the order of j. In this case, the following branch of the function $\xi(\alpha) = \xi_1 + i\xi_2$ was chosen:

$$t_1 = \left[1/2\left(S + \left(S^2 + 4R^2\right)^{1/2}\right)\right]^{1/2},$$

$$t_2 = \operatorname{sgn} R\left[1/2\left(-S + \left(S^2 + 4R^2\right)^{1/2}\right)\right]^{1/2},$$

where

$$S = t_1^2 - t_2^2 = (\mathrm{Re}\,\alpha)^2 - (\mathrm{Im}\,\alpha)^2 - \nu_0^2,$$

$$R = 2 t_1 t_2 = (\mathrm{Re}\,\alpha)(\mathrm{Im}\,\alpha) - \varepsilon\nu_0/2. \qquad (38)$$

Having applied the Fourier transformation to (23), we obtained the boundary condition for equation (35) when y = 1

$$\left(\frac{dH}{dy}\right)_{y=1} = G(\alpha). \qquad (39)$$

where

$$G(\alpha) = \int_{-\infty}^{0} g(x) e^{-i\alpha x}\,dx + \int_{0}^{\infty} g(x) e^{-i\alpha x}\,dx,$$

$$= \int_{0}^{\infty} \frac{a}{a_0}\left(\frac{\partial\Phi}{\partial y} - M\frac{dY}{dx}\right) e^{-i\alpha x}\,dx + I(\alpha). \qquad (40)$$

Function $I(\alpha)$ and (40) is associated with the specific damping law of vibrations of the boundary surface when $x \to \infty$.

Using (40), we find the final expression for the solution $H(\alpha, y)$:

$$H(\alpha, y) = G(\alpha) K_0(ty)/t K_0'(t). \qquad (41)$$

With the aid of the inverse Fourier transformation, we obtain $\Psi(x, y)$

$$\Psi(x, y) = \frac{1}{2\pi}\int_{i\delta-\infty}^{i\delta+\infty} H(\alpha, y) e^{-i\alpha x}\,d\alpha \qquad (0 < \delta < k_2). \qquad (42)$$

Using the results obtained above, one can construct an iteration process of solving equations (18), (19) with boundary conditions (20) -(24). It consists in the following:

1. When $x > 0$ the zero approximation $n^0(x)$ of function $n(x)$ is assigned.

2. One determines the solution $\Phi(x, y)$ which describes the perturbed flow in the jet according to (25)-(33).

3. Integration of the equation

$$M\frac{dY}{dx} = \nu Y + \left(\frac{\partial\Phi}{\partial y}\right)_{y=1}, \quad Y(0) = 0, \qquad (43)$$

which, associates perturbation of the boundary of a jet Y with the potential Θ is determined by the right hand part in the boundary condition (23).

4. The solution $\psi(x,y)$ which describes the perturbed state of the exterior medium is determined according to (34), (42). The first approximation for $\Pi(x)$ is determined according to the obtained solution:

$$\Pi^{1}(x) = I_{\varepsilon} + I_{\varepsilon} \Psi \qquad (44)$$

5. The described process is multiply repeated so long as the sequential approximations $\Pi^{n}(x)$ and $\Pi^{n+1}(x)$ are not sufficiently close to $0.....$ in the entire range. We note that it is desirable to refine the successive approximations of Π^{n} according to forumulas of the following type in order to insure and speed up convergence of the iteration cycle:

$$\tilde{\Pi}^{n} = F(\Pi^{n}, \tilde{\Pi}^{n-1}, \Pi^{n-2}, \ldots)$$

In this work, the method of the false position [5] was used for such refinement. This method is a generalization of the method of secants to the case of the operator equations.

The described algorithm was performed on the computer. In this case, the Laplace and Fourier transformations were made numerically according to the Simpson formula on segments of a finite line divided into 95 intervals. With suffificiently long lengths L, of these segments, the solutions practically did not depend upon L.

In order to test the accuracy of the obtained solutions, the latter were placed in the equations and boundary conditions (18)-(23). Calculations showed that these relationships are satisfied with good accuracy.

In the plane case, the original equations (4) and equation (17) should be replaced by equations:

$$\beta^{2}\frac{\partial^{2}\psi}{\partial x^{2}} - \frac{\partial^{2}\psi}{\partial y^{2}} + 2M\frac{\partial^{2}\psi}{\partial x \partial \tau} + \frac{\partial^{2}\psi}{\partial \tau^{2}} = 0 \qquad (45)$$

$$\frac{\partial^{2}\psi}{\partial x^{2}} + \frac{\partial^{2}\psi}{\partial y^{2}} - \frac{\partial^{2}\psi}{\partial \tau_{\varepsilon}^{2}} - \varepsilon\frac{\partial \psi}{\partial \tau_{\varepsilon}} = 0 \qquad (46)$$

Equations (18), (19), (26), (29) and (35) also correspondingly change; the relationship with angle Θ in all formulas is naturally absent.

The solutions to the differential equations for the images G and H of potentials F and Ψ in the plane case are written via the Poiner and not the Bessel functions. Namely, instead of (32) we have

$$G(p,y) = \begin{cases} A(p)\operatorname{ch}\mu y & \text{when } j = 0 \\ A(p)\operatorname{sh}\mu y & \text{when } j = 1 \end{cases} \tag{47}$$

and instead of (37) we have

$$H(\alpha,y) = A(\alpha)e^{-\alpha y} \text{ when } j = 0 \text{ и } 1 \tag{48}$$

We now note that if one sets $\Pi^0(x) \equiv 0$ in the iteration cycle described above, and one limits oneself to the zero approximation, then we obtain a solution to the problem in the simplified statement. In such a solution, one ignores the secondary acoustical emission from the surface of the jet.

The inverse Laplace transformation (33) when $\Pi(x) \neq 0$ can be made analytically, using the Jordan lemma and Cauchy theorem of residues, similar to the way this was done for the plane case in [1, 2]. We here write the single solution for the plane (m = 0) and cylindrical (m = 1) solution for the antisymmetrical (j = 1) perturbations in the exterior acoustical waves.*/

$$F(x,y) = F_1 + iF_2 = \Phi(x,y)\exp(-i\alpha x)$$

$$F_1 = \frac{p_0}{T^M}\left\{\frac{1}{c-d}\left[f_m^{(1)}(y)\sin\frac{dx}{\beta} - f_m^{(0)}(y)\sin\frac{cx}{\beta}\right] - \right.$$

$$\left. - \sum_{n=1}^{\infty} \frac{cd + \Lambda_{mn}^2}{(c^2-\Lambda_{mn}^2)(d^2-\Lambda_{mn}^2)\Lambda_{mn}} f_{mn}^{(1)}(y)\sin\frac{\Lambda_{mn}x}{\beta}\right\}$$

$$F_2 = \frac{p_0}{T^M}\left\{\frac{1}{c-d}\left[f_m^{(1)}(y)\cos\frac{dx}{\beta} - f_m^{(0)}(y)\cos\frac{cx}{\beta}\right] - \right. \tag{49}$$

$$\left. - \sum_{n=1}^{\infty} \frac{c+d}{(c^2-\Lambda_{mn}^2)(d^2-\Lambda_{mn}^2)} f_{mn}^{(0)}(y)\cos\frac{\Lambda_{mn}x}{\beta}\right\}$$

---

*/ - The solution to the problem in the simplified presentation for the cylindrical case was obtained by a student at Moscow State University, V. V. Labutina.

where

μ_n - the n-th root of the Bessel function T_1.

We note that the solutions obtained from (49) in the cylindrical case for pressure perturbation p' and the velocity components Φ_x have infinite discontinuities on characteristics BC, CD, FG, GH (Figure 1). A similar result was earlier obtained in a work [6] during investigations of perturbed, supersonic steady-state flow in cylindrical tubes and jets during an investigation. One can assume that this effect, associated with the description of the reflection of discontinuities from the axis by linearized equations of gas dynamics, has an effect on the solution only in the vicinity of the discontinuity lines. This is also confirmed by calculations that were made especially, in which the condition $\Phi = 0$ or $\partial\Phi/\partial y = 0$ was set not on the axis, but on a certain cylindrical surface of small radius δ surrounding the axis.

It is also important to note that the solution for the boundary of the perturbed jet and the distribution of pressure on the jet boundary do not have discontinuities.

2. Investigation of obtained solutions. We shall initially refer to the solution to the problem in the simple statement (49). By investigating the singular points of the solution (49), one can as was done in [1,2], derive a formula for critical frequencies of the exterior acoustical waves, with which, as will be shown below, one deals with maximum intensification of perturbations in the jet. We shall write the general formula for the plane (m = 0) and cylindrical (m = 1) cases, both for the symmetrical (j = 0), and for the

antisymmetrical (j = 1) perturbations in the exterior wave:

$$Sh_n = \frac{\omega_n 2R}{a_1} \qquad (50)$$

Here, Strouhal number, calculated according to the linear frequency , velocities of sound in the exterior medium a_1, and diameter width of jet 2R; n = 1, 2, 3,..., and functions h(n) is defined as:

$$\qquad (51)$$

By , we have in mind, respectively, n-th roots of the Bessel functions T_0 and T_1. We shall give the first three values of the functions h(n) for the cylindrical case:

when $j = 0$ $h(n) = 0.76,\ 1.76,\ 2.75$
when $j = 1$ $h(n) = 1.22,\ 2.23,\ 3.23$

We note that the relationship of critical frequencies for the plane and cylindrical cases which correspond to precisely the same value of n does not depend upon the parameters which determine flow in the jet and in the exterior medium, and is always greater than unity.

In Figure 2, according to the formula (50), the relationship $Sh_n(M)$ is plotted when n = 1 for a cylindrical cold jet (stagnation temperature T_0 which is equal to temperature of the exterior medium T_e)in the case of an antisymmetrical acoustical field. Here, too, a semi-empirical relationship between the frequency of the discrete component (the first tone) and parameters of the circular jet and the exterior medium

$$Sh_1 = \frac{0,85}{\sqrt{M^2 - 1} + a_e/a} \qquad (52)$$

are obtained in [7] when processing a large number of experimental data obtained from different authors is given. The dash line in Figure 2 plots the scatter boundaries of the experimental data. The coincidence of our results with the experimental data can be considered satisfactory, particularly at low M nubmers of the jet. For comparison, Figure 2 also plots the relationship $Sh_n(M)$ for the plane, antisymmetrical case.

Figure 2

1--critical frequency of the antisymmetrical, exterior acoustical wave for the cylindrical case; 2--the same, for the plane case; 3--empirical relationship of the frequency of the discrete component in the noise spectrum of the circular jet [7]; --- - scatter boundaries of experimental data

We shall now proceed to examine solutions to the non-simplified problem */. We shall chiefly investigate the behavior of the value K_p, which is the ratio of the amplitude of pressure perturbations in any particular point of the jet or exterior medium to the amplitude P of the exterior acoustical wave (8). For points within the jet, K_p is the coefficient of intensification of pressure perturbations in the jet in comparison with the assigned perturbations (8) which characterize basic emission. For the exterior medium, K_p is the amplitude of pressure pulsations caused both by the basic emission (8) and by secondary emissions from the edge of the oscillating jet. We shall also examine perturbations of pressure in the exterior medium due solely to secondary emissions; their amplitude, related to P, shall be designated as K'_p. Subsequently, inasmuch as the characteristic dimension of our problem is the length of a unit of the jet $L = 2a$, $\beta = \sqrt{M^2-1}$ (Figure 1), we shall use the coordinate $x = x/\beta$, y during the analysis.

Figure 3

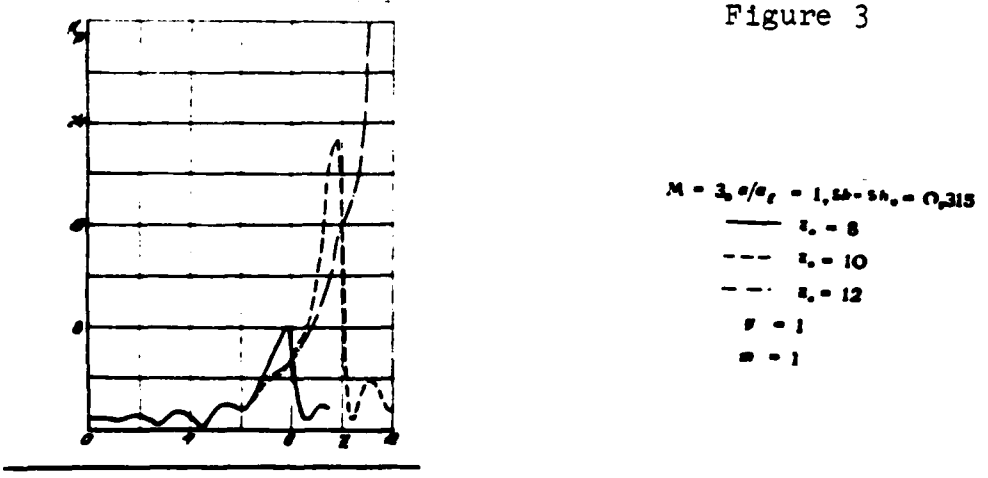

*/ Everywhere, unless otherwise stated, the case of the antisymmetrical acoustical field (j = 1) is investigated.

It is primarily necessary to explain what effect the boundary condition (18) of rapid damping of boundary oscillations of the jet behind the cross section $z = z_0$ set by the authors has on the solution in the region $z < z_0$, inasmuch as this condition, of course, quite crudely simulates the termination of effective interaction of the jet and the exterior medium existing in reality. Figure 3 plots relationships with the coordinate z of the value K_p on the boundary of the cylindrical jet for calculation with $M = 3$, $a/a_r = 1$, $Sh = Sh_0 = 0.315$. Comparing the solutions obtained when $z_0 = 8$, 10 and 12, one can see that a common curve exists with which the curve $K_p(z, z_0)$ merge which corresponds to various z_0. The divergence of curves $K_p(z, z_0)$ from the common curve begins approximately when $z = z_0 - 2$ for each z_0. The curves $K_p(z, z_0)$ behave similarly when $y < 1$, i.e., within the jet.

In $y = 1$, the relationship $K_p(z)$ in the vicinity of the point $z = z_0$ has the character of a rapidly dampning flare (Fig. 3). The value of this flare depends upon the selected law of dampning of vibrations of the boundary surface when $z > z_0$. Cases were examined in the work when the displacement value of Y when $z > z_0$ either identically equals 0, or decreases to 0 with the increase in z exponentially or according to a parabolic law. However, the solution when $z < z_0$ outside the small vicinity of the point z_0 is practically not affected by the selected damping law.

Thus, one can conclude that if at least for $z_0 \leqslant 12$, the effect of the boundary condition when $z \geqslant z_0$ is only felt on the solution to our problem when $z < z_0$ in the vicinity of a point $z = z_0$, with a length on the order of 1 jet unit (for pressure). In this case, the case examined in Figure 3, when amplitude of pressure perturbations K_p on the boundary of the jet rapidly increases with distance from the nozzle is the most unfavorable one. In those cases when a noticeable increase in K_p on the boundary of the jet with the increase z does not occur, the effect of the boundary condition when $z > z_0$ on the solution is still weaker.

We finally note that the solution which describes vibrations of the jet boundaries when $z < z_0$ does not practically depend on the choice of z_0, and the condition set when $z > z_0$.

The figure 4 compares the simplified solution (49) and the complete solution obtained numerically for the plane case. The distribution of the amplitude of pressure perturbations K_p within the jet ($y = 0.5$) along the z coordinate for a version $M = 3, a/a_1 = 1$, $Sh = Sh_* = 0.26$, is plotted.

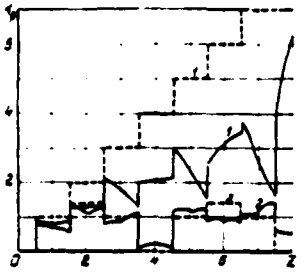

$m = 0$, $M = 3, a/a_1 = 1$.
1. $Sh = Sh_* = 0,26$.
2. $Sh = 0,5 \cdot Sh_* = 0,13$
——— complete solution
----- simplified solution

Figure 4

Comparison of the data in Figure 4 shows that even in a case when one takes the secondary acoustical emission from the boundary of the jet into account, the value of K_p at the critical frequency increases, on the average, with distance from the nozzle cross-section; in this case, during the transition through each discontinuity surface, value K_p increases. Doubtlessly, pressure perturbations are smaller here (1.5 - 2 times) than in the simplified solution which does not take into account the removal of acoustical energy from the jet's surface. We note that the segments of the jet on which K_p diminishes pertain to characteristic triangles of the type C D E in Figure 1, one of whose sides is the boundary of the jet from which the acoustical energy is removed. On the other hand, the segments on which K_p conserves a constant value or increases pertain to triangles of the D E F type, not associated with the jet boundary.

A comparison of the complete and simplified solutions is also made in Figure 4 for the frequency $Sh = 0.5\, Sh_*$. Both solutions are similar and are periodic solutions.

Figure 5

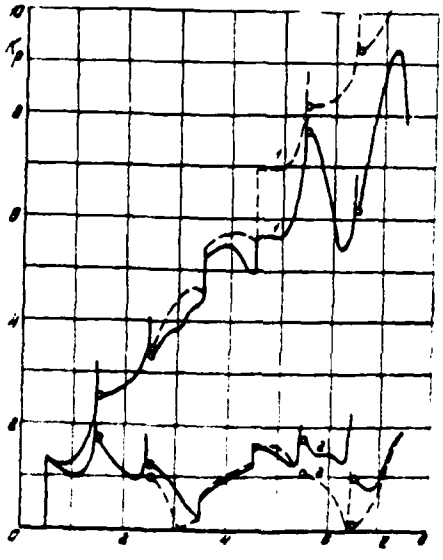

$m = 1$,
$M = 3, a/a_* = 1.$
$Sh = Sh_* = 0{,}315$
$Sh = 0.5\ Sh_* = 0{,}157.$
—— complete solution
--- simplified solution

A similar comparison was made in Figure 5 for the cylindrical case. Here the value K_p once again increases with distance from the nozzle at the critical frequency $Sh = Sh_*$, on the average, and at the frequency $Sh = 0.5\,Sh_*$ relationship $K_p(z)$ is periodic. One can note that the effect of secondary emission on the perturbed flow in the jet is weaker in the cylindrical case than in the plane case.

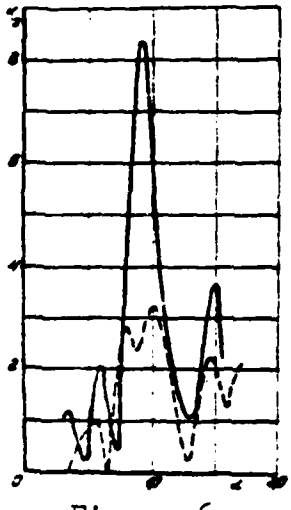

Figure 6

$M = 3,\ a/a_* = 1,\ z = 8,$
$y = 0{,}5$

—— $m = 1$,
--- $m = 0$.

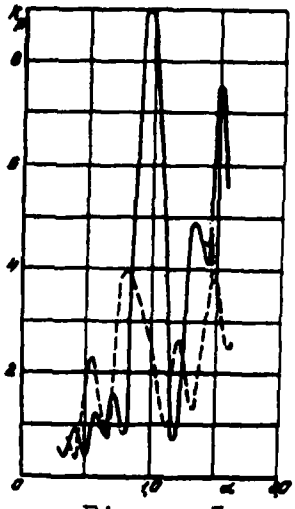

Figure 7

$M = 3,\ a/a_* = 1,\ z = 7.$
$y = 0{,}8$

—— $m = 1$,
--- $m = 0$.

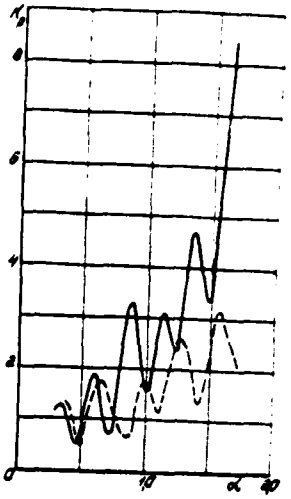

Figure 8

$M = 3,\ a/a_1 = 1,\ z = 7,\ y = 1$

— $m = 1$.

-- $m = 0$.

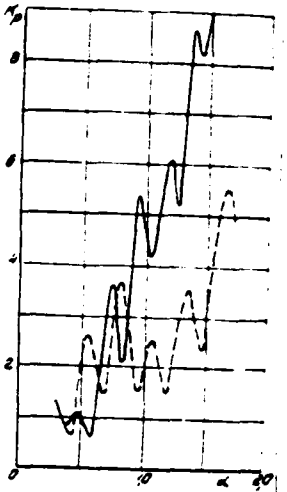

Figure 9

$M = 3,\ a/a_1 = 1,\ z = 8,\ y = 1$.

— $m = 1$.

--- $m = 0$.

Figures 6 and 7 plot the relationships of the K_p value within the jet ($y = 0.5$) for cross section $z = 6$ and 7 with the ratio α of the frequency of exterior acoustical wave Sh to the critical frequency Sh_* calculated according to (50), when $n = 1$. Taking into account the removal of acoustical energy from the boundary of the jet does not lead to a noticeable change in the value of the critical frequency, whose formula was derived when solving the problem in the simplified statement, for the cylindrical jet. For cold jets, the maximum K_p is reached as it were when $\alpha = 1$, i.e., . When the jet is heated, one observes a slight decrease in the frequency which corresponds to the peak of the value K_p, as in Figures 6 and 7; however, even for an infinitely heated jet , displacement according to the peak frequency of the value K_p relative to $\alpha = 1$ does not exceed 5-7%.

Curves have an absolute maximum when for the plane jets when $z = 6$ and other whole even values of z. Additionally, one has a local maximum when whose value is comparable to the value of the absolute maximum. It is interesting that when the curve for the whole, odd z (for $z = 7$ in Figure 8) has an

absolute maximum, but when $\alpha = 1$ the maximum does not exist at all, and instead of it, one has a point of inflection. Thus, in the plane case secondary acoustical emission from the jet surface leads to the appearance of still another frequency at which perturbations develop in the jet which are comparable to perturbations at the critical frequency.

We note that significantly greater perturbations develop in the cylindrical jet at the critical frequency than in the plane one; relationships $K_p(\alpha)$ are characterized by more clearly pronounced peaks.

We return to the behavior of the relationship $K_p(\alpha)$ on the boundary of the jet (Figures 8,9). In the simplified solution, K_p is the amplitude of the exterior wave (8) when $y = 1$, such that $K_p(1)$. The relationships $K_p(\alpha)$ in the complete solution are depicted by the curves with a large number of maxima and minima. In this case, the values of the extrema increase with the increase in the frequency α, and a particularly sharp increase in the value K_p is observed when $\alpha > 1$; this increase is the more intensive, the further we are from the nozzle.

Figure 10 investigates the effect of the Mach number of the jet M and the ratio a_1/a_0 of velocities of sound in the jet and in the exterior medium on the distribution $K_p(z)$ on the boundary of the jet for critical frequencies in the cylindrical case. Value K_p does not strongly differ from the amplitude of exterior acoustical waves (i.e., from 1) $z = 3-6$. When $z > 6$, the contribution of secondary emission from the surface of the jet to total emission is the basic one, and the value of K_p increases very rapidly with the increase in z, exceeding the amplitude of the base wave 5-10 times when $z = 8$, and 10-20 times when $z = 9$ (the effect of the boundary condition when $z = 10$) is already felt in the data when $z = 9$, to the point). For cold jets, the intensive increase of K_p begins earlier relative to z (i.e., closer to the nozzle) with a decrease in M number of the jet; we note that when $M = 4$, such an increase is generally not observed. In the case of the jet with different temperatures,

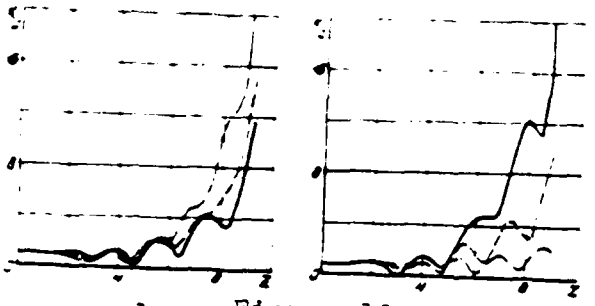

Figure 10

$\gamma = 1$, $M = 3$, $m = 1$

a)

	a/a_*	$Sh = Sh_*$
——	0,8	0,28
- - -	1	0,315
- · -	100	0,43

б) $\gamma = 1$, $T_* = T_e$, $m = 1$

	M	a/a_*	$Sh = Sh_*$
——	2	0,75	0,38
- - -	3	0,8	0,28
- - -	4	0,44	0,20

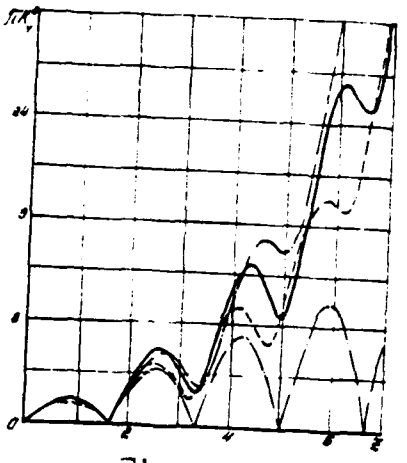

Figure 11

	M	a/a_*	$Sh = Sh_*$
——	3	0,8	0,28
- -	3	1,00	0,43
- · -	2	0,75	0,38

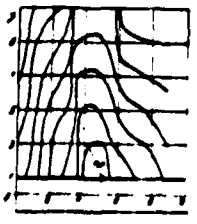

$m = 0$, $M = 3$, $a/a_* = 1$,
$Sh = Sh_* = 0,28$, $\Delta\varphi = 30°$.

Figure 12

a more rapid increase in K_p (z) is observed for the hotter jets, although the differences here are not very significant.

The value K_p behaves similarly as well on the surface of the plane jet.

The behavior of K_p within the jet at the critical frequency is characterized by the fact that prior to [illegible], the relationship between K_p and the coordinate z is close to monotonic increase (Figure 5). In this case, the complete and simplified solutions are similar; the relationships [illegible] nearly do not differ until z = 5, corresponding to various [illegible]. When z > 6 in regions of continuity, K_p, one has sharp drop and increases in K_p. Such a character of the behavior of K_p is clearly defined for a jet with small M.

Figure 11 plots the relationship between coordinate z and the value [illegible] for the case of the critical frequency:

$$K_y^* = \frac{\gamma M^2}{\rho_0 T} K_y$$

where K_y - amplitude of vibrations of the jet boundary. A comparison was made for the relationships [illegible] for the simplified and complete solutions. These two solutions, as in the case with the pressure distributions, are similar when z < 5, but a sharp increase in the scale of vibrations of the jet occurs for the complete solution at higher values of z. In both cases, the jet vibrates, significantly deforming (bending). There are points on the boundary of the jet which remain stationary for the simplified solution. In the complete solution these points correspond to points of the minimum range of vibrations of the stream boundary. We note that the value [illegible] for the simplified solution with the given [illegible] and [illegible] does not practically depend upon the parameters [illegible]. The most rapid increase [illegible] with the increase in z is observed for cold jets with small Mach numbers for the complete solution.

It is interesting to examine a perturbed flow in the exterior medium due to secondary emission from the jet surface. Figure 12

plots lines of equal phase (through 90°) of the secondary acoustical emission (for pressure) in the plane case when $M = 3, a/a_i = 1, Sh = Sh_0 = 0.28$. It is evident from the graph that pressure perturbations in the exterior medium caused by pulsations of the jet in it, propagate approximately like cylindrical waves with a center in the mid point of the third unit of the jet.

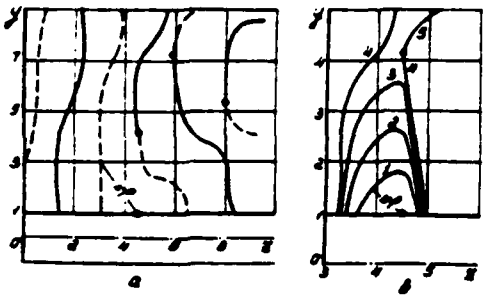

Figure 13

$m = 1, \quad M = 3, \quad a/a_i = 0.8, \quad Sh = Sh_0 = 0.28.$

a. —$\Delta\varphi = 0$ ---$\Delta\varphi = 180°$

b. 1. $\Delta\varphi = 22°,5.$ 2. $\Delta\varphi = 45°.$ 3. $\Delta\varphi = 67°,5.$
4. $\Delta\varphi = 90°.$ 5. $\Delta\varphi = 270°.$

The picture of secondary emission in the case of the cylindrical jet is somewhat more complicated (in Figure 13, for M = 3, $a/a_i = 0.8$ (cold jet), $Sh = Sh_0 = 0.28$). . In this case, we once again observe the presence of an effective source of emission situated on the surface of the jet within the confines of its third unit (when z = 4.5). In the vicinity of the point z = 4.5, the equiphase lines are closed lines with a pole at this point (Figure 11B). However, far from the source one has points in which the amplitude of the secondary emission vanishes. Not one, but several sets of phase lines run through such points, and with the transition through such a point the phase changes in jump fashion by 180°. In this case, within the confines of the calculated region (up to $y \leq 8$), one does not detect a tendency toward formation of closed lines with a common pole. Thus, unlike the plane case, perturbations in the exterior medium propagate as waves from a certain effective source only in a comparatively small vicinity of the source, and subsequently the picture is more complex in the far acoustical field.

Qualitatively, the picture of phase lines is precisely the same with other M, a/a_* as well. The position of the effective source depends weakly on M; for heated jets, the source is displaced further from the nozzle cross section, but remains within the confines of the third cell even for an infinitely heated jet.

The Figure 14 plots the relationship between the amplitude of pressure perturbations in the exterior medium K'_p, due to secondary emission with the polar angle (the pole in the effective source on the surface of the jet, i.e., when $\gamma = 1$, $\bar{x} = 4.5$, 0° corresponds to the direction from the source to the nozzle) at distances from the source $\bar{r} = 0.5\beta$ and $\bar{r} = 1.5\beta$ for a case $M = 3$, $a/a_* = 0.8$, $\Delta h_0 = 0.28$,

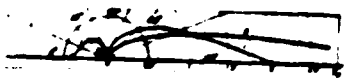

Figure 14

$n = 1$, $M = 3$, $a/a_* = 0.8$, $\Delta h_0 = 0.28$. Полюс в точке (1) $\bar{x} = 4.5$, $\gamma = 1$, 0° – направление от полюса к сопл. (2). 1. $\bar{r} = 0.5\beta$, 2. $\bar{r} = 1.5\beta$.

Key:
(1) pole and the point
(2) direction from pole to nozzle

As is evident from the constructed diagram, secondary emission from the surface of a pulsating jet at the critical frequency has the form of emission from a dipole with an axis parallel to the jet axis.

We shall interpret the obtained results according to secondary emission and its effect on flow in the jet:

At the critical frequency, secondary emission from the surface of the jet or at least near this surface has the form of emission from an effective source situated within the confines of the third jet cell;

at basic emission frequencies comparable with the critical frequency and exceeding it, the amplitude of secondary emission can noticeably exceed the amplitude of the base emission;

a sharp increase in the amplitude of the secondary emission on the surface of the jet and in the scale of vibrations of the boundary of the jet begins beyond the third-fourth cells of the jet;

it also leads to a significant change in the character of perturbed flow in the jet;

The increase in the value $\varkappa$ observed at jet Mach numbers M < 3 is particularly sharp for cold jets; on the other hand, when M > 4 secondary emission does not make an important contribution to total emission; for jets with identical M and different temperatures, differences are not very great;

The conclusions that were drawn are identically valid for plane and cylindrical jets and in the cylindrical case the noted characteristics of secondary emission appear more sharply.

It is interesting to compare the obtained results with the data of an experiment, photography of plane and circular jets, which study the sound of the discrete frequency cited in works [8-14], which make it possible to draw a schematic picture of jet pulsations (Figure 15).

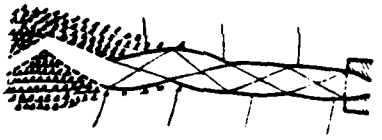

Figure 15

In all the photographs one can clearly see the first two cells of the jet, whose displacement relative to the steady-state position is practically absent. This is in agreement with our data, according to which the amplitude of secondary emission in small in this region, as are displacements of the jet boundary. The two succeeding cells are also quite clearly evident in the photographs; however, their vibrations are already extremely noticeable; vortices break away from the surface of the jet into the surrounding medium. According to our own results, a noticeable increase in the amplitude of secondary emission and the scale of jet vibration begins within limits of the third-fourth cells. This increase in the linear solution becomes exceedingly rapid behind the fourth cell of the jet. In the full scale model, the presence of non-linear and dissipated mechanisms limits the increase in pulsations. Actually, it is evident, according

to the photographs that a powerful formation of vortices begins behind the fourth cell and the jet practically disintegrates. The jet cells behind the fourth cell in certain photographs are indistinguishable, while on others they are visible with great difficulty--this depends upon the conditions of the experiments, specifically, on the presence of reflecting surfaces in the acoustical field of the jet, for example, the end of the nozzle which is not covered with sound absorbing material.

The Figure 16 gives a qualitative comaprison of our results with experimental data [14] for a sonic, super-expanded jet. In the experiment, the pressure drop in the nozzle receiver and the surrounding medium was $p_0/p_\infty = 3.07$, which corresponds to an average M number of the jet of ~ 1.5. The points in Figure 16 plot the values of the amplitude of pressure fluctuations Δp_z near the surface of the jet, due both to the emission of noise by the jet and to the presence of pulsations with a discrete frequency, taken from [14]. The maxima and minima in the distribution of Δp_z are in fact due to the presence of discrete pulsations. One can note that the positions of these extrema coincide well with the positions of the extrema and the distribution of K_p when $y = 1$, plotted according to the result of our calculations for a cold jet with $M = 1.5$, affected by an exterior acoustical wave with a frequency Δp_z . It is evident according to the photograph [14], that when $z > 8$, i.e., where a rapid increase in K_p takes place in the linear solution, the jet has totally disintegrated; the noise spectrum of the jet is even in this region, without discrete components, and Δp monotonically diminishes.

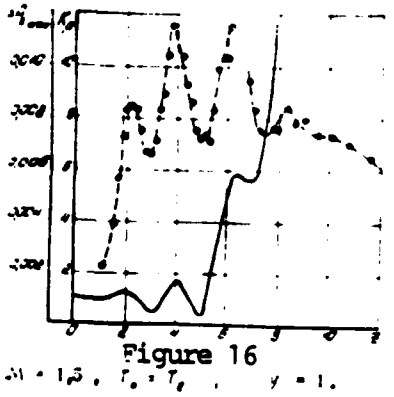

Figure 16

Thus, there is a qualitative coincidence between our results and the experimental data, and the deterioration of the jet corresponds to a rapid growth in perturbations on the surface of the jet in the linear solution.

We note that the picture of acoustical waves emitted by jets can be reduced to a picture of spherical waves emitted by a certain effective source, with good accuracy. The position of the source can be determined according to photographic data. The measurement of photographs made in a number of works shows that that the effective source lies within the region of the sixth-eighth cells of the jet. It is interesting that one other source of emission was detected in an experiment [10] with plane jets besides the basic one. The additional source is located at the beginning of the third jet cell. This source can evidently be compared with the effective source of secondary emission, which we discussed above on the basis of the results of our calculations.

We shall now turn to an investigation of the problem of interaction of the cylindrical jet with a symmetrical acoustical field ($j = 0$). Figure 17 plots the relationship between frequencies Sh of the exterior waves of the amplitude of pressure perturbations K_p for a cross section $z = 6$ when $y = 0$ (axis of the jet) and $y = 1$ (boundary closed) for a case [illegible]. There is a maximum within the jet K_p at a frequency equal to the critical frequency [50]. When $Y = 1$, secondary emission does not make a noticeable contribution to total emission.

Figure 18 compares the amplitudes of vibrations of the boundary of the jet [illegible] in the symmetrical and antisymmetrical cases with critical frequencies of the corresponding perturbations. In the symmetrical case, the value of [illegible] increases on the average linearly with the increase in z unlike the antisymmetrical case, where the scale of vibration of the jet sharply builds up with large z.

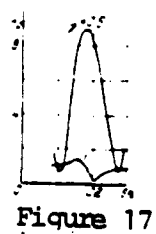

Figure 17
$m = 1$, $j = 0$, $M = 3$, $a/a_1 = 1$, $z = 6$.

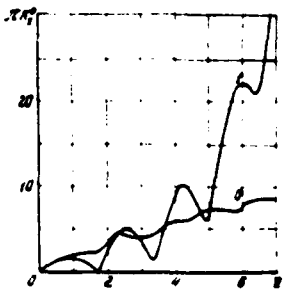

Figure 18

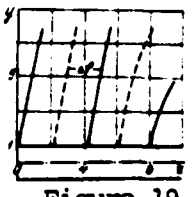

Figure 19
$m = 1$, $j = 0$, $M = 3$, $a/a_1 = 1$, $Sh = Sh_0 = 0.18$, $\Delta\varphi = 180°$.

The cited data indicate that the jet in the symmetrical, exterior acoustical field is more stable than in the antisymmetrical one. This result is in accord with the fact that no jet emission of sound at a discrete frequency with a symmetrical character of the acoustical field is observed in experiments.

Figure 19 plots phase lines of the secondary emission of the jet, confirmed by the effect of the symmetrical pressure wave at a frequency equivalent to the critical frequency. It is curious that these lines are parallel straight lines throughout nearly the entire calculated region, such that in this case secondary emission is a plane wave inclined toward the jet axis at an angle of about~60°.

3. The effect of a subsonic satellite flow. One can solve the problem of the interaction of the supersonic jet with the exterior acoustical field with the presence of a subsonic satellite flow in the exterior medium with the Mach number M_e. In this case, the basic equations and calculation formulas only change slightly. Certain results of solving this problem for the antisymmetrical case will be given below.

By using the simplified statement of the problem, one can derive the formula for critical frequencies of exterior acoustical waves in the examined case:

$$\Omega_{kp} = \frac{\sqrt{n^2-1}}{a_0} \cdot \frac{h(n)}{\sqrt{\left(\frac{a_0}{a}\right)^2 - \frac{n^2-1}{\gamma M_e^2}}\left(\frac{a_0}{a} - \frac{n^2-1}{\gamma M_e^2}\right)} \qquad (53)$$

where the function h(n) is defined in (51).

Figure 20 plots the relationship between the critical frequency Ω_{kp} and the number M_e of the satellite flow for a cold cylindrical jet with M = 2.5. The same figure plots A. G. Yepifanskiy's experimental data on the frequency of the discrete component of the cold jet in the satellite flow. In the experiment, the discrete component was registered with numbers $M_e = 0.6-0.7$ at 2 close frequencies (1 and 11 in Figure 20). The coincidence of our results with the experimental data when $M_e \approx 0.6-0.7$ is satisfactory with respect to the frequency value.

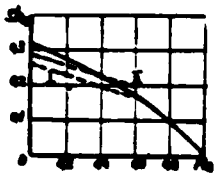

Figure 20

M = 2,5 ; $r_0 = r_c$

- critical frequency of antisymmetrical, exterior acoustical wave for the cylindrical case; - - - experimental relationship of frequencies of the discrete components in the noise spectrum of the circular jet.

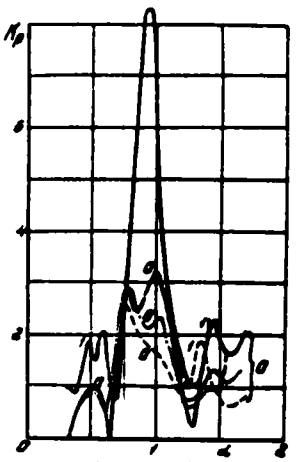

Figure 21

M = 3, $a/a_c = 1$, $0 - m = 0$, $1 - m = 1$

—— $M_e = 0$ --- $M_e = 0{,}28$ --- $M_e = 0{,}5$

$z = 6$, $y = 0{,}5$

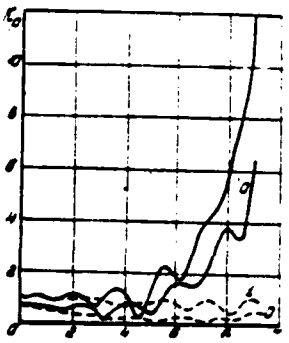

Figure 22

M = 3 ; $a/a_c = 1$; $y = 1$; $Sh = Sh_c$, $0 - m = 0$, $1 - m = 1$

—— $M_e = 0$

-- $M_e = 0{,}5$

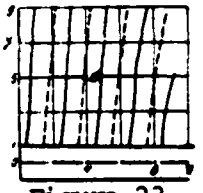

Figure 23

$m = 1$, $M = 3$, $M_e = 0{,}5$, $a/a_c = 1$, $Sh = Sh_c = 0{,}18$, $= 180°$.

Relationships between the value K_p within the jet and the ratio α of the frequency of exterior waves to the critical frequency (53) for $n = 1$ appear in Figure 21 for several values for M_e. In the cylindrical case, formula (53) derived when solving the problem in the simplified presentation, determines the frequency value at which the jet maximally intensifies the perturbations transmitted to it, and then, when one takes secondary emission into account. The presence of satellite flow slightly alters the value of K_p within the jet. In the plane case, one observes displacement of the basic maximum of the curve $K_p(\alpha)$ with the critical frequency $\alpha = 1$ to a frequency $\alpha = 0{,}8$, with

the increase in the M_e number; in the vicinity of the latter frequency, the value of K_p weakly depends on M_e.

Figure 22 gives the distribution of K_p along the boundary of the jet for $M = 3, a/a_1 = 1, M_1 = 0$ and 0.5. All data pertain to cases of critical frequencies of exterior waves. With the presence of a satellite flow on the surface of the jet in the entire calculated segment (up to z = 10), secondary emission proves to be slight and the amplitude K_p of total emission is nearly 1. Thus, the presence of a satellite flow has a stabilizing effect on the jet. These data are in accord with the results of an experiment, according to which jets in a satellite, subsonic flow do not emit sound of a discrete frequency when $M_1 > 0.6 - 0.7$.

Figure 23 plots the phase lines of secondary emission from the surface of a cylindrical jet situated in a satellite flow ($M = 3, M_1 = 0.5, a/a_1 = 1$) with a critical frequency of the exterior wave $Sh = Sh_1 = 0.18$. It is interesting that the picture of the phase lines in this case does not have anything in common with the corresponding picture for the case of a jet flowing into a flooded space (fig 13). With the presence of the satellite flow, perturbations caused in the exterior medium by jet pulsations propogate like plane waves, inclined toward the jet axis. This picture of phase lines is very similar to the picture for the case of symmetrical jet pusations (fig 19). These data and those given above indicate that both the presence of a satellite flow during antisymmetrical perturbations in the exterior acoustical field and "symmetrization" of perturbations have an identical, stabilizing effect on the jet.

4. Basic conclusions. On the basis of the results of the investigation of solutions to the problem of the interaction of a supersonic jet with the exterior acoustical field (in the linear approximation and the simplified presentation for the plane case in [1,2], in the linear approximation and the complete presentation for the plane and the cylindrical cases in this work, and the nonlinear solution in the simplified presentation for the plane case in [1,2]) one can draw the following conclusions:

/. The authors' hypothesis that the supersonic jet, because of its periodic (cellular) structure has properties of a unique resonator is confirmed: During interaction with the exterior acoustical field, the jet intensifies the perturbations transmitted to it from the outside at certain, entirely determined frequencies. In accordance with the model of the phenomenon, accepted in the work, the emission of sound at a discrete frequency by supersonic jets should, in fact, occur at these critical frequencies. This is confirmed by comparing values of critical frequencies calculated according to the formulas cited in the work with the experimental values of frequencies of the discrete components of the noise spectrum of the supersonic jets.

2. During the interaction of a supersonic flowing into a flooded space with the antisymmetrical acoustical field, perturbations on the jet's surface rapidly increase with distance from the nozzle cross-section; the development of perturbations is particularly rapid behind the fourth jet cell. This effect does not exist if the jet flows in a subsonic satellite flow with a sufficiently high M_e number, as well as during the interaction of the jet with the symmetrical acoustical field. In all cases when the results of the calculations could be compared with the experimental results, it proved that the presence of emission at a discrete frequency in the experiment corresponds to the rapid development of perturbations on the jet surface in the calculation.

3. The investigation of the nonlinear solutions shows that the jet ceases to intensify the perturbations arriving from the outside with sufficiently high amplitudes of the exterior acoustical waves. This indicates the possible mechanism of limiting the growth of pulsations in the jet, which leads to the establishment of self-excited vibrations. It is in fact the jet which intensifies the perturbations transmitted to it by the exterior wave. In this case, perturbations of already high intensity are emitted in the region of its disintegration, which will be intensified in their turn by the jet, etc. However, when sufficiently high perturbations develop in the jet, this leads to the distortion of its periodic structure and deterioration of its resonator properties, as a result of which the increase in perturbations ceases.

4. In order to culminate the study of the examined problem in the linear approximation, it is necessary to investigate the effect of the form of basic emission ψ_0, as well as the waves reflected by the various screens.

The linear solutions make it possible to obtain the statistical characteristics of the acoustical field, which take into account the random character of jet pulsations [1,2]. Great interest also attaches to the further study of this problem in the linear presentation, specifically the mechanism of acoustical wave emission from the region of jet disintegration.

REFERENCES

1. Лебедев М.Г., Телешин Г.Ф. Последование взаимодействия сверхзвуковой струи с акустическими волнами. Изв. АН СССР, МЖГ, № 4, М., 1970.

2. Лебедев М.Г., Телешин Г.Ф. Взаимодействие сверхзвуковой струи с акустическими волнами. В сб. "Аэродинамика больших скоростей". Труды Института механики МГУ, № 5, 1970.

3. Грей Э., Мэтьюз Г.Б. Функции Бесселя. ИЛ, М., 1953.

4. Нобл Б. Метод Винера – Хопфа. ИЛ, М., 1962.

5. Коллатц Л. Функциональный анализ и вычислительная математика. "Мир", М., 1969.

6. Уорд Дж. Н. Осесимметричные сверхзвуковые потоки в областях, включающих ось, – линейное приближение. В сб. "Современное состояние аэродинамики больших скоростей", ИЛ, т. 1, М., 1955.

7. Акуфиев В.М., Комаров В.В., Купцов Б.М., Полынков Л.А., Сергиенко А.А. Дискретная составляющая в спектре шума сверхзвуковых струй. Изв. АН СССР, МЖГ, № 3, 1969.

8. Маркин В.М. Некоторые последования акустического излучения воздушной сверхзвуковой струи. Кандидатская диссертация. Акустический ин-т АН СССР, М., 1969.

9. Powell A. On the noise emanating from a two - dimensional jet above the critical pressure. The Aeronautical Quarterly, vol. IV, pt. II, 1953.

10. Hammitt A.G. The oscillation and noise of an overpressure sonic jet. Journ.Aero/Sci., 1961, vol.28, N 9.

11. Mörle M. Emissions acoustiques associées aux jets d'air supersoniques. Journ de Mécanique, 1965, vol.4, N 3.

12. Davies M.G., Oldfield D.E.S. Tones from a choked axysimmetric jet. Acustica, 1962, vol. 12, N 4.

13. Poldervaart L.J., Vink A.T., Wijnands A.P.J. The photographic evidence of the feedback loop of a two-dimensional screeching jet of air. The 6 th Int. Congress on acoustics, Tokyo, 1968, P-101 - P - 104.

14. Laffiter W.L., Hubbard H.H. The near noise field of static jets and some model devices for noise reduction. NACA Rep., n 1261, 1956.

STABILITY OF AN AXISYMMETRICAL COMPRESSED, NON-VISCOUS WAKE

by

S. Ya. Gertsenshteyn and A. V. Kashko

The article gives certain results of calculating the stability of flow in the wake behind a body moving (flying) at hypersonic velocity. Wave numbers, rates of propagation and amplification coefficients were obtained which are characteristic for the vibrations which arise in the wake. The relationships between these values and the Mach number and the temperature drop on the axis of the wake and the periphery are examined.

The article also gives a brief survey of theoretical investigations on stability of flow in the far wake.

1. It is well known from many experimental works [1,2] that sinusoidal oscillations appear in the supersonic wake behind the "throat" (at a distance of 10-15 diameters of the body). These oscillations develop quite rapidly and at a distance of approximately 25 diameters downstream from the "throat" of the wake, flow becomes turbulent. A study of the given oscillations is of certain interest and a number of theoretical works have been devoted to this question.

Basically, results were obtained for plane wakes. The purpose of this work is to study axisymmetrical compressible wakes.

We note that the analogy between plane and axisymmetrical wakes is far from complete. For example, it has been shown in the axisymmetrical case for quite "smooth" profiles [11], that 2-dimensional, increasing oscillations do not exist and only a 3-dimensional, sinusoidal wave can develop in the flow. In the plane case, however, according to the Squire theorem, plane perturbations are the most unstable ones. As the conducted calculations show, the corresponding numerical data for axisymmetrical and plane wakes also significantly differ.

Evidently, Helmholtz first explained the appearance of oscillations in the wakes with instability at the vortex layers which form in the wakes. Raley [3] examined and solved the problem of the stability of the vortex sheet. He also solved the problem of stability of the vortex layer of finite thickness. The problem of flow stability in a wake with vortex distribution of finite intensity was first examined by G. I. Petrov [4]. In this work the velocity profile has been replaced by a broken line consisting of 5 components (fig. 1); the solution was obtained by analogy with the above-mentioned Rayleigh solution. With the aid of comparatively simple calculations, it was specifically demonstrated in a work [4] that the antisymmetrical perturbations developed more intensively than the symmetrical ones. In this work [4] with the aid of the generalized Rayleigh method, an examination was made of stability of an axisymmetrical wake relative to zonal oscillations. Certain results of a work [4] were duplicated and refined in the work of Michalke and Schade [12]. The work [12] also employed the Rayleigh method, but the velocity profile was replaced by a broken line with a significantly larger number of components than in the work [4].

We note that the overwhelming majority of works on wake stability relate to the plane wake. Basically, three works [11, 4, 13] contain results on the stability of axisymmetrical wakes. The stability of flow relative to the zonal oscillations was examined in a work [4], as has already been mentioned above. A work [11] derives certain estimates and criteria which are necessary and sufficient for the existence of neutral and increasing oscillations, by analogy with the known criteria for the plane case. Greatest interest attaches to the necessary condition for the existence of increasing perturbations, obtained in a work [11]. It will be briefly explained below how this condition can be obtained and what conclusions can easily be drawn from it.

The problem of the stability of an axisymmetrical wake in an ideal, incompressible fluid can pertain to a problem for eigenvalues for a second order equation

$$(U-c)\frac{d}{dz}\left\{\frac{\tau}{n^2+\alpha^2\tau^2}\frac{d(\tau G)}{dz}\right\}-(U-c)\tau G-\tau G\frac{d}{dz}\left(\frac{\tau U'}{n^2+\alpha^2\tau^2}\right)=0 \qquad (1)$$

Here the boundary conditions - conditions of solution limitation when $\tau = 0$ and $\tau \to \infty$. $U(z)$ - basic flow velocity profile, α and n - assigned parameters (perturbation was presented in the following form):

$$q' = \hat{q}(z)\exp(i\alpha x - i\alpha ct + in\varphi)$$

By multiplying equation (1) by $\frac{\tau\bar{G}}{U-c}$ (here $\bar{G}$ is a function conjugate of G) and integrating the obtained expression from $\tau = 0$ to $\tau \to \infty$, having used the known boundary conditions, integrating by terms, and by separating the real and imaginary part, one easily can obtained:

$$c_i\int_0^\infty |q|^2 Q'\,dz = 0 \qquad (2)$$

here

$$q(z)=\frac{\tau}{U-c}G(z),\quad Q=\frac{\tau U'}{n^2+\alpha^2\tau^2}.$$

If $c_i \neq 0$, then it follows from (2) that Q' can change sign in the interval $(0,\infty)$, i.e., when $c_i \neq 0$ should vanish at a certain point of the interval $(0,\infty)$. For example, it is easy to show from this necessary condition that $q' \neq 0$ for $U(z) = U_0/(1+\frac{r^2}{r_0^2})^2$ when n = 0.

It was shown in work [11] that increasing perturbations can only exist for this profile when n = 1, i.e., only the "sinusoidal" oscillations can be unstable.

It was noted in a work [11] that this conclusion can be related solely to the "smoothed" velocity profile.

The given conclusion is not true for profiles with a sharp velocity change. No specific calculations relative to increasing perturbations are given in work [11].

Work [13] is chiefly devoted to plane wakes in a compressible, non-viscous fluid. Only individual calculations are given for the axisymmetrical case in the work for a Gaussian distribution of the velocity profile $U(r) = e^{-r^2}$ when n = 1, i.e., for the "sinusoidal" waves. A work [13] not only gives specific calculations, but also derives certain necessary criteria for the existence of neutral

perturbations and a certain sufficient condition for the existence of increasing perturbations. The conducted investigation is similar to investigations made in the case of the incompressible fluid [5,6]. The authors also used the investigations of Lynn and L. Liz, which are unpublished in the Soviet Union, and which deal with the stability of a compressible boundary layer. In addition to the work referenced above [13], stability of the compressible plane wake is investigated in works [7,14,15]. Works [7,14] investigate the plane case. A work [15] examines the plane and axisymmetrical cases. The basic flow in this case is assumed to be constant in the vicinity of the axis, i.e., stability of an axisymmetrical vortex sheet in a compressible gas was examined.

2. In order to investigate oscillations in an axisymmetrical wake, one can take the original equation system in the cylindrical coordinate system [8]:

$$
\begin{aligned}
&\frac{\partial v_z}{\partial t} v_z + \frac{1}{r}\frac{\partial v_z}{\partial \theta} v_\theta + \frac{\partial v_z}{\partial z} v_z + \frac{\partial v_z}{\partial t} - \frac{1}{r} v_\theta^2 = -\frac{1}{\rho}\frac{\partial P}{\partial z}\\
&\frac{1}{r} v_z v_\theta + \frac{\partial v_\theta}{\partial t} v_z + \frac{1}{r}\frac{\partial v_\theta}{\partial \theta} v_\theta + \frac{\partial v_\theta}{\partial z} v_z + \frac{\partial v_\theta}{\partial t} = -\frac{1}{r\rho}\frac{\partial P}{\partial \theta}\\
&\frac{\partial v_z}{\partial t} v_z + \frac{1}{r}\frac{\partial v_z}{\partial \theta} v_\theta + \frac{\partial v_z}{\partial z} v_z + \frac{\partial v_z}{\partial t} = -\frac{1}{\rho}\frac{\partial P}{\partial z}\\
&\frac{\partial \rho}{\partial t} + \frac{\partial(\rho v_z)}{\partial z} + \frac{1}{r}\frac{\partial(\rho v_\theta')}{\partial \theta} + \frac{\partial(\rho v_z)}{\partial z} + \frac{\rho v_r}{r} = 0\\
&c_v \rho \frac{dT}{dt} = A\frac{P}{\rho}\frac{d\rho}{dt}\\
&P = \rho R T.
\end{aligned}
\qquad (3)
$$

We shall present the sought solution to the system in the form of the sum of the basic flow

$$
\begin{aligned}
&\bar{V}_{осн}\,(v_{осн\,z} = V_{z(r)},\ v_{осн\,r} = 0,\ v_{осн\,\theta} = 0,\\
&\tau_{осн} = \bar{T}_{(r)},\ P_{осн} = \bar{P},\ \rho_{осн} = \bar{\rho})
\end{aligned}
$$

and a certain, sufficiently small perturbation:

$$v_z + V_z + v_z' \quad , \quad v_r + v_r' \quad , \quad v_\theta + v_\theta' \quad ,$$

$$p + \bar{p} + p' \quad , \quad \rho + \bar{\rho} + \rho' \quad , \qquad (4)$$

$$T + \bar{T} + T' \quad .$$

Having substituted (4) in (3), and ignoring the terms which are quadratic relative to the perturbation components, we obtain a system consisting of 6 linear equations relative to 6 unknown functions:

$$v_r' \quad , \quad v_z' \quad , \quad v_\theta' \quad , \quad \rho' \quad , \quad T' \quad , \quad p' \quad :$$

$$\frac{\partial v_r'}{\partial t} + V_z \frac{\partial v_r'}{\partial z} = -\frac{1}{\rho} \frac{\partial p'}{\partial r}$$

$$\frac{\partial v_\theta'}{\partial t} + V_z \frac{\partial v_\theta'}{\partial z} = -\frac{1}{r\rho} \frac{\partial p'}{\partial \theta}$$

$$\frac{\partial v_z'}{\partial t} + v_r \frac{\partial V_z}{\partial r} + V_z \frac{\partial v_z'}{\partial z} = -\frac{1}{\rho} \frac{\partial p'}{\partial z}$$

$$\frac{\partial \rho'}{\partial t} + v_r \frac{\partial \bar{\rho}}{\partial r} + V_z \frac{\partial \rho'}{\partial z} + \bar{\rho}\left[\frac{\partial v_r'}{\partial r} + \frac{1}{r}\frac{\partial v_\theta'}{\partial \theta} + \frac{\partial v_z'}{\partial z} + \frac{v_r'}{r}\right] = 0$$

$$\bar{\rho} \frac{\partial T'}{\partial t} + \bar{\rho}\left[v_r \frac{\partial \bar{T}}{\partial r}\right] = (\gamma - 1)\bar{\rho}\left[\frac{\partial v_r'}{\partial r} + \frac{\partial v_z'}{\partial z} + \frac{1}{r}\frac{\partial v_\theta'}{\partial \theta} + \frac{v_r'}{r}\right] \qquad (5)$$

$$p' = \rho' \bar{T} + \bar{\rho} T' \quad .$$

If all perturbation components are sought in the form,

$$q' = \hat{q}(r) \exp[i\omega t + i\alpha z + i\beta\varphi] \quad ,$$

then it is easy to obtain a system of ordinary differential equations from the system (5) for determining the function $\hat{q}(r)$:

$$i\beta \hat{v}_r + V_z i\alpha \hat{v}_r = -\frac{1}{\rho} \hat{p}'$$

$$i\beta \hat{v}_\theta + V_z i\alpha \hat{v}_\theta = -\frac{1}{r\bar{\rho}} i\beta \hat{p}$$

$$i\beta \hat{v}_z + \hat{v}_r \bar{V}_z'(r) + i\alpha \bar{V}_z(r) \hat{v}_z = -\frac{1}{\bar{\rho}} i\alpha \hat{p}$$

$$i\beta \hat{\rho} + i\alpha V_z \hat{\rho} + \bar{\rho} \hat{v}_r + \bar{\rho}\left[\hat{v}_r' + \frac{1}{r} i\beta \hat{v}_\theta + i\alpha \hat{v}_z + \frac{\hat{v}_r}{r}\right] = 0$$

$$\bar{\rho} i\beta \hat{T} + \bar{\rho} \hat{v}_r \bar{T}'(r) + \bar{\rho} i\alpha V_z \hat{T} = (\gamma - 1)\bar{\rho}\left[i\alpha \hat{v}_z + \hat{v}_r' + \frac{1}{r} i\beta \hat{v}_\theta + \frac{\hat{v}_r}{r}\right] \qquad (6)$$

$$\hat{p} = \hat{\rho} \bar{T} + \bar{\rho} \hat{T}$$

We shall insert the dimensionless variables: [illegible]

[illegible] (7)

System (6), in the dimensionless variables has the form:

[illegible] (8)

[illegible] (9)

[illegible] (10)

[illegible] (11)

[illegible] (12)

[illegible] (13)

Here M is the Mach number: [illegible]

It is subsequently convenient to reduce the system (8) tc 1 equation. We shall write the equation for pressure [illegible]. It is preliminarily expedient to obtain the expression for [illegible] through [illegible] and [illegible]. For this purpose, it is sufficient to substitute the expression for [illegible] from equation (8) in equation (10). Having substituted the expression for [illegible] from equation (13) in equation (12), we then obtain the relationship between [illegible], obtained from equation (11), having substituted the expression equation (13) in equation (12), instead of [illegible] its expression through [illegible] and [illegible]. If one now uses the expressions already found for [illegible] and [illegible] via [illegible] and [illegible], then we obtain the following equation for [illegible]:

[illegible] (14)

Here

$$\alpha_1 = i[\beta + \alpha V_2] \ .$$

3. Boundary conditions for Equation (14) may be respresented simply: at z = 0 p(0) = 0 and at $z \to \infty$ the solution $p(z)$ must be bounded in absolute value. However, close to the point $z = 0$ it is advantageous to integrate Equation (14) numerically, since expressions of the form $\frac{1}{z}$ and $\frac{1}{z^2}$ are included in the coefficients of the equation. Therefore it makes sense to use the asymptotic representation of the solution in the vicinity of zero.

To perform a numerical calculation, it is necessary also to replace the boundary condition at infinity by the boundary condition at a finite distance. This may be done by using the asymptotic expansions. Below we give the corresponding calculations.

If at $z \to 1$ $V_1 = 1$ and $\bar{r} = 1$, the Equation (14) assumes the form

$$\hat{p}\left(\frac{1}{i(\beta+\omega)}\left[(\beta+i\omega)^2 + \frac{r^2}{z^2 M^2} + \frac{\alpha^2}{M^2}\right]\right) - \hat{p}'\frac{1}{i(\beta+\omega)}\frac{1}{M^2} - \frac{1}{i(\beta+\omega)}\hat{p}'\frac{1}{M^2}\frac{1}{z} = 0. \qquad (15)$$

Or

$$\hat{p}'' + \frac{1}{z}\hat{p}' + \hat{p}\left(-\frac{r^2}{z^2} - \alpha^2 + M^2(\alpha+\beta)\right) = 0 \ . \qquad (16)$$

The asymptotic behaviour at infinity of the bounded solution of Equation (16) is well known [9,10]:

$$P(\tau) = \text{const}\ \frac{1}{\sqrt{\tau}}\, e^{-\lambda\tau} \quad . \tag{17}$$

where $\lambda^2 + M^2(\alpha+\beta)^2 - \alpha^2$

and $\mathrm{Re}\,\lambda > 0$. (18)

We shall not consider the case $\mathrm{Re}\,\lambda = 0$, since at $M^2(\alpha+\beta)^2 - \alpha^2 < 0$ the boundary condition at infinity is automatically satisfied for any β (case of a continuous spectrum). Using (17), we may readily see that for very large values of τ the following relations must be satisifed with great accuracy:

$$P + \frac{1}{2}\frac{1}{\tau}P + \lambda P = 0 \quad . \tag{19}$$

This relationship (19) will replace the boundary condition at infinity below.

Let us write the asymptotic solution of Equation (14) in the vicinity of zero. Equation (14) may be rewritten in the following form:

$$\hat{P}'' + \left[\frac{\beta a_1' + \beta a'}{\beta a_1} + \left[\frac{a_1'}{a_1} - \frac{1}{\tau}\right]\right]\hat{P}' + \left[\frac{a_1^2 M^2}{\tau^2} + \frac{\tau^2 + \alpha^2\tau^2}{\tau^4}\right]\hat{P} \quad . \tag{20}$$

Let us give the solution of Equation (20) in the form of the series

$$P = \tau^{\lambda}\sum_{0}^{\infty} C_n \tau^n$$

Collecting terms of the form $\tau^{\lambda-1}$, we have

$$\lambda(\lambda-1)C_0 + \lambda(-C_0) + \gamma^2 C_0$$

from which we have

$$\lambda^2 + \gamma^2$$

The remaining coefficients of the series may be readily determined by means of C_0. For example, collecting terms of the form $r^{\lambda-1}$, we obtain C_1:

$$C_1\lambda(\lambda+1)+(\lambda+1)C_1+\gamma^2C_1+\lambda C_0\left[\frac{(\partial a_1)'}{\partial a_1}\Big|_{r=0}+\frac{a'}{a}\Big|_{r=0}\right]$$

Thus, in the vicinity of zero the unknown solution behaves like r^{γ}. It is assumed that $\gamma\neq 0$. For $\gamma=0$ we may obtain the corresponding asymptotic representation by analogy with the previous one [27].

4. These calculations make it possible to obtain the representation of the nature of vibrations in a supersonic medium. As an example, we examined flow in the medium behind a body in the range of Mach numbers from 10 to 30. The flow instability is considered in the wake behind the "throat", at a distance 10 - 15 times greater than the body dimensions. Data on the velocity and temperature distribution were taken from [1,2,13]:

$$U=1-\Delta u e^{-\eta^2},$$

$$T=1+\Delta T e^{-\eta^2},$$

$$z=\int_0^{\eta}\frac{d\eta}{T(\eta)},$$

$$\Delta u=1-f'=1-(1-M_\infty^{-2})^{1/2}$$

$$\frac{h_0(0)}{h_\infty}=(1-f'^2)\gamma=1-\frac{M_\infty^2}{2}.$$

Here $U(\eta)$ is the dimensionless velocity; $T(\eta)$ is the temperature distribution; $h_0(0)$ - enthalpy in the cross section we selected on the wake axis; h_∞ - enthalpy in the advancing stream.

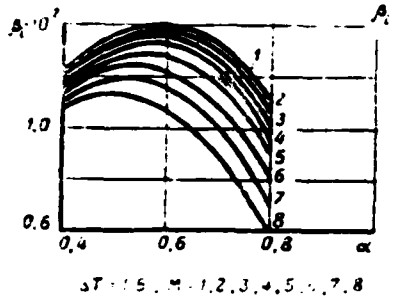

Figure 1

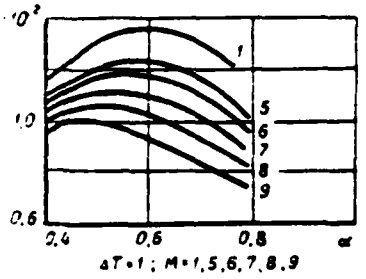

Figure 2

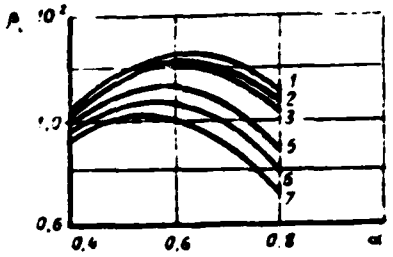

Figure 3

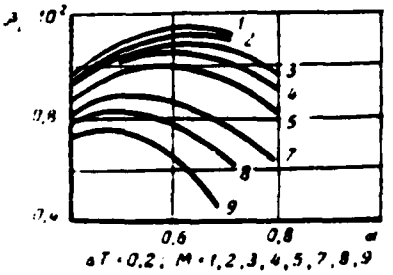

Figure 4

The results of the calculations are partially given on graphs 1 - 6. As shown in Figures 1,2,3,4, with an increase in the Mach number the amplification coefficient decreases, but very little. There the well known sharp increase in stability of flow with an increase in the Mach number can be better explained by the large phase propagation rate of perturbations in the compressed wake (Figure 5) - (the perturbations very rapidly drift along the stream, without becoming developed). It is of interest to compare the results obtained with the well known results [13] on the stability of plane streams. The comparison shows that the amplification coefficients for plane streams are approximately four times greater than for axisymmetric streams.

These calculations also show that with an increase in the Mach number, the extremal wave number α^*, which corresponds to the maximum amplification coefficient, decreases, and

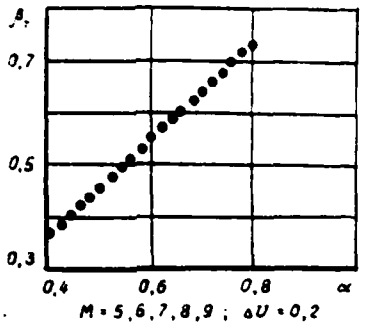

Figure 5

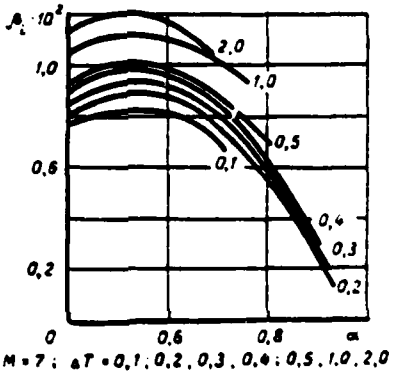

Figure 6

the phase velocity c_r^* remains almost unchanged. We should also note that the phase velocity changes little with a change in the wave number α (for fixed Mach number) - Figure 5.

Separate calculations were made to clarify the effect of a hot "core" for an axisymmetric wake.

With an increase in ΔT (from 0.1 to 2.0), the amplification coefficient αc_i increases by approximately a factor of 1.5 (Figure 6). The extremal wave number α^*, with an increase in ΔT from 0.1 to 2.0, decreases by approximately 1/10 of the initial value. The perturbation propagation rate in the range examined changes very little. We should note that the

for the observer, who moves at the perturbation propagation rate $c_1 = \frac{a_1}{a}$, the local flow velocity, whose stability is being studied, is less than the speed of sound. This occurs in the entire range in which ΔT and M change.

REFERENCES

ЛИТЕРАТУРА

1. Лиэ Л. Ракетная техника и космонавтика, № 2, 1964.
2. Лакуэнд Р.С. Ракетная техника и космонавтика, № 4, 1966.
3. Рэлей. Теория звука, т. 1 - 2.
4. Петров Г.И. Труды ЦАГИ, № 304, 1937.